Design and evaluation of a new diagnostic instrument for osmotic gradient ektacytometrie

Arie Eric Oren Finkelstein

UNIVERSITÉ PARIS-EST

ÉCOLE DOCTORALE MSTIC

MATHÉMATIQUES ET SCIENCES ET TECHNOLOGIES DE L'INFORMATION ET DE LA COMMUNICATION

THÈSE DE DOCTORAT

DISCIPLINE : ELÉCTRONIQUE, OPTRONIQUE ET SYSTÈMES

PRÉSENTÉE PAR

Arie Finkelstein

DESIGN AND EVALUATION OF A NEW DIAGNOSTIC INSTRUMENT FOR OSMOTIC GRADIENT EKTACYTOMETRY

---

dirigée par: Gaelle Lissorgue

Soutenue le 28 juin 2017 devant le jury composé de :

Pr. Georgiev Vjacesclav	University of West Bohemia	Rapporteur
Pr. Hamam Yskandar	Tshwane University of Technology	Rapporteur
Pr. Lissorgue Gaelle	ESIEE Paris	Directeur de thèse
Pr. Rocaries François	Tshwane University of Technology	Examinateur
MdC Georgiev Daniel	University of West Bohemia	Examinateur
Pr. Français Olivier	ESIEE Paris	Examinateur

ACKNOWLEDGEMENTS

I would like to thank the reviewers of my thesis, Yskandar Hamam and Vjačeslav Georgiev for carefully reading my dissertation and for their useful suggestions for improvements.

Thanks also to François Rocaries, Olivier Français, and Daniel Georgiev for agreeing to be examiners on the thesis jury.

I am grateful to my thesis director, Gaelle Lissorgues, for her extremely patient and efficient supervision of this thesis.

Thanks to Gilles Bertrand for creating the contact between the Bicêtre hospital hematology department and the ESIEE Paris Embedded Systems department where I was employed. It was this contact that first brought to my interest the subject of RBC deformability.

My thanks to Therese Cynober, Loic Garçon and Véronique Picard, from the Bicêtre hematology department for the fruitful years of collaboration in the project of modernising the Technicon Ektacytometer owned by their laboratory.

My very special thanks to Frans Kuypers from Children's Hospital Oakland Research Institute (CHORI), California, USA, for his hospitality and for our fruitful collaboration in the Microfluidic Ektacytometer project covered by this thesis.

Thanks to James Casey from Berkeley University, California, USA, and Gregor Havkin, Cold Spring Harbor Laboratory, NY, USA, for very useful discussions and comments on the manuscript of this thesis.

Thanks to Moshe Machover and Emmanuel Frajoun for their contribution to style and proofing of math formulae.

Thanks to Olivier De Cambry, for his valuable advice in the use of Mathematica software.

Thanks to Genevieve Baudoin, for her follow up and support of my research activities, as a manager of research at ESIEE Paris.

The study described in chapter 4 was performed within the framework of a research contract between CHU de Bicêtre and ESIEE during 2006 and 2008 and partially funded by CHU de Bicêtre.

I wish to thank Hugues Talbot, Suat Topsu, Thérèse Cynober, Loïc Garçon , Gregor Havkin and Frans Kuypers for their contribution as co-authors of the journal article on which chapter 4 is based (Finkelstein et al., 2013).

I also wish to thank the following persons for their contribution to the research project described in chapter 4: Michel Couprie for his valuable advice in image processing, Thibaut Barati and Olena Tankyevych for image processing software development, and Ivan Swiac, Etienne Desjardins and Michel Pellegrin for GUI software development, Bruno Capellazzi for mechanical work and Leon Heller for ARM microcontroller embedded software development.

I wish to thank Rowley Associates for the donation of Crossworks ARM Development Environment software which was used to develop the embedded control program.

Finally, my thanks to my children Thierry and Maya, and my friends Francine, Abdou, Nicole and Louise for their encouragement, and a tribute to my mother and my late father and stepfather, who brought me up in the spirit of curiosity for innovation and science in the benefit of humanity.

ABSTRACT

The ability of red blood cells (RBC) to change their shape under varying conditions is a crucial property allowing the cells to traverse capillaries narrower than their own diameter. Ektacytometry is a technique for measuring deformability by exposing a highly diluted blood sample to shear stress and evaluating the resulting elongation in RBC shape using a laser diffraction pattern.

Two main methods are used to characterize RBC deformability in ektacytometry:

(1) In "Shear Scan" the cells are mixed with a high-viscosity solution of normal physiological osmolality while increasing shear stress is applied to the mixture. The diffraction pattern therefore shows the mean deformability as a function of shear stress at physiologic tonicity (Groner et al., 1980).

(2) In "Osmotic Scan", the shear stress is kept constant, but RBCs are mixed in a medium where osmolality is increased gradually. The diffraction pattern then shows deformability as a function of osmolality. This mode is also known as "osmotic gradient ektacytometry", and provides information on membrane stiffness, intracellular viscosity and surface-area-to-volume ratio (Clark et al., 1983).

Measurement of RBC deformability in Osmotic Scan mode has made it possible to diagnose several hereditary disorders related to cell membrane or hemoglobin defects such as spherocytosis, eliptocytosis, or stomatocytosis. RBC deformability depends on both cytosolic and membrane parameters and measurement of the osmotic deformability profile has been used to monitor patient treatment, aimed at normalization of RBC properties.

Ektacytometry has been dominated by the Taylor-Couette cylinder shearing technique for the last four decades. However, equipment based on flow channel shearing is simpler, cheaper and easier to maintain. Thus, in recent years several studies have shown that the results obtained by this technique, in the shear scan ektacytometry mode, are valid for clinical use. However, no osmotic gradient ektacytometer in a flow channel was designed and built up until the present research project.

In this dissertation the design, construction and testing of an osmotic gradient ektacytometer based on a flow channel is described in detail. The new instrument

has several advantages over the currently used rotating cylinder technique. These are:

- Lower quantities of blood sample are required - important for newborn babies and experimental mouse models used in bio clinical studies.

- Closed circuit design giving better sterile conditions and lowering sample contamination risk.

- Closed circuit allows monitoring of additional parameters like oxygenation and temperature. It also permits the instrument to be more compact in size and lighter.

- No moving parts in the flow channel leading to lower power consumption, lower production/manufacturing cost, and simplification of maintenance.

- Test conditions are closer to blood vessel physiology.

- Provides better precision because shear stress does not depend on viscosity under constant pressure across the channel.

The research involved the design of several components:

- A new hydraulic system intended to create varying osmolality solution with a fixed viscosity.

- The use of various sensors and associated electronics for the measurement of temperature, conductivity, differential pressure and laser beam intensity.

- Design of an electronic board (based on a microcontroller programmed to control valves and pumps and to communicate with user interface program on a computer).

Comparative experiments were performed in order to determine the most effective means of measuring the elliptical shape of the diffraction pattern which represents the average RBC deformability. Results obtained by a camera were compared to those obtained by a four quadrant photodiode detector.

The study was also complemented by a theoretical analysis based on fluidic modeling, in order to correlate experimental results with the Taylor-Couette

cylinder ektacytometer operation principle, and to optimize the design of the full device.

The shear stress distribution in a shear driven flow system (Taylor-Couette cylinders) is different than that generated in a pressure driven flow in a channel. In a Taylor-Couette system all RBCs are exposed to the same shear stress, but in a flow channel the distribution of shear stress is not uniform. This means that the interpretation of the diffraction pattern in these two different systems represents potentially different deformability "indexes". This difference is assessed theoretically but the results need to be verified experimentally for a variety of pathologies in order to confirm that they both give comparable results in clinical use. A small number of pilot experiments performed to date show comparable results.

The dissertation is divided into seven chapters including a general introduction and conclusions. A short description of the thesis structure is found at the end of the introduction chapter, section1.6 "Aim, objectives and Dissertation Overview ".

CONTENT

1 INTRODUCTION 1

1.1 HISTORY 2

1.2 BLOOD 3

1.3 RED BLOOD CELLS 3

1.4 DEFORMABILITY OF RBCS4

1.5 PATHOLOGICAL DISORDERS AFFECTING RBC DEFORMABILITY 7

1.5.1 Hereditary Spherocytosis (HS) 10

1.5.2 Hereditary Elliptocytosis (HE) 10

1.5.3 Hereditary Ovalocytosis (SAO) 10

1.5.4 Hereditary Stomatocytosis (HSt) 11

1.5.5 Sickle cell disease 12

1.6 AIM, OBJECTIVES AND DISSERTATION OVERVIEW 12

2 STATE OF THE ART 15

2.1 RBC DEFORMABILITY MEASUREMENT TECHNIQUES 15

2.1.1 Introduction 15

2.1.2 Measurement techniques of single cells 15

2.1.3 Measurement techniques of RBC populations 27

2.2 EKTACYTOMETER COMMERCIAL APPLICATIONS 31

2.2.1 Technicon 32

2.2.2 Lorca (Laser-assisted Optical Rotational Cell Analyzer)34

2.2.3 RheoScan-D 36

2.2.4 Rheodyn SSD 37

2.3 CONCLUSIONS 38

3 COMPARISON BETWEEN PRESSURE AND SHEAR DRIVEN FLOWS FOR OSMOLALITY GRADIENT EKTACYTOMETRY.....39

3.1 INTRODUCTION **ERREUR ! SIGNET NON DEFINI.**

3.2 THEORETICAL BACKGROUND 39

3.3 CYLINDRICAL COUETTE FLOW 44

3.4 PLANE ROTATIONAL COUETTE FLOW 48

3.5 PLANE-POISEUILLE FLOW 50

3.6 CONCLUSIONS 55

4 COMPARISON BETWEEN A CAMERA AND A FOUR QUADRANT DETECTOR, IN THE MEASUREMENT OF RED BLOOD CELL DEFORMABILITY AS A FUNCTION OF OSMOLALITY 59

4.1 INTRODUCTION 59

4.2 THEORETICAL BACKGROUND 59

4.3 EXPERIMENTAL APPARATUS AND METHODS 61

4.4 RESULTS AND DISCUSSION 65

4.5 CONCLUSIONS 67

5 MODELLING AND MATHEMATICAL ANALYSIS 69

5.1 MODELING USING MATLAB/ SIMULINK 69

5.2 PRACTICAL CONSIDERATIONS 76

5.2.1 Example 77

5.2.2 Calculation 78

5.3 CONCLUSIONS 79

6 DESIGN AND PROOF OF PRINCIPLE..... 81

6.1 INTRODUCTION 81

6.1.1 Process and venue used for testing 81

6.2 HYDRAULIC SYSTEM 84

6.2.1 Initial design 84

6.2.2 Hydraulic system Second design 87

6.2.3 Flow cell choice 90

6.2.4 Optical system 93

6.2.5 Hardware composition 95

6.2.6 Software 103

6.3 PROOF OF PRINCIPLE 105

6.3.1 Sample preparation 105

6.3.2 Solution preparation 106

6.3.3 Osmolality calibration 108

6.3.4 Osmoscan curves 110

6.4 CONCLUSIONS 113

7 CONCLUSIONS 115

8 REFERENCES 117

9 APPENDIX 129

9.1 SCIENTIFIC COMMUNICATIONS BY ARIE FINKELSTEIN 129

9.1.1 International journals 129

9.1.2 Conferences 130

9.1.3 Internal communications 130

LIST OF TABLES

TABLE 1: LORRCA MAXSIS AND TECHNICON MAIN DIFFERENCES 36

TABLE 2: COMPARISON OF FEATURES OF CYLINDRICAL COUETTE FLOW AND PLANE-POISEUILLE FLOW 56

TABLE 3: COMPARISON OF FORMULAS FOR CYLINDRICAL COUETTE FLOW *VS.* PLANE-POISEUILLE FLOW 57

TABLE 4: THE TABLE INDICATES THE SETTINGS AS DEPICTED IN STEPS 1-5 87

TABLE 5: CALCULATED FLOW RATES, PRESSURES AND TUBE LENGTHS FOR THREE DIFFERENT HEIGHT IBIDI SLIDES (L=50MM, W= 5MM). SEE MORE DETAILS ABOVE. 92

TABLE 6: CHANNEL HEIGHT MEASUREMENTS, WITHIN SAME BATCH, FOR IBIDI μ-SLIDE I (PROVIDED BY IBIDI) 93

TABLE 7: CONDUCTIVITY BOARD VOLTAGE MEASUREMENT FOR SEVERAL CONDUCTIVITY VALUES 97

TABLE 8: COMPARISON OF PRESSURE MEASUREMENTS BETWEEN A NEEDLE GAUGE AND TWO PRESSURE SENSORS 103

TABLE 9: COMPOSITION OF CALIBRATION SOLUTIONS 108

TABLE 10: MEASURED VALUES FOR OSMOLALITY CALIBRATION 109

TABLE 11: COMPARING THE INDICATOR POINTS ON CURVES IN FIGURE 60 AND FIGURE 61 FOR THE SAME BLOOD SAMPLE OBTAINED BY THE MICROCHANNEL DEVICE AND THE TECHNICON EKTACYTOMETER 112

LIST OF FIGURES

FIGURE 1: ERYTHROCYTE BICONCAVE SHAPE. 4

FIGURE 2: EFFECT OF DEFORMABILITY ON HIGH-SHEAR VISCOSITY OF BLOOD. 5

FIGURE 3: OSMOTIC DEFORMABILITY PROFILES OF RED CELLS FROM NORMAL CONTROL, 8

FIGURE 4: IMAGES OF PATHOLOGIC RBC. 9

FIGURE 5: DEFORMATION OF A CELL DUE TO NEGATIVE PRESSURE IN A MICROPIPETTE. 17

FIGURE 6: SCHEMATIC DIAGRAM OF A RHEOSCOPE 18

FIGURE 7: OPTICAL TWEEZERS FORCES. 20

FIGURE 8: A TYPICAL SETUP OF OPTICAL TWEEZERS. 21

FIGURE 9: A SINGLE BEAM RBC LASER TRAPPING TECHNIQUE 22

FIGURE 10: SCHEMATICS OF AFM OPERATION. 23

FIGURE 11: SCHEMATIC OF RBC OPTICAL MAGNETIC TWISTING CYTOMETRY (OMTC) TESTS. 24

FIGURE 12: EXPERIMENTAL SETUP FOR WDPM. 26

FIGURE 13: (A) QPI OF BLOOD SMEAR USING FPM 26

FIGURE 14: IMAGES OBTAINED BY CDOT, QPI METHOD. 27

FIGURE 15: SCHEMATIC REPRESENTATION OF THE FILTRATION APPARATUS. 28

FIGURE 16: TYPICAL SHEAR SCAN DEFORMABILITY CURVE.30

FIGURE 17: TYPICAL OSMOSCAN CURVES. 31

FIGURE 18: A BLOCK DIAGRAM OF THE TECHNICON EKTACYTOMETER 33

FIGURE 19: SCHEMATIC DIAGRAM OF LORCA RBC DEFORMABILITY MEASUREMENT SYSTEM.34

FIGURE 20 : THE LORRCA MAXSIS EKTACYTOMETER. 35

FIGURE 21: SCHEMATIC DIAGRAM OF THE RHEOSCAN-D SLIT-FLOW EKTACYTOMETER 37

FIGURE 22: VARIOUS SHEARING GEOMETRIES USED TO MEASURE RED BLOOD CELL DEFORMABILITY **ERREUR ! SIGNET NON DEFINI.**

FIGURE 23 : VISCOSITY OF DILUTED BLOOD SUSPENTION VS. HEMATOCRIT. 41

FIGURE 24: VELOCITY PROFILES FOR POISEUILLE FLOW 44

FIGURE 25: ENTRANCE EFFECT IN A FLOW CHANNEL. 44

FIGURE 26: COUETTE CYLINDERS 45

FIGURE 27: PLANE COUETTE FLOW: VELOCITY PROFILE OF FLUID BETWEEN TWO PARALLEL PLATES WITH ONE PLATE MOVING AT CONSTANT VELOCITY. 47

FIGURE 28: CROSS SECTION OF PARALLEL DISK RHEOMETER. 48

FIGURE 29: PRESSURE DRIVEN FLOW: VELOCITY PROFILE OF FLUID THROUGH A CHANNEL. 51

FIGURE 30: VELOCITY PARABOLIC PROFILE AND SHEAR STRESS LINEAR PROFILE IN PLANE-POISEUILLE FLOW. 53

FIGURE 31: AN ILLUSTRATION OF THE H/W RATIO INFLUENCE ON THE VELOCITY PROFILE, IN A RECTANGULAR CHANNEL 54

FIGURE 32: SCREEN SHOT OF THE DIFFRACTION IMAGE 63

FIGURE 33: MODIFIED TECHNICON EKTACYTOMETER 64

FIGURE 34: SCREEN SHOT OF THE CUSTOM APPLICATION COMPARING TWO DIFFERENT WAYS TO MEASURE EI FROM THE DIFFRACTION PATTERN 64

FIGURE 35: A TYPICAL OSMOTIC DEFORMABILITY CURVE INDICATING THE POINTS USED FOR COMPARISON OF THE DIFFERENT MEASUREMENT 65

FIGURE 36: EXPERIMENTAL CURVE. THE TOP CURVE WAS OBTAINED BY THE FOUR QUADRANT DETECTOR AND THE BOTTOM ONE BY THE CAMERA. 66

FIGURE 37: SCHEMATIC DIAGRAM OF THE FLODIF HYDRAULIC SYSTEM. 70

FIGURE 38: HYDRAULIC SYSTEM MATLAB SIMULINK MODEL 72

FIGURE 39: CURVES OF OSMOLALITY (MOSM/KG) VS TIME (MINUTES), OBTAINED WITH MATLAB SIMULINK FOR SEVERAL FLOW RATES 73

FIGURE 40: SIMULATION EXAMPLE OF THE EVOLUTION OF VOLUME (GREEN CURVE RIGHT AXIS) AND OSMOLALITY (BLUE LEFT AXIS) IN THE STEER TANK 79

FIGURE 41: PICTURE OF INITIAL HYDRAULIC SYSTEM EXPERIMENTAL SETUP. 85

FIGURE 42: FIVE STATES OF OPERATION FOR ONE EXPERIMENT: 86

FIGURE 43: SECOND DESIGN IMPROVED HYDRAULIC SYSTEM 88

FIGURE 44: HYDRAULIC SYSTEM OF THE SECOND DESIGN 90

FIGURE 45: LASER TUBE WITH OPTICAL SYSTEM. 94

FIGURE 46: FLOW CELL WITH BOTTOM FEED LINE AND TOP WASTE LINE. 94

FIGURE 47: FOUR QUADRANT DETECTOR ON SLIDING BASE. 95

FIGURE 48: ANALOG TO DIGITAL CONVERSION UNIT (NI USB6009) WITH RELAY CARD FOR SOLENOID VALVE AUTOMATION. 96

FIGURE 49: CONDUCTIVITY MEASUREMENT CARD WITH CONDUCTIVITY AND TEMPERATURE MEASUREMENT UNIT. 98

FIGURE 50: FOUR QUADRANT DETECTOR CIRCUIT 99

FIGURE 51: ORIENTATION OF THE FOUR QUADRANT DETECTOR (LEFT) AND ITS MASK (RIGHT) 99

FIGURE 52: ARM LPC2148 MICROCONTROLLER BOARD (RIGHT), CONDUCTIVITY MEASUREMENT BOARD (LEFT) AND QUADRATURE PHOTODETECTOR ANALOG INTERFACE (ON BREADBOARD) 100

FIGURE 53: ANALOG POWER SUPPLY UNIT 101

FIGURE 54: ANALOG AND SWITCHING POWER SUPPLIES, PHOTODETECTOR CARD AND RELAY CARD 101

FIGURE 55: PRESSURE SENSORS CARD 102

FIGURE 56: SCREENSHOT OF WINEKTA PROGRAM 104

FIGURE 57: COMPUTER PROGRAMME FOR USER INTERFACE USING LABVIEW 105

FIGURE 58: OSMOLALITY CALIBRATION CURVE 109

FIGURE 59: CURVES OBTAINED ON THE 0.1MM FLOW CELL BEFORE OSMOLALITY CALIBRATION. 110

FIGURE 60: CURVE OBTAINED ON THE FLOW CELL OF H=0.1MM AFTER OSMOLALITY CALIBRATION. 111

FIGURE 61: CURVE OBTAINED ON THE TECHNICON EKTACYTOMETER. 112

LIST OF ABBREVIATIONS AND ACRONYMS

FloDiF – The name invented for the microfluidic ektacytometer

RBC – Red Blood Cell

WBC – White Blood Cell

S/V – Surface to Volume ratio

TT – Tank Treading

ID – Internal Diameter

AFM – Atomic Force Microscopy

MA – Micropipette Aspiration

MTC - Magnetic Twisting Cytometry

OT – Optical Tweezers

SD – Standard Deviation

EI – Elongation Index

DI – Deformation Index

PVP – Polyvinylpyrrolidone

RPM - Revolutions per Minute

HeNe – Helium Neon

MCHC - Mean Corpuscular Hemoglobin Concentration

ARM Advanced RISC Machine

JTAG Joint Test Action Group

CCD Charge-Coupled Device

HE Hereditary Elliptocytosis

HS Hereditary Spherocytosis

HST Hereditary Stomatocytosis

DHSt Dehydrated Hereditary Stomatocytosis (xerocytosis)

OHSt Overhydrated hereditary Stomatocytosis

AIHA Autoimmune hemolytic anemia

HPP Hereditary Pyropoikilocytosis

SAO Southeast Asian Ovalocytosis

1 INTRODUCTION

Circulation of Red Blood Cells (RBC) throughout the vascular system is essential for delivery of oxygen to body tissues. Most of the oxygen exchange with the tissues is done in the smallest capillaries of the body, and the diameter of those is generally smaller, by as much as one third, than the diameter of the RBC. Therefore, the ability of RBC to repeatedly and reversibly deform is crucial for proper circulation and oxygen exchange. In fact, during the four months average lifespan of an RBC in humans, it goes through nearly a quarter of a million cycles of stretching and relaxation.

Flaws in RBC deformability result in failure of the RBC's to circulate properly in the capillaries, as well as to a decrease in their flow rate in macrovascular vessels, due to deterioration of the shear thinning property compared to healthy blood. (Chien, 1975) (SCHMID-SCHöNBEIN et al., 1969). Decrease in RBCs' deformability can result from hereditary or acquired pathologies such as sickle cell anemia, spherocytosis, elliptocytosis, stomatocytosis, auto-immune hemolytic anemia and malaria. RBC deformability disorders are genetically sustained in human populations in areas where malaria is endemic. Despite their severe health effects,

they confer survival advantages for those affected by the heterozygous[1] form and who contract malaria (Haldane, 1949) (Allison, 1964). For this reason the majority of these pathologies are geographically confined to the tropics and subtropics. Due to poverty in some of these regions, there is a lack of commercial interest and a striking lack of resources allocated for research, diagnosis and treatment in this field.

The study of Red Blood Cell (RBC) disorders is of primary importance, not only for diagnosis and treatment, but also because it may one day lead to understanding the mechanisms preventing malaria which may, in turn, contribute to a discovery of efficient preventive means.

My work has been motivated by the desire to contribute to both research and treatment of hereditary RBC disorders.

1.1 History[2]

RBCs were first discovered by Jan Swammerdam, in 1658, but a first published report only appeared in 1674 by Antonie Van Leeuwenhoek who also described their form changing feature (Van Leeuwenhoek, 1674). A modern milestone in the field was the work of Färaeus and Lindqvist showing that blood viscosity decreases strongly with reduced diameter of the tube (below a critical value of 0.3 mm) (Fahraus and Lindqvist, 1931). The role of deformability for the survival and proper functioning of RBC has long been known. However, its measurement only started in 1964 when Rand and Burton introduced the micropipette aspiration technique (Rand and Burton, 1964). In the following years several other methods of measuring RBC deformability were published including filtration, optical trapping, rheoscopy, flow channels and ektacytometry as detailed in § 2.1.

---

[1] There is a recent controversy regarding the disadvantage of the homozygous form (Pasvol, 2009)

[2] A more detailed historical review can be found in (Bessis and Delpech, 1981) and (Mohandas and Gallagher, 2008)

1.2 Blood

Blood is a non-Newtonian, viscoelastic and thixotropic suspension composed of roughly half plasma and half cellular particles. The particles are mostly cells and cell fragments: red blood cells (RBC), white blood cells (WBC), and thrombocytes (platelets). RBCs make around 98% of the total volume of cells in the blood. The average RBC's hematocrit (fraction of the total blood volume) is 45% in men and 42% in women.

Plasma, the extracellular portion of blood, consists of water (92%), proteins, nutrients, minerals, waste products, hormones, carbon dioxide, glucose, electrolytes and clotting factors. It is a Newtonian fluid with normal viscosity range of 1.10 – 1.30 cP at 37°C.

Blood viscosity, which has a crucial impact on circulation, may be subjected to several anomalies and depends on hematocrit, RBC deformation, aggregation and plasma viscosity. These factors are dynamic and vary with shear stress. Normal blood viscosity range is 3-4 cP at 37°C

Blood flow in vessels with diameter between 10μm to 300μm has significant non-Newtonian properties known as the Fahræus–Lindqvist effect (Fahraus and Lindqvist, 1931).

1.3 Red Blood Cells

Red blood cells count well over half of the total number of cells in a human body (Bianconi et al., 2013). Around 2.4 million of them are replaced each second in an adult body (Sackmann, 1995). Mammalian RBCs are non-nucleated cells. Their nucleus and mitochondria are expelled during bone marrow extrusion and cell maturation. Higher hemoglobin content improves their capacity for oxygen storage and diffusion. Moreover, the bi-concave cell shape of normal RBCs, which improves their deformability, and hence their circulation, would not be possible with the presence of a nucleus. The human normal RBC has an average diameter of a 7.82μm (SD ±0.58μm), and an average thickness of 2.58 μm (SD ±0.27μm) at the wider parts

and 0.81µm (SD ±0.35µm) in the center (Evans and Fung, 1972). RBCs of neonates, compared to adult cells, have 21% larger volume, 13% greater surface area and 11% wider diameter (Linderkamp et al., 1983).

The biconcave shape of a normal RBC gives it another advantage in achieving an efficient oxygen transfer since its average surface area of ~140 μm^2 is considerably higher than 97 μm^2, which is the surface area of a sphere having the same 90 fL volume [3] (Canham, 1970) (Lenard, 1974). The cell shape is a result of the interaction between the membrane, a network of skeletal proteins and the cytoplasm. Aging cells are removed from circulation by the spleen after a four months average lifespan, in which they travel around 400 km distance (Sackmann, 1995).

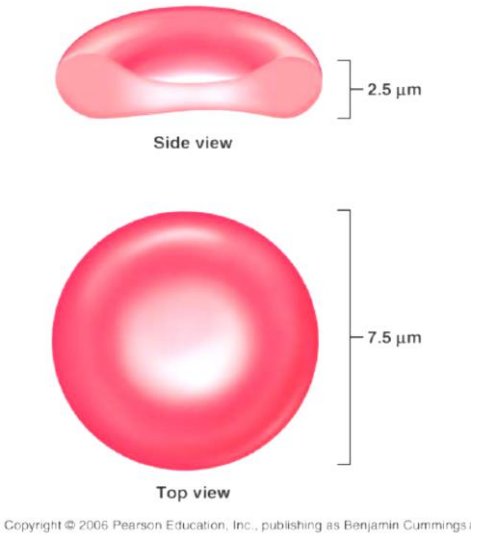

Figure 1: Erythrocyte biconcave shape. (©2006 Pearson Education. From http://www.lamission.edu/lifesciences/lecturenote/AliPhysio1/Blood.pdf, accessed 23 March 2017)

1.4 Deformability of RBCs

In order to assure proper transport of oxygen and carbon dioxide through body organs, red blood cells must be capable of repeatedly deforming, allowing them to

[3] Some controversial aspects of this view can be found in (Stier et al., 2013)

traverse capillaries narrower than their own diameter. Furthermore, deformability of RBC improves circulation also in macrovascular vessels since it's responsible for the reduction in blood viscosity (Figure 2).

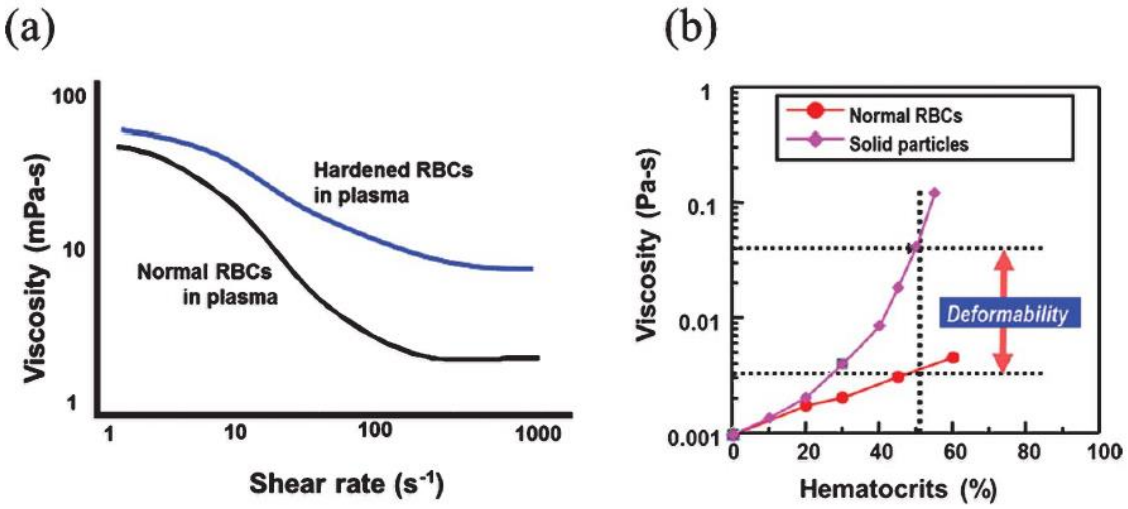

Figure 2: Effect of deformability on high-shear viscosity of blood. from (J. Kim et al., 2015)

The Deformability of RBCs is defined as their ability to modify their shape in response to externally applied forces. In blood circulation these forces are forms of stress either imposed by fluid flow with cell to cell interactions or by a vessel wall.

Human RBCs take around one minute to complete one cycle of circulation. In their lifetime RBCs are repeatedly subject to deformation, in around one hundred and fifty thousand circulation cycles.

The degree and other characteristics of deformability of RBCs depend on multiple factors related not only to the general flow conditions such as vessel geometry, blood pressure, blood viscosity, hematocrit and temperature, but also to the cell biomechanical and biochemical characteristics.

Three main cell properties responsible for RBC deformability are: cell surface to volume ratio (S/V), intracellular viscosity and cell membrane viscoelastic properties (Chien et al., 1978).

The biconcave geometry gives the cell an excess of surface area allowing it to easily fold and elongate under smaller forces. The mean volume of RBC is 94 fl (SD ±14fl)

and its membrane's surface area is 135 μm^2 (SD $\pm 16 \mu m^2$)(Evans and Fung, 1972)(McLaren et al., 1987). This represents an increase in membrane surface area, compared to a sphere of an equal volume, by a factor of 1.4. The larger surface area allows for a more efficient gas exchange and for substantial changes in shape under shearing forces, with very little area expansion. The maximal fractionnal area expansion, producing lysis, was uniformly distributed between 2% and 4% average (Evans et al., 1976). The biconcave shape is due to the mechanical and biochemical properties of the membrane, which is composed of a phospholipid bilayer supported by cytoskeletal proteins.

The RBC membrane surrounds a liquid cytoplasm whose viscosity depends mainly on hemoglobin concentration (MCHC). Its value is ~7 cP for normal MCHC of ~32 g/dl. It rises sharply with MCHC in a nonlinear fashion: it's nearly quadrupled at an MCHC of 40 g/ml (Chien, 1987). MCHC varies with changes in plasma osmolality leading to hydration or dehydration of the cell. It also increases with cell aging resulting in decreased deformability of old cells (Sutera et al., 1985). For a healthy RBC, the viscosity contrast λ, defined as the ratio of cytosol over blood plasma viscosity, is approximately $\lambda=5$ (Fischer et al., 1978) (Fedosov et al., 2014). The higher this contrast is the higher is the threshold shear stress in which RBCs, flowing in the macro circulation, change from tumbling motion (rigid body rotation) into tank tread motion[4] (where the membrane turns around the cell content) (Fischer and Korzeniewski, 2013). The increase in threshold has an effect on the whole blood viscosity and hence results in reduced flow rate. Tank tread motion has an important effect on RBC deformability since the induced cell membrane rotation transmits the external shear into the cell interior, causing it to participate in flow and behave more like a fluid (Keller and Skalak, 1982).

[4] An intermediate regime of motion called swinging was found at around $\lambda=4$, between tumbling and tank-treading motion regimes (Abkarian et al., 2007)

High elasticity of the membrane and cytoskeletal structure is an important determinant in the ability of RBCs to deform. The cell membrane can repeatedly elongate, under stress, to a length of over twice its diameter. This deformation is reversible, so the cell acquires back the biconcave discoid shape after the shear stress is removed. In other words the cell is highly elastic and also has a memory of its shape. The rim for instance is always formed by the same membrane elements. These elements regain their original position after tank treading movement under shear (Fischer, 2004). RBCs have a quick response time to deformation and recovery, of approximately 80 ms (Chien et al., 1978).

1.5 Pathological disorders affecting RBC deformability[5]

A short review of RBC abnormalities characterized by RBC deformability alteration follows with a focus on hereditary hemolytic anemias. Some of these present very similar symptoms and a correct specific diagnosis is critical.

Since most of these hereditary disorders confer resistance to Malaria they are significantly more prevalent in regions where Malaria is endemic (Allison, 1964; Kwiatkowski, 2005).

Many studies demonstrate that RBC deformability is altered when either membrane or cytosol is altered. The source for these alterations could be either acquired or hereditary.

In these abnormalities, altered cell geometry is manifested in alteration of S/V ratio and results in decreased cellular deformability, compromised red cell function, osmotic fragility and lessened survival of the RBC. This is the case of sickle cell disease (SC), hereditary spherocytosis (HS), hereditary elliptocytosis (HE),

[5] This section is based on *Pathobiology of Human Disease* (Linda M. Mcmanus, 2014) and *Red cell membrane : past, present and future* (Mohandas and Gallagher, 2008)

hereditary stomatocytosis (HSt), thalassemia or malaria(Allard et al., 1978; Mokken et al., 1992).

The Ektacytometer is useful—for both diagnosis and medical follow up treatment—in RBC abnormalities characterized by decreased cell deformability.

Ektacytometer shear scan curves show abnormal deformability, but they give similar curves for several pathologies, therefore they do not reveal enough information for specific differential diagnoses. Osmotic scan curves give distinctive curves for different pathologies. Some examples are found in Figure 3. Extensive information for the interpretation of osmotic scan Ektacytometry curves can be found in (Clark et al., 1983; Johnson and Ravindranath, 1996; King et al., 2015; Mohandas et al., 1980)

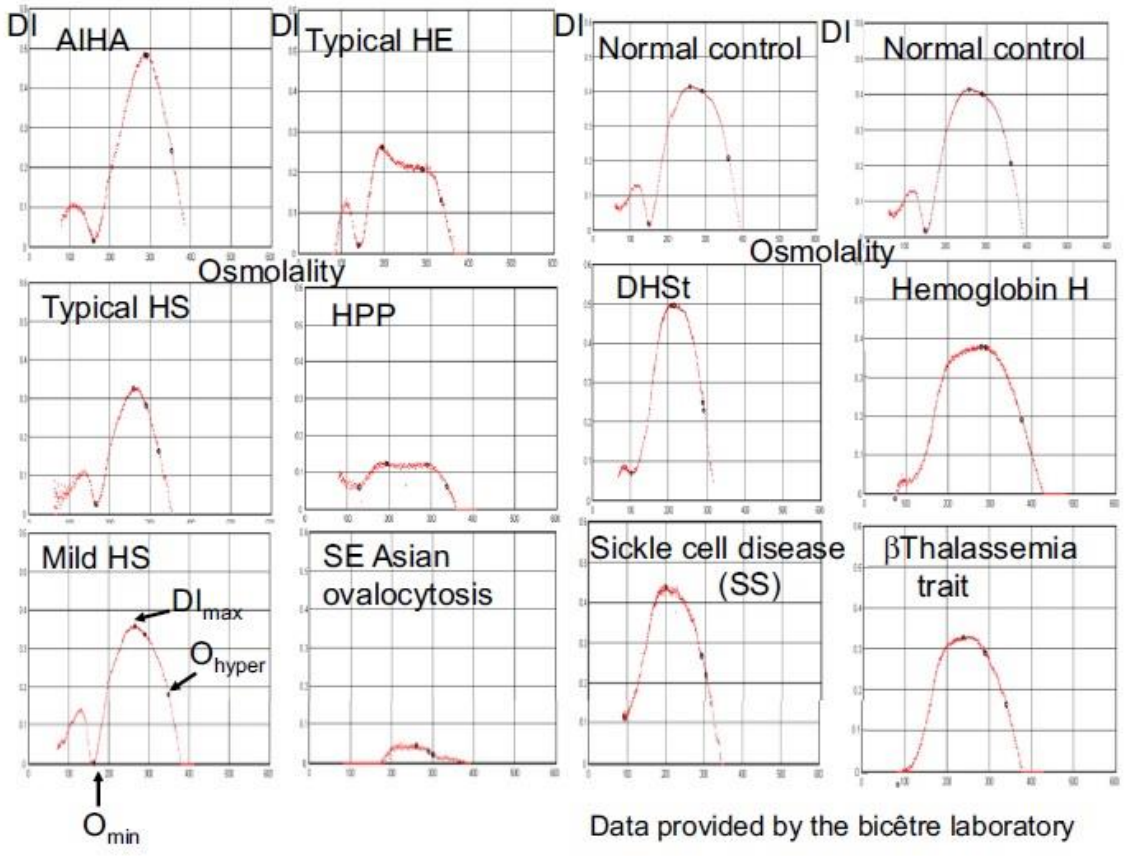

Figure 3: Osmotic deformability profiles of red cells from normal control, AIHA, HS, HE/HPP, DHSt, and hemoglobinopathies. From (King et al., 2015)

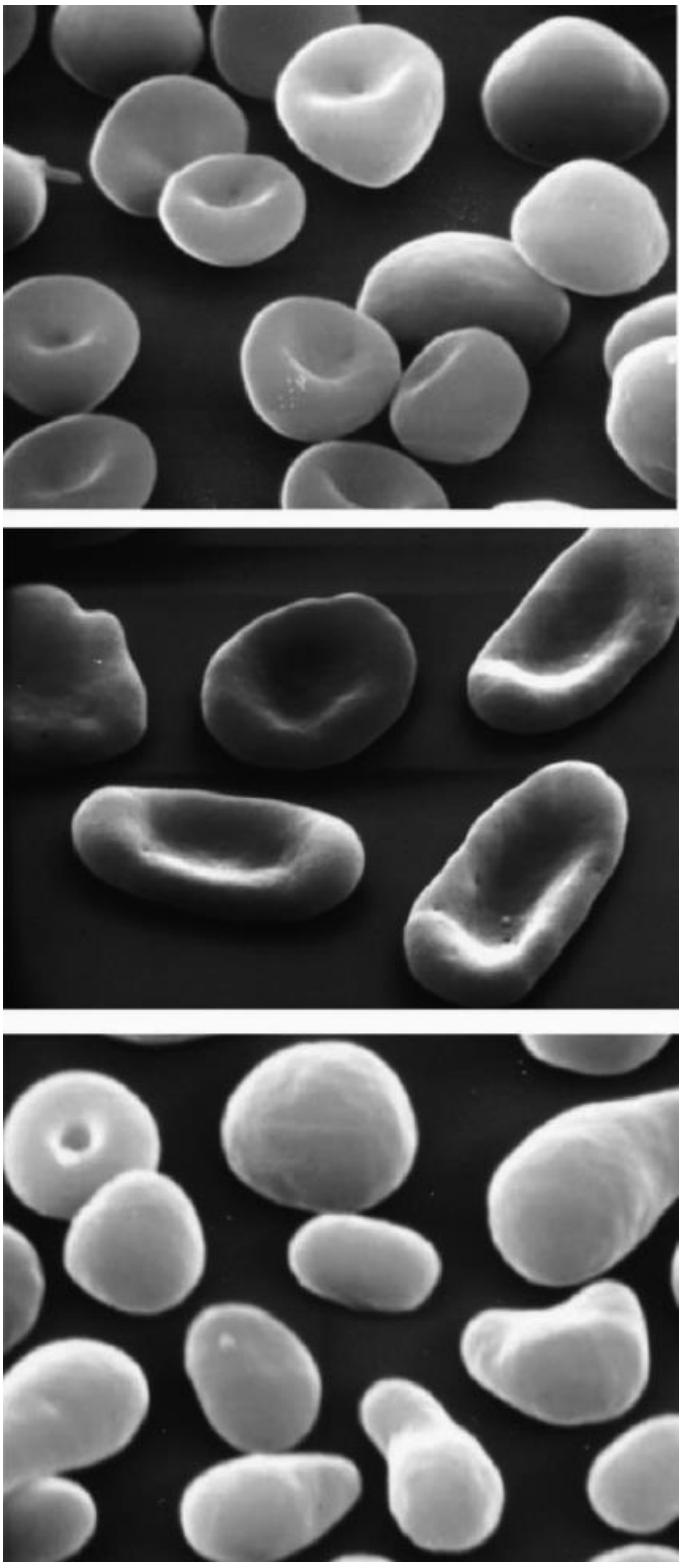

Figure 4: Images of pathologic RBC. Hereditary spherocytosis (top panel), nonhemolitic Hereditary elliptocytosis (middle panel) and fragmented red cells in hemolytic HE (bottom panel) from (Mohandas and Gallagher, 2008)

1.5.1 Hereditary Spherocytosis (HS)

Hereditary Spherocytosis, affects all ethnic groups but is more common in people of northern European ancestry (2 in 10000)(Eber and Lux, 2004). Clinical manifestations of HS are highly variable ranging from mild to very severe anemia. A common feature of all forms of HS is loss of RBC membrane surface area resulting in change of cell shape from discocytes to stomatocytes to spherocytes (Figure 4). Reduction in membrane surface results in reduced deformability and inability to effectively traverse the spleen, which sequesters and removes spherocytes from circulation. Splenectomy reduces the severity of anemia by increasing the life span of spherocytic red cells.

1.5.2 Hereditary Elliptocytosis (HE)

Although HE has a worldwide distribution, it's more common in Malaria endemic regions with prevalence between 0.6% to 1.6% in West Africa (Dhermy et al., 2007). Most cases of HE are heterozygous and hence asymptomatic. Around 10% of patients, mostly homozygous for HE variants, experience mild to severe anemia, including the severe variant hereditary pyropoikilocytosis (HPP). A mechanically unstable membrane results in progressive loss of membrane surface area and transformation of cell shape from discocyte to elliptocyte, as a function of time in the circulation (Figure 4). As with HS, splenectomy increases the life span of fragmented red cells and thus reduces the severity of anemia.

1.5.3 Hereditary Ovalocytosis (SAO)

Rigid membrane is a distinguishing feature of hereditary ovalocytosis (Mohandas et al., 1984). The geographic distribution is highly correlated to Malaria infected zones mainly in South East Asia. SAO prevalence can reach 6.6 to 20.9% in several groups of Malayan aborigines (Amato and Booth,1977). Despite a marked increase in cell membrane rigidity (4 to 8 times less elastic than normal membrane as assessed by Ektacytometry and micropipette aspiration) most affected people experience minimal hemolysis. Except for one reported case (Picard et al., 2014) the

homozygous form has not been described and is thought to be lethal (Liu et al., 1994).

1.5.4 Hereditary Stomatocytosis (HSt)

HSt is a rare hemolytic anemia, characterized by RBC taking a form of a cup with a mouth shape (stoma) area. Several varieties of HSt were identified, with two main ones associated with the status of hydration of the cell. The impact on osmotic gradient ektacytometry curves is a curve shifted to the left (DHSt) or to the right (OHSt) of a normal deformability curve.

1.5.4.1 Hereditary Xerocytosis (also called DHSt Dehydrated Hereditary Stomatocytosis)

DHSt is the least severe but the more common of the HSt conditions. Its prevalence is estimated as 1 patient out of 50,000 individuals contrary to OHSt with 1 patient per 100,000 individuals (Hereditary Stomatocytosis - Anaemias - Enerca, *European Network for Rare and Congenital Anaemias*). Due to dehydration, the cell MCHC and cytoplasmic viscosity are increased. Cell dehydration has a marginal effect on survival of DHSt cells. DHSt is therefore associated with well compensated anemia with a mild to moderately enlarged spleen.

1.5.4.2 Overhydrated hereditary Stomatocytosis (OHSt)

OHSt is a rare disorder where RBC over hydration results in increased cell volume with no increase in surface area. Unlike in DHSt, the cell survival in OHSt is significantly compromised leading to moderately severe to severe anemia. Cells with increased sphericity are sequestered by the spleen. However while splenectomy is beneficial in management of HS and HE, it is completely contraindicated in both types of hereditary stomatocytosis because of an increased risk of venous thromboembolic complications. Osmotic scan ektacytometry is very important in providing a proper diagnosis of HSt.

1.5.5 Sickle cell disease

Sickle cell disease (SCD) or sickle cell anemia is an inherited blood disorder characterized by abnormal mechanical and rheological behavior of RBCs. SCD is caused by sickle hemoglobin (HbS), a variant hemoglobin (Hb) molecule resulting from a point mutation in the β-globin gene. Upon deoxygenation, HbS polymerizes or self-assembles inside the RBC and significantly alters and damages the cytoskeleton and membrane cortex, resulting in a sickle-shaped RBC. This sickle RBC has decreased deformability, causing abnormal rheology in sickle-cell blood and eventually various complications of SCD: painfull crisis, ischemia and organ damage can result when microcirculation is impeded due to the poorly deformable RBCs. As a result of these complications, a study conducted in the United States during the 1980s showed a decrease of roughly 25 to 30 years in life expectancy of sickle cell anemia patients (Platt et al., 1994). Since the last two decades, new treatments improve life expectancy.

1.6 Aim, objectives and Dissertation Overview

The aim of this dissertation is to explore the theoretical basis, build a prototype and produce a proof of concept for a new diagnostic instrument of hereditary RBC disorders, based on a microfluidic method.

In order to achieve this aim I explored the following objectives:

1. Describe the current state-of-the-art in the field, including research and commercial applications, so as to place my work in the context of existing technology. This is described in chapter 2 “State of the Art”.
2. Study the theoretical difference between the current method used in osmolality gradient Ektacytometry diagnosis based on rotating concentric cylinders, and my proposed microfluidic method. This is explored in

chapter 3 “Comparison between Pressure and Shear driven flows for Osmolality Gradient Ektacytometry”.

3. Compare the two methods of measurement of deformability of RBCs that are used in Ektacytometry: photodetectors and a camera. The comparison allowed me to choose the preferred method to employ in the current work. This comparison is done in chapter 4 “Comparison between a camera and a four quadrant detector, in the measurement of red blood cell deformability as a function of osmolality”.

4. Model the hydraulic system in order to evaluate flow rate magnitudes necessary to achieve proper osmolality increasing solution for Osmoscan curves. This is explored in chapter 5 “Modelling and Mathematical analysis”.

5. Design and build a prototype, based on knowledge acquired in previous chapters, and compare measurement results with an Ektacytometer using rotating cylinders. This is explored in chapter 6 “Design and Proof of principle”.

6. Conclusions from this study are presented in chapter 7.

2 STATE OF THE ART

2.1 RBC Deformability Measurement Techniques[6]

2.1.1 Introduction

The RBC Deformability measurement techniques can be categorized in two main groups: Measurement of cell population deformability and measurement of individual cell deformability[7]. Techniques used on individual cells are mostly used in research and are rarely suitable for clinical use.

2.1.2 Measurement techniques of single cells

2.1.2.1 Micropipette Aspiration (MA)

The micropipette aspiration technique was first developed by Mitchinson and Swann in 1954 as an instrument they called "Cell Elastimeter" (Mitchison and

[6] This section is based on the following sources: (Musielak, 2009) (Baskurt et al., 2009) (Dobbe, 2002) (Kim Y. et al., 2012) (Kim J. et al., 2015)

[7] Sometimes a different categorisation is used: flow systems and single-cell systems

Swann, 1954). The technique was later applied to RBC by Rand and Burton (Rand and Burton, 1964) and was introduced as a laboratory clinical tool in the early 1970's by Evans (Evans, 1973). The RBC is aspirated by a glass micropipette of internal diameter between 1 to 3 μm to which a negative pressure is applied. The length of the aspirated part of the cell depends on the amount and duration of the suction pressure, the micropipette diameter and the cell properties. There are three phases in this aspiration process. First a small part of the cell membrane produces a tongue, inside the micropipette, of an equibiaxial form (Figure 5). Increased aspiration pressure results in a longer aspirated section that starts to buckle. At a certain point, the aspiration pressure reaches a threshold level causing the cell to flow inside the tube. In some cases the cells are osmotically swollen into a nearly spherical form prior to the aspiration. Comparing their aspiration rate to cells in isotonic conditions can give supplementary information (Hochmuth, 2000)

The instrument consists of three parts: a pressure controller, a chamber where the cells are aspirated by the micropipette and a microscope.

Different mechanical properties of the cell can be determined by various measurements:

- Time required for the aspirated part of the cell to withdraw and return to its original shape after release of pressure. The shape recovery time constant depends primarily on the membrane viscosity and its elasticity, cytoplasm viscosity and cell thickness.
- Pressure that is required to aspirate a length of the cell equal to the radius of the pipette.
- Ratio of the aspirated length to the micropipette radius at a given pressure.
- Critical pressure above which the cell flows inside the micropipette.

The MA technique allows measurement of different mechanical properties of individual cells such as membrane viscosity, elasticity and bending modulus (Hochmuth et al., 1979) (Artmann et al., 1998) (Brooks and Evans, 1987) (Evans,

1983) (Chien et al., 1978). It is a useful research tool, but it is not practical for clinical use due to its time consuming procedure. Moreover, due to numerous approximations, results need validation by other measurement methods.

Attempts for the automation of an MA system have not found a commercial application (Heinrich and Rawicz, 2005) (Shojaei-Baghini et al., 2013).

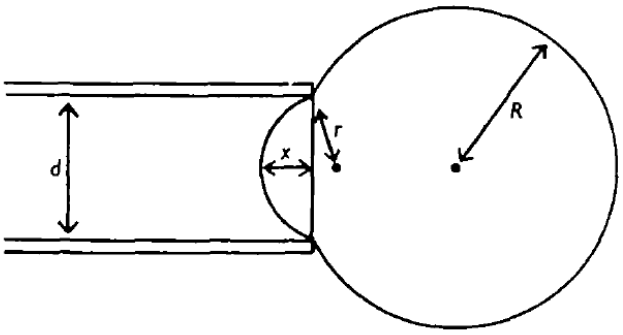

Figure 5: Deformation of a cell due to negative pressure in a micropipette. From (Mitchison and Swann, 1954)

2.1.2.2 Rheoscopy

This method was introduced in 1969 (Schmid-Schoenbein et al., 1969) for the measurement of single red blood cell deformability

A Rheoscope consists of a rheological chamber (flow system) placed on an inverted microscope stage, and equipped with means for optical measurement.

One variant of rheoscope uses a transparent cone-plate viscometer as the rheological chamber. Cells suspended in the viscometer are subjected to a constant shear and are photographed through a microscope (Figure 6). Photographic images are measured and cell elongation (E) is calculated from the length and width of the ellipsoid image.

Elongation is defined as *E= (L-W)/(L+W)*. Shear force acting on the RBC can be varied either by changing the viscosity of the suspending fluid or the speed of rotation of the cone. The effects on cell dimensions can be directly measured.

A microfluidic Rheoscope is obtained by using a flow channel as the flow system (Zhao et al., 2006).

Several versions of a Rheoscope whereby the deformation is measured automatically rather than directly observed, were proposed using video or high speed CCD cameras. One such design is based on rotating parallel plates establishing the shearing system, and determination of cell deformability by an image processing algorithm (Dobbe et al., 2002). Another design is based on a microfluidic channel (Bransky et al., 2006). The automated versions of a Rheoscope can yield histograms for cell deformability and thus give information about deformability distribution of RBC population. However, the technology is still limited by time consuming computer processing and by inaccuracies in image interpretations for complex geometrical forms.

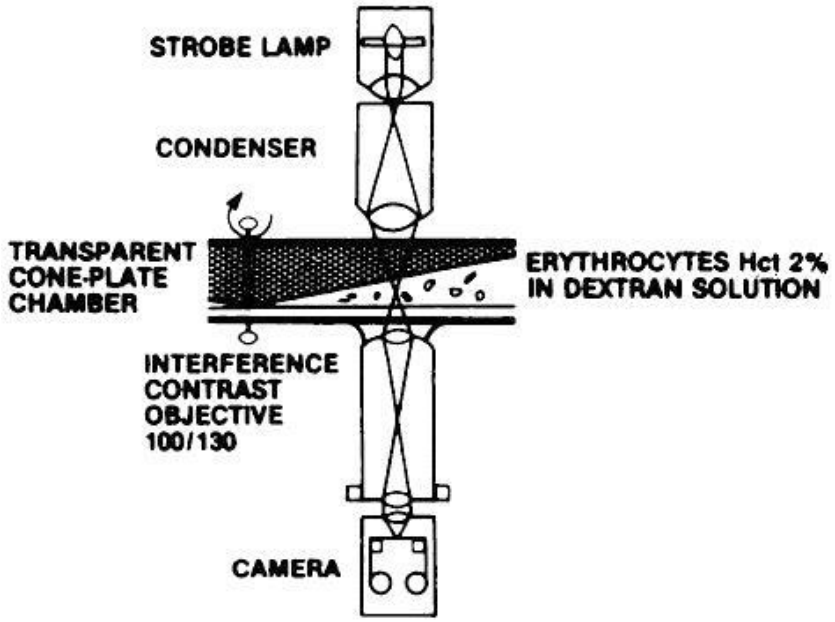

Figure 6: Schematic diagram of a Rheoscope (Groner et al., 1980)

2.1.2.3 Optical Tweezers (OT)

The founding principles for the optical tweezers, also called «laser trapping», were first discovered by Arthur Ashkin in 1970 (Ashkin, 1970). He showed that microscopic dielectric particles can be lifted and held, both in air and water, by highly focused optical beams (Ashkin and Dziedzic, 1971). However it was only in 1986 that these beams were employed in an instrument (Ashkin et al., 1986) The technique was later labeled « optical tweezers » since it allows picking up and moving small particles using an optical beam. The physical principle is based on a balance of two types of optical forces, created by the interaction with a small spherical dielectric particle. These forces consist of the light scattering forces acting along the wave propagation direction and gradient electric forces acting in a lateral direction towards the beam center (Figure 7). The magnitude of these forces is of the order of pico Newtons (pN).

In the case of transparent dielectric beads whose diameter is greater than the wavelength of the laser beam, the forces can be explained by the effect of refracted rays. The refracted rays exit the bead in a direction different from which they entered. This indicates that the momentum of light has changed. An opposite momentum change on the particle is created according to conservation of linear momentum. A detailed explanation of the Physical forces involved, using two distinct approaches, ray optics and electric field associated with the light, can be found in Contemporary Physics by Justin E. Molloy and Miles J Pudgett (Molloy and Padgett, 2002).

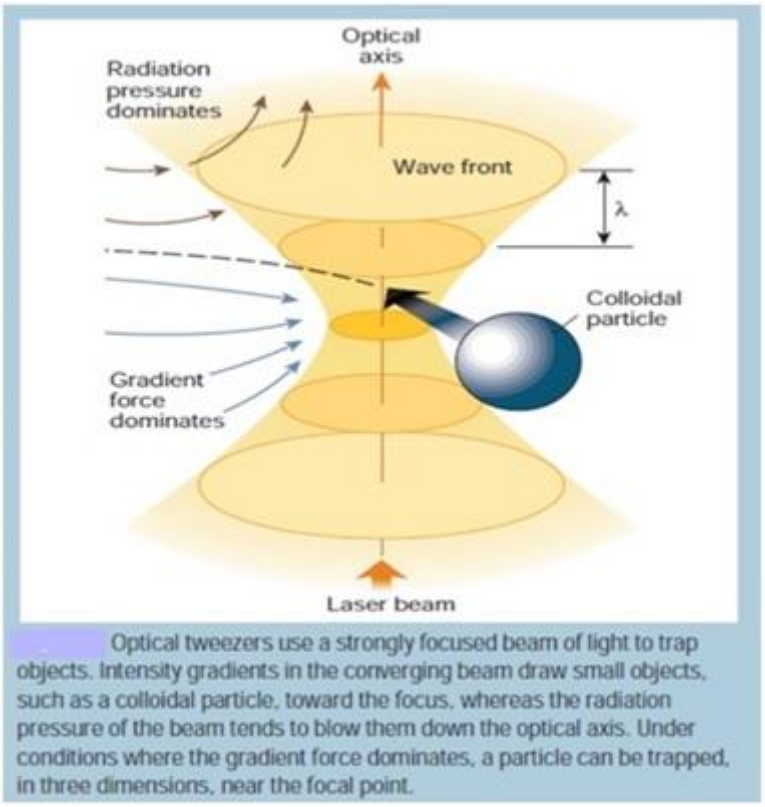

Figure 7: Optical tweezers forces. From (Grier, 2003)

OT can be constructed by modifying an inverted microscope. A typical setup is shown in Figure 8.

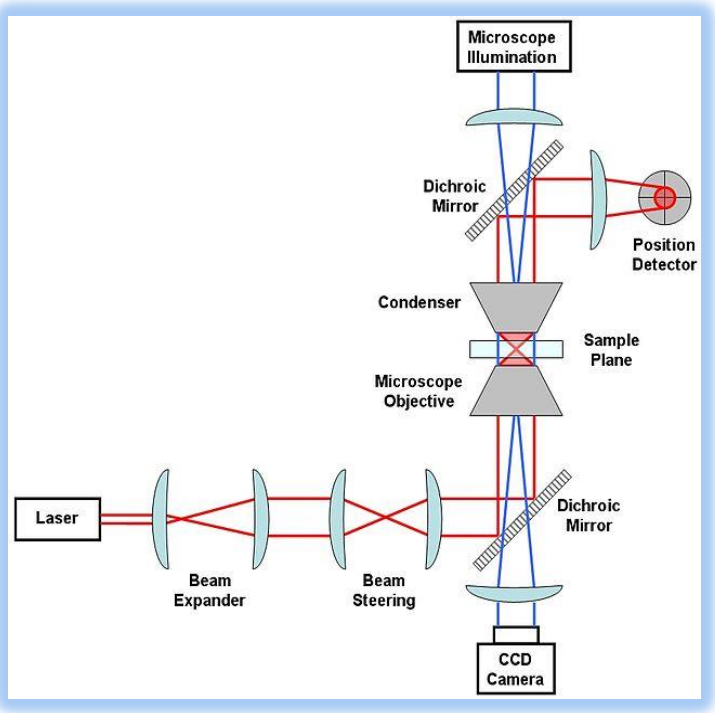

Figure 8: A typical setup of Optical tweezers. Image courtesy of Wikipedia user RockyRaccoon (Public Domain) (http://en.wikipedia.org/wiki/File:Generic_Optical_Tweezer_Diagram.jpg accessed 10 April 2015)

OT have been used to measure RBC deformability (Hénon et al., 1999) (Dao et al., 2003). An Nd:YAG laser source of 1064 nm wavelength is used because of the low absorption coefficient at this wavelength. The beam intensity is up to a few Watts and the light absorption can cause damage to the trapped cell by heating (Block, 1992). Two Microspheres are attached to the cell opposite sides. One of the beads is also attached to the microscope slide which is fixed to the stage. The other bead is lifted slightly by laser trapping. The stage is shifted in such a way that the cell is stretched (Figure 9) until it escapes from the trap. The stage shift is measured for several laser intensities. In this way the maximum elongation of the cell can be measured with respect to a calibrated trapping force. It is also possible to obtain projected dimensions with a CCD camera. With an applied force of 193 pN on a normal RBC an elongation of 50% and a reduction of the short axis by 40% were

observed (Mills et al., 2004). From its dimensional variation in response to optical force, using a mathematical model, the shear modulus of a normal RBC was calculated to be approximately 10μN/m, (Dao et al., 2003).

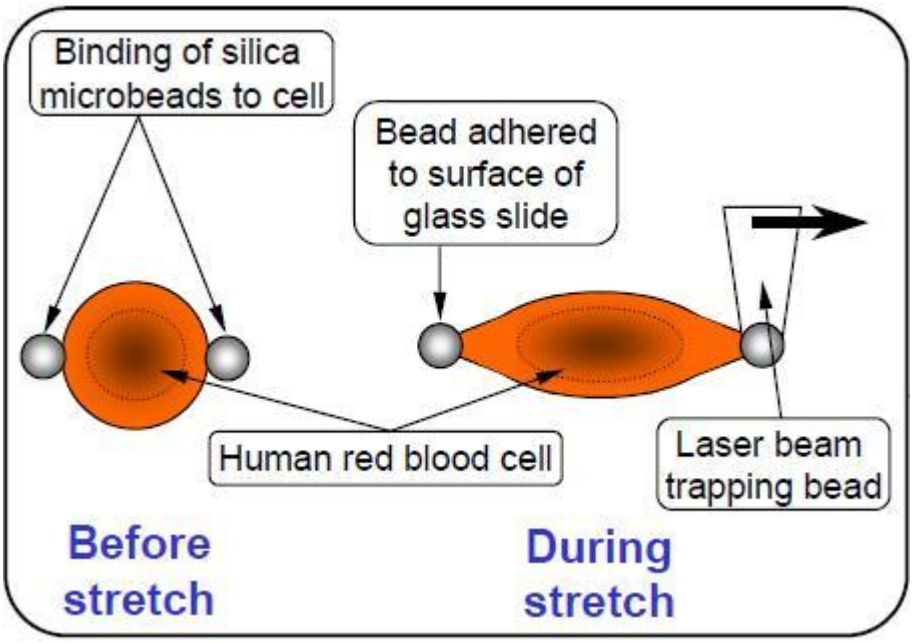

Figure 9: A single beam RBC laser trapping technique (from Dao et al., 2003)

2.1.2.4 Atomic Force Microscopy (AFM)

Atomic Force Microscopy (AFM) is a scanning technique providing images of surfaces on a sub nanometer (atomic) scale. It can also measure surface forces (Binnig et al., 1986). A probe composed of a spring arm and a microscopic tip moves across the surface having a physical contact with it. The vertical displacement of the arm caused by the examined surface is amplified by a laser beam and a quadrant photo detector. The quadrant detector measures very small changes in laser beam position reflected by the cantilever arm surface. (Figure 10) The signal from the quadrant photo detector is used as a feedback for the control of the microscope

stage piezoelectric scanner. This way the tip follows the surface changes without breaking. The displacement of the tip is recorded and used to create the surface image. Several variants to the contact imaging mode are used: a tapping mode or a non-contact mode. Other deflection measurement methods are used such as piezoelectric detection, laser Doppler vibrometry, optical interferometry and capacitive detection.

AFM can also be used in order to measure individual RBC deformability. For this purpose a parabolic or spherical tip is used. A force on the order of several nN is applied to the tip and the stage displacement is first measured against a hard material and then against the cell. The Young's modulus E is calculated from the indentation relative to the applied force taking into account the tip radius (Weisenhorn et al., 1993).

The principle is based on an early instrument called Cell Poker (McConnaughey and Petersen, 1980).

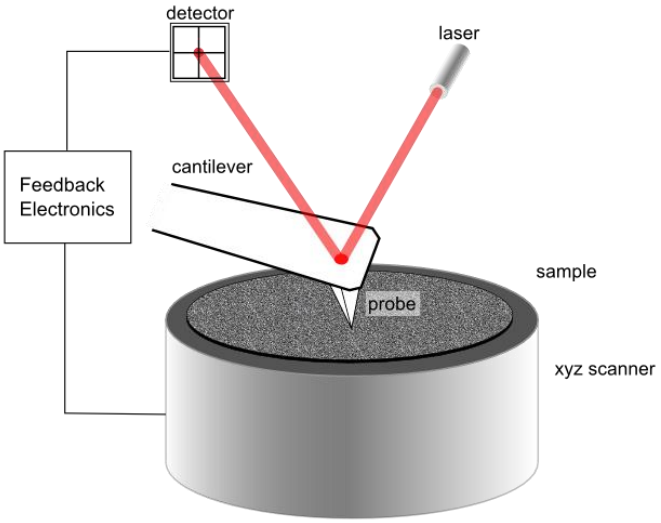

Figure 10: Schematics of AFM operation.

From (Eaton and West, 2010)

2.1.2.5 Magnetic Twisting Cytometry

Magnetic Twisting Cytometry (MTC) applies a magnetic field of a precise magnitude to ferrimagnetic microbeads attached to the cell membrane. The resulting displacement of the microbeads is measured and gives information on the cell mechanical properties (Wang et al., 1993). Either a static or an oscillating magnetic field is used and the microbeads displacement is recorded by a CCD camera. The displacement is then computed from the image and the magnitude of rotation and translation is presented as a function of the applied torque (Figure 11).

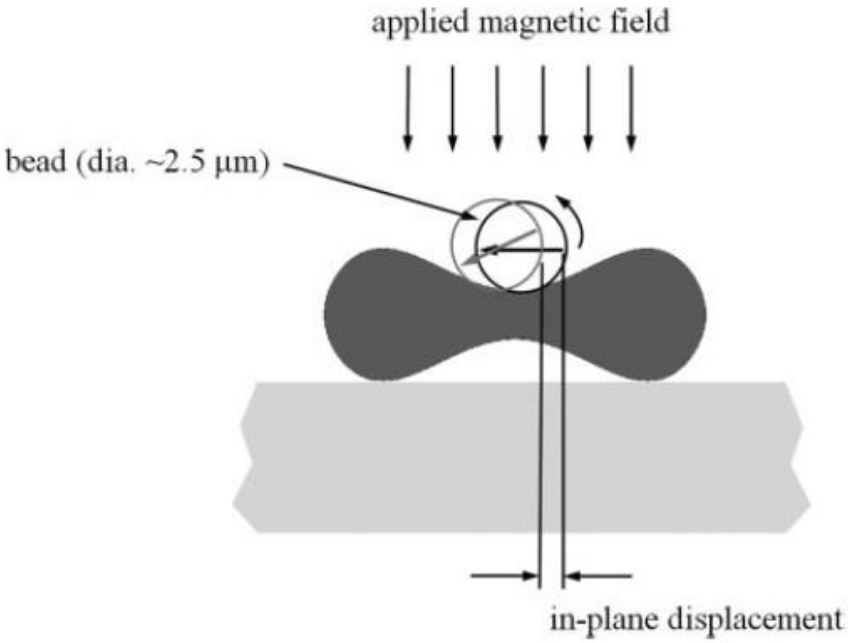

Figure 11: Schematic of RBC optical magnetic twisting cytometry (OMTC) tests. A magnetic field is applied normal to the magnetization of the bead to generate a torque on the bound bead. The applied torque deforms the cell, which causes the bead to rotate and translate. The in-plane displacement of the bead is tracked optically. From (Puig-de-Morales-Marinkovic et al., 2007)

The advantage of this method is that it allows the measurement of both static and dynamic (time dependent) deformability. Applying oscillating magnetic force at

different frequencies can give additional information for the cell deformability properties (Puig-de-Morales-Marinkovic et al., 2007).

2.1.2.6 Quantitative phase imaging

Quantitative phase imaging (QPI) has the potential of revealing unique cellular information. Unlike other measurement techniques described in this chapter, QPI does not employ an external force on the cell, but rather measures intrinsic nanoscale fluctuations (also called flickering) in cell membrane and uses them as an indicator of linear mechanical response, correlated to RBC deformability (Brochard and Lennon, 1975; Popescu et al., 2006b). Measurement, by QPI, of linear response properties of the RBC membrane at varying states of osmotic stress makes it possible to experimentally probe the nonlinear elastic membrane response (Park et al., 2011).

QPI is suitable for RBC studying since the cell is thin, nearly transparent and weakly absorbs or scatters light. Therefore, light amplitude information does not provide a good image contrast. The contrast information is obtained by measuring the significant phase delay on top of light intensity. QPI offers quantitative measures of thickness and refractive index of the cell. Since the actual phase of light field varies extremely fast (femtoseconds scale), it is only possible to experimentally access phase difference between fields by interferometry. Several two-dimensional and three dimensional QPI methods exist differing mainly by the interferometric experimental technic employed. A detailed description of these technics as well as the theoretical and historical context of interferometry is described in (Lee et al., 2013; Mir et al., 2012). A diagrammatic example of a QPI technique, called White-Light Diffraction Phase Microscopy (wDPM), can be found in Figure 12. Images obtained by another QPI technique, Fourier Phase Microscopy (FPM), are shown in Figure 13.

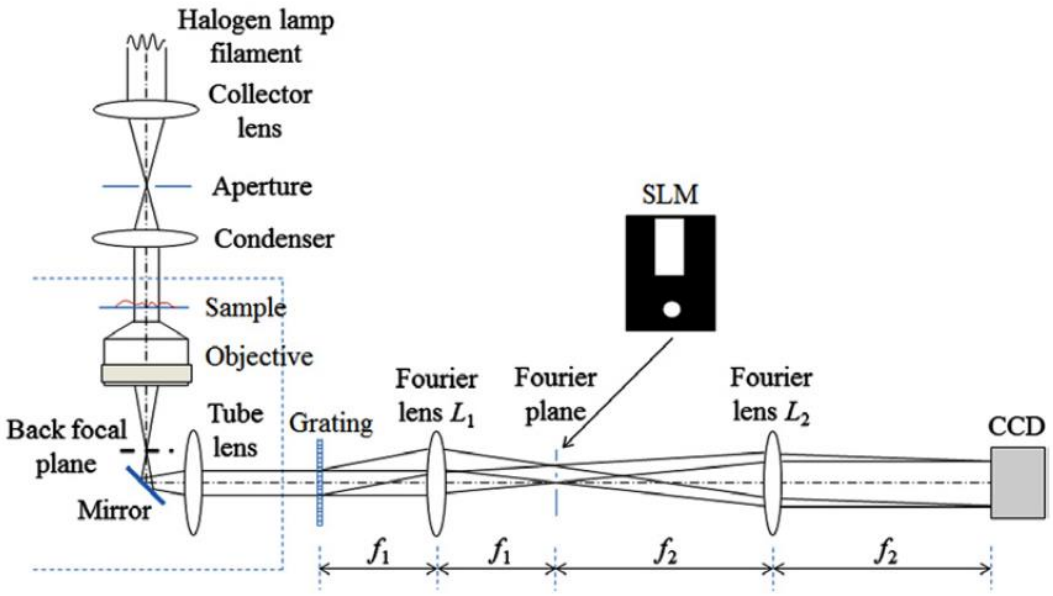

Figure 12: Experimental setup for wDPM. From (Bhaduri et al., 2012)

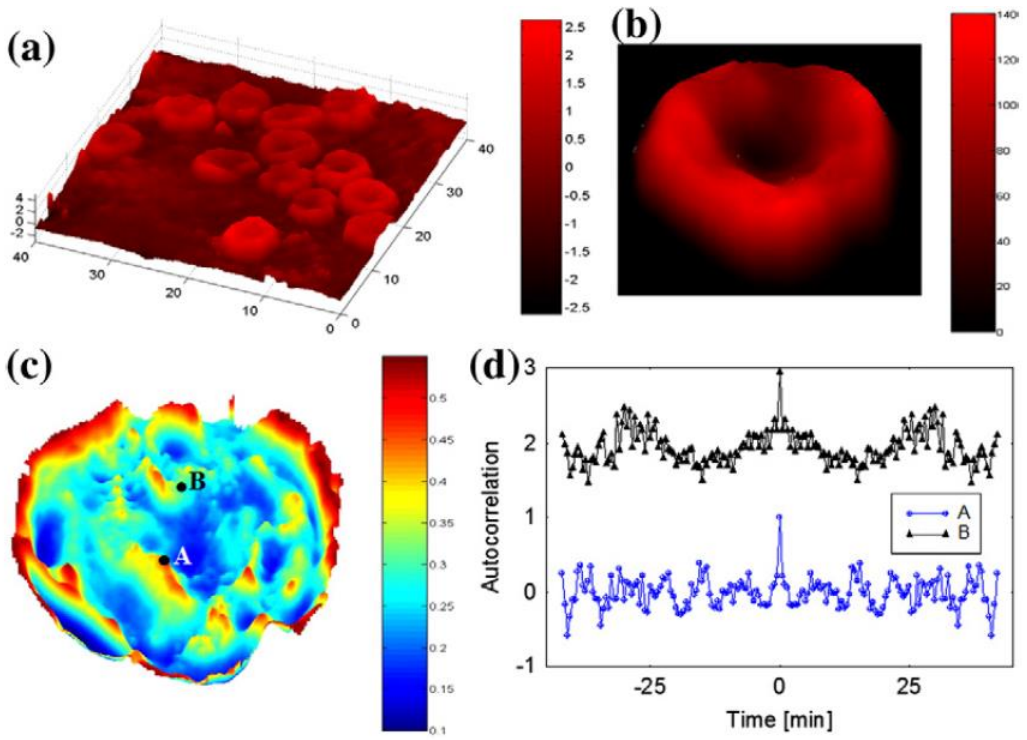

Figure 13: (a) QPI of blood smear using FPM; the color bar indicates thickness in microns. (b) Surface image of a single red blood cell; the color bar shows the phase shift in nm. (c) Average frequency map of the cell, calculated from the FPM time-lapse dataset; the color bar has units of min−1. (d) Normalized autocorrelations associated with temporal fluctuations of the points shown in (c). The top curve was shifted for better visibility. From (Popescu et al., 2006a)

Some other QPI methods were used for RBC studies. Diffraction phase microscopy (DPM) has been used to measure and compare the shear moduli of healthy RBCs as well as those invaded by malaria organisms (Plasmodium falciparum)(Park et al., 2008). Common-path diffraction optical tomography (cDOT) has been used to study blood storage effect on RBC surface area and deformability (Park et al., 2016). Images obtained by this technique are shown in Figure 14.

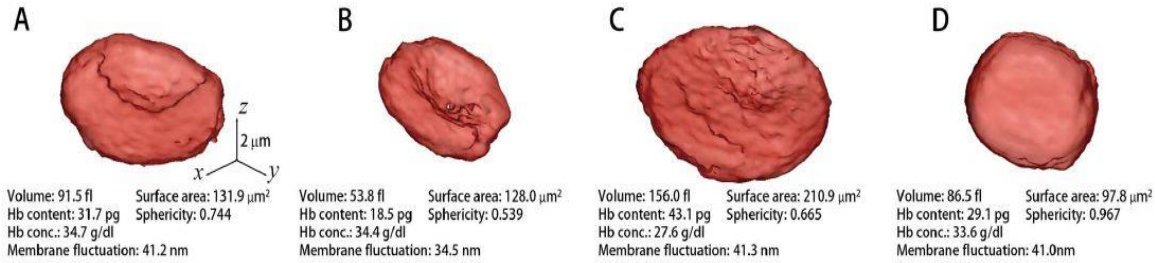

Figure 14: Images obtained by cDOT, QPI method. 3D rendered iso-surfaces of refractive index maps of individual RBCs from (A) healthy, (B) iron deficiency anemia, (C) reticulocyte, and (D) hereditary spherocytosis, red blood cells (Kim et al., 2014)

2.1.3 Measurement techniques of RBC populations

2.1.3.1 Filtration

Filtration is a simple technique, where whole blood or diluted blood suspension is pressured against a filter membrane with pores diameter inferior to the cell diameter. Only deformable cells can pass through the filter. A filter of 5 μm pores is normally used with gravity effect or a pressure gradient applied across the membrane. Either a positive pressure (Schmid-Schönbein et al., 1973) or a negative pressure (Reid et al., 1976) can be used. The filterability index is given by the filtered volume per minute. This technique is very frequently used because of its low cost and simplicity. However, it has several disadvantages as results depend on cell size and the occlusion of pores by white blood cells. If washed erythrocytes are used, the process not only risks removing non deformable RBCs but it is also time consuming (Stuart, 1985). Small non deformable cells can pass through the filter

pores and are considered deformable. It also has a poor reproducibility and impossibility of detecting minor deformability due to lack of filters homogeneity.

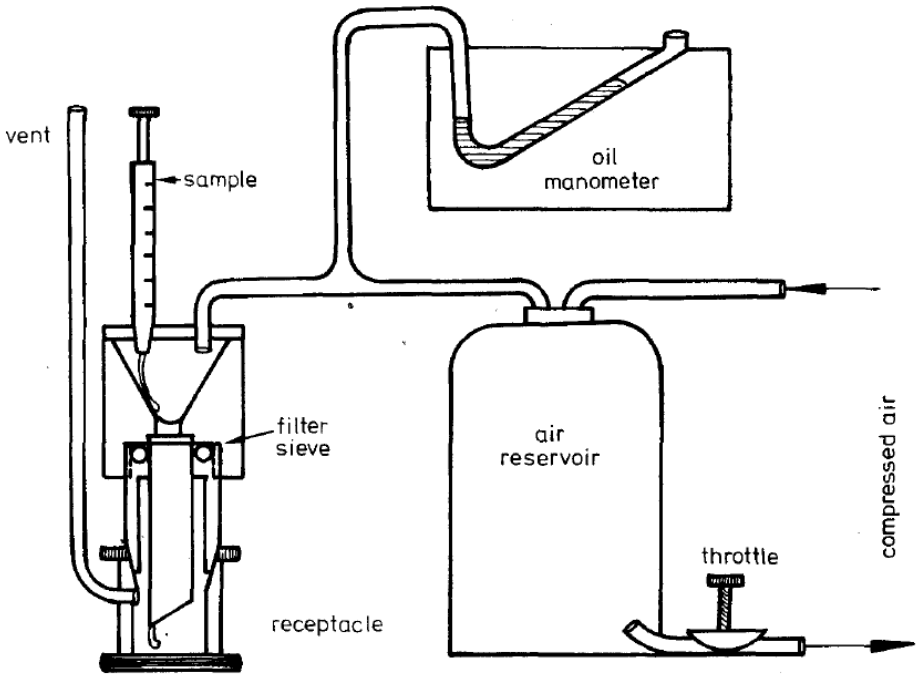

Figure 15: Schematic representation of the filtration apparatus.

From (Schmid-Schönbein et al., 1973)

2.1.3.2 Cell Transit Analyzer

The cell transit analyzer is similar to filtration but allows for an automatic measurement of a large number of individual cells. A diluted suspension of RBC is put under pressure against a membrane with several dozens of 3µm to 6µm cylindrical pores. A pure physiological buffer is placed on the other side of the membrane. Two electrodes are placed in the reservoirs on both sides of the membrane. Conductance is measured between the electrodes using a 100 KHz signal. The passage of a non-conductive cell through a pore results in small perturbation in the overall conductivity. Counting the generated resulting pulses

and analyzing their duration and rise time, gives indication of cell deformability (Koutsouris et al., 1987). The measurement principle is an extension of the Coulter principle (Frank and Hochmuth, 1987).

The advantage of this technique is that it allows for the measurement of a large number of individual cells, giving information on deformability distribution and detecting subpopulations with different ability to deform. However, this technique, like the filtration technique is unable to measure badly non deformable cells since they occlude the pores. On the other hand, small non deformable cells are counted as deformable. Using the conductivity perturbation pulse length and intensity as an indication of cell deformability is problematic since it is influenced by cell size and by the form the cell obtains while passing through the pore. Some deformable cells obtain a cup shape occluding the pore and some are folded leaving a slit that allows a path for electrical current (Reinhart et al., 1991).

2.1.3.3 Ektacytometry

Ektacytometry is an optical deformability measurement technique of RBC population, originally developed in France by Bessis in the 1970s (Bessis and Mohandas, 1975). In this technique a highly diluted red cell suspension is exposed to laser light and the diffraction pattern created by the laser beam, going through the suspension, is measured. When RBCs suspended in a high viscosity liquid, are exposed to a shear stress in a flow, they deform, which is in turn reflected by a change in the diffraction pattern of the laser beam. The diffracted pattern has the same eccentricity as the average of the exposed cells but is rotated by 90°. The measurement of the diffraction pattern eccentricity therefore provides a quantitative measure for the average RBC deformability. Two methods exist for the evaluation of the diffraction pattern elongation: Measuring light intensity with photodiodes at defined locations or using a camera with image analysis (Finkelstein et al., 2013). The results are expressed as elongation index (EI) or deformation index

(DI) both reflect the aspect ratio of the elliptical diffraction pattern and increase with cell deformability (*see section* 4.3 Equation 24).

There are three different technics for RBC shearing: cylindrical Couette flow (rotating cylinders), planar rotational Couette flow (parallel plates) and plane Poiseuille flow (microfluidic channel).

In ektacytometry, two main modes are used to characterize RBC deformability: Shear Scan where the cells are kept in a constant osmolality and an increasing shear stress is applied (Figure 16), and Osmotic gradient (OsmoScan) where shear stress is kept constant, but cells are mixed in a medium where osmolality is gradually increased (Figure 17).

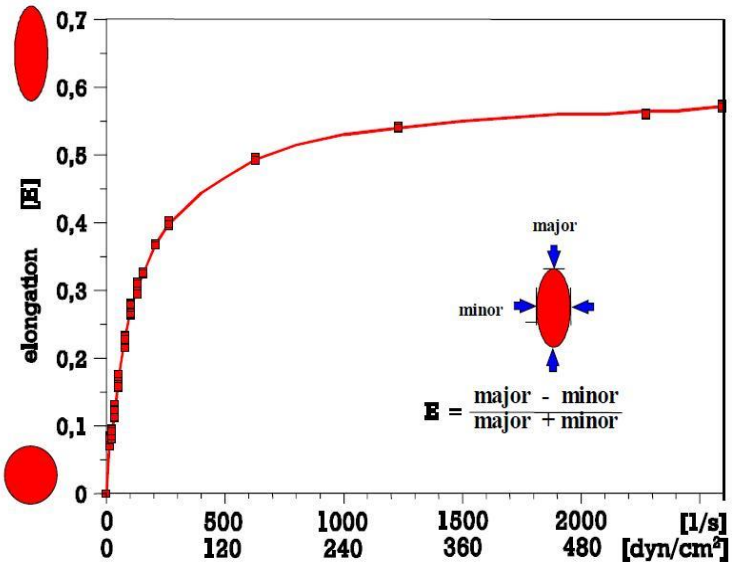

Figure 16: Typical shear scan deformability curve. From (Bayer et al., 1994)

The advantage of Osmoscan over Shear scan is that it allows not only to measure the deformability of the cells but also to attribute low deformability to specific cell defaults such as cell membrane or intracellular viscosity (Clark et al., 1983; Johnson and Ravindranath, 1996). Typical osmoscan curves for several RBC disorders are shown in Figure 17.

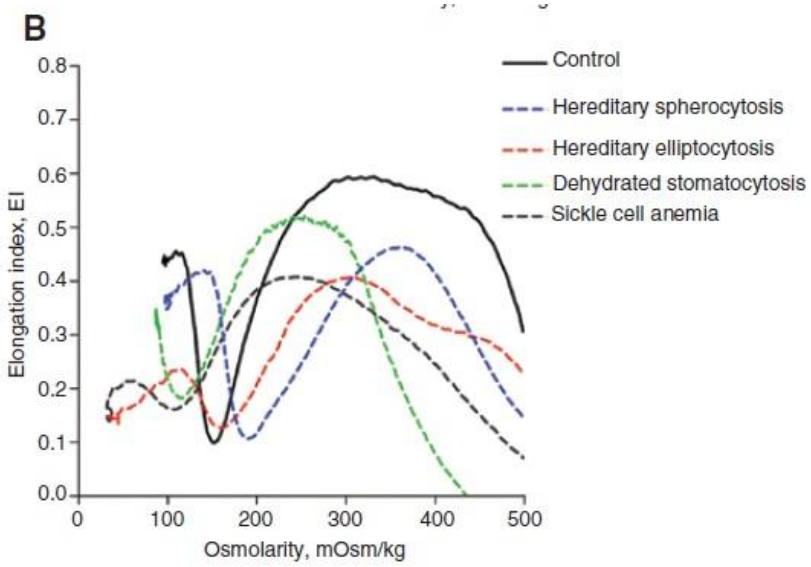

Figure 17: Typical osmoscan curves. from (Lazarova et al., 2017).

Ektacytometry is a very practical laboratory technic, allowing, in an automated quick experiment, to evaluate the mean deformability of RBC population. However, it doesn't give detailed information regarding the distribution of the deformability in a mixed cell population.

Several geometries were used as shearing techniques: Couette cylinders, parallel plates, and flow channel. These geometries are described in detail in chapter 3.

Since my work is dedicated to the design and fabrication of a prototype for a new Ekacytometer, I review hereafter, the current available commercial Ektacytometers.

2.2 Ektacytometer Commercial Applications

The first prototype of an Ektacytometer was developed in Bicêtre hospital near Paris, by Bessis and Mohandas in the early nineteen seventies, and had a stationary internal cylinder and a rotating external cylinder. Nearly twenty years later a commercially available Ektacytometer was produced by Technicon (*Technicon* Instruments, Tarrytown, NY, USA). It was very similar to the Bicêtre hospital prototype but had an internal rotating cylinder and an external stationary one. Several dozens of them were sold but their production was stopped several years

later. There are still a few functioning units in some hospitals in France and in the USA.

Currently, there exist three commercially-available ektacytometers having different shearing geometries: Couette cylinders (Lorca), rotating parallel plates (Rheodyn SSD) and a flow channel (RheoScan-D). All three allow only shear scan and a comparison study was conducted between them (Oguz K Baskurt, 2009). A recent variant of Lorca, called Lorrca MaxSis based on Couette cylinders shearing technique, allows osmotic gradient ektacytometry.

2.2.1 Technicon

(*Technicon* Instruments, Tarrytown, NY, USA)

The Technicon Ektacytometer, built and commercialized in the early 1990s, comprises a shearing system based on two concentric transparent cylinders having an inner cylinder diameter of 50.7mm and a gap of 0.5mm. The inner cylinder rotates at controlled speeds between 0 to 255 RPM while the outer cylinder is stationary. The sample preparation unit is comprises a steer tank and peristaltic pumps where blood is highly diluted with a Polyvinylpyrrolidone (PVP) transparent solution of 20 cP viscosity. The sample is pumped into the space between the cylinders and sheared by the inner cylinder rotation. A HeNe laser source of 1mW beam of 632.8nm wavelength and 1mm diameter crosses the sheared blood sample. The diffracted laser pattern is projected on a mask containing four holes nearly equidistant from the beam center (there is a slight difference between the distance of the two vertical wholes and the two horizontal wholes in order to compensate for the lens effect of the cylinders). A quadrant photodiode detector is placed behind the mask and measures the light intensities behind the four holes (see section 4.3 Figure 32 and Equation 24). An average of the light intensities through the two vertical holes A_1, A_2 is calculated and so is the case for the two horizontal holes B_1, B_2. Thus errors due to non-perfect centration are eliminated. In the case of a round diffraction image the average vertical and the average horizontal light intensities

should be equal. In the case of an elongated light diffraction pattern the average vertical light intensity will be superior to the average horizontal one (the elongated diffracted image is rotated 90° with respect to the elongated cells. Hence the difference between vertical and horizontal light intensities gives an indication of the elongation rate. This difference is divided by the sum of intensities A+B so elongation values stay within the value limits of +/- 1.

The Technicon Ektacytometer comprises four modes of operation:

Shear scan (called RPM scan in the Technicon manual) and osmoscan where described earlier in section 2.1.3.3.

Time scan: The viscometer rotates at a very high speed for four minutes. During this time elongation is measured and recorded. This mode is used for the fragility assay, where cells are submitted to very high shear stress and their fragmentation is monitored by the decrease of elongation index with time.

Relaxation scan: The viscometer rotates at a pre-set maximum speed and then abruptly stops. Elongation is measured every 20ms for one second after rotation is stopped. This mode is used to study the speed in which the cell returns to its original form after shear stress is removed.

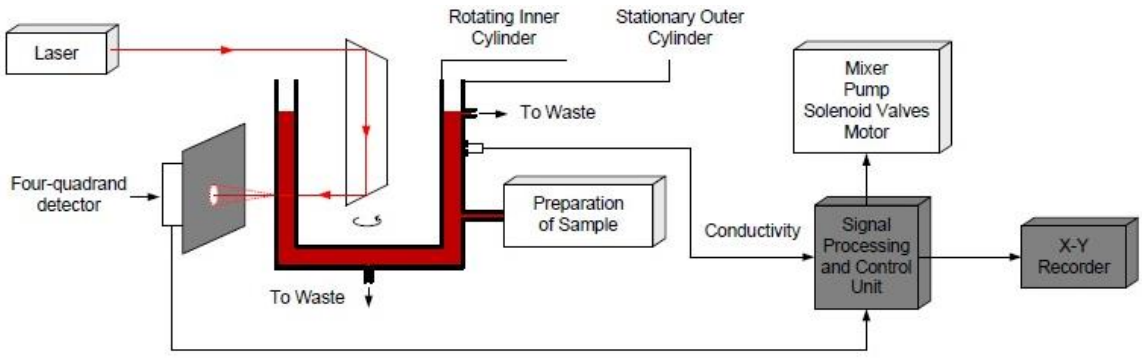

Figure 18: A block diagram of the Technicon Ektacytometer (Swaič, 2007)

2.2.2 Lorca (Laser-assisted Optical Rotational Cell Analyzer)

(RR Mechatronics, Hoorn, the Netherlands)

The Lorca (also called Viscoscan) has a very similar shearing geometry to the Technicon Ektacytometer described above and to the original first Ektacytometer prototype developed by Bessis and Mohandas (Bessis and Mohandas, 1974)(Bessis and Mohandas, 1975)(Bessis et al., 1980) . The transparent cylinders have a gap of 0.3 mm between them. An increasing speed of rotation is applied to the internal cylinder resulting in an increasing shear stress of 0.3 to 75 Pa, acting on the RBC suspended in the solution between them having a viscosity of 30 cP (Hardeman et al., 1994). A laser diode traversing the diluted RBC solution produces a diffraction pattern. The diffraction pattern is captured by a CCD camera. An image processing algorithm calculates an elongation index based on the image pattern. The corresponding shear stress is calculated from the speed of rotation, viscosity, and cylinder geometry. This instrument is temperature controlled for 37°C.

Osmolality gradient ektacytometry (Osmoscan) is not available on this instrument.

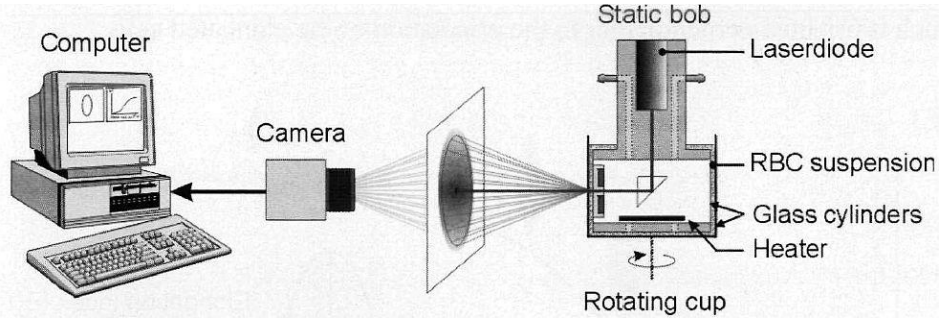

Figure 19: Schematic diagram of Lorca RBC deformability measurement system. from (Dobbe, 2002)

2.2.2.1 Lorrca MaxSis

Lorrca MaxSis is a recent modification introduced to the original Lorca, in order to allow its use in Osmolality gradient Ektacytometry (Osmoscan mode). It's the only commercially available Ektacytometer, in Osmoscan mode, following the cessation of the Technicon's production around two dozens of years ago. It's very similar to the Technicon described in 2.2.1. It uses Couette cylinders for shearing and a laser source. However the interpretation of the laser diffraction pattern is obtained by a camera and an image processing algorithm rather than by photodiodes. A comparison of Lorrca MaxSis main features to the Technicon is shown in Table 1.

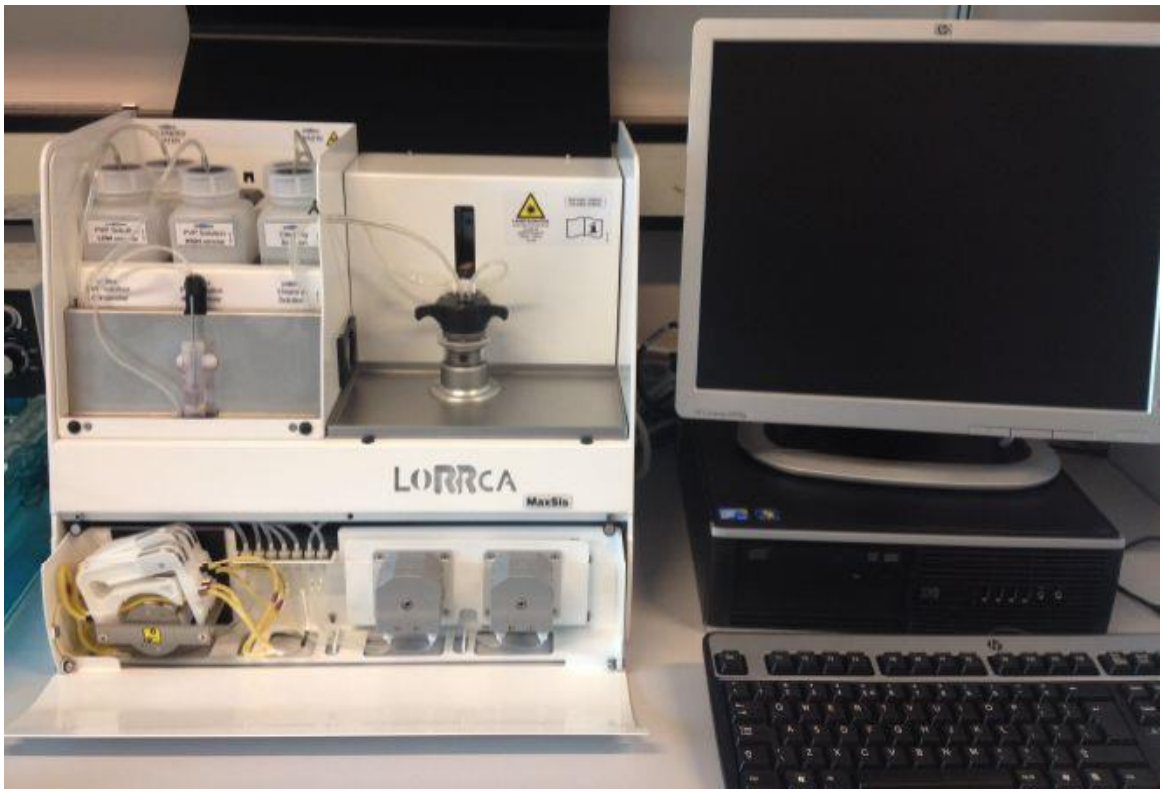

Figure 20 : The LORRCA MAXSIS Ektacytometer. From (Lazarova, www document)

Table 1: Lorrca Maxsis and Technicon main differences

	Lorrca MaxSis	Technicon
Diffraction measurement	Camera	Photodiodes
Rotating cylinder	External	Internal
Viscosity of solutions	20 cP	30 cP
Laser source	Laser Diode	Helium Neon

2.2.3 RheoScan-D

(RheoMeditech, Seoul, Korea)

Described as Laser Diffraction Slit Flow Rheometer or Microfluidic Ektacytometer, this instrument is using, as a shearing device, a disposable flow channel of precise dimensions (0.2 mm high × 4.0 mm wide × 40 mm long).

A blood sample diluted in a viscous transparent solution flows through the channel due to a diminishing vacuum pressure. A laser beam traverses the RBC suspension and creates a diffraction pattern projected on a screen. A CCD video camera captures the images and an Elongation Index (EI), as a measure of the RBC deformability, is determined from the iso-intensity curves in the diffraction pattern using an ellipse-fitting program. The EI is recorded with respect to the average shear stress, which is calculated from the measured pressure. RBC average deformability is obtained for a range of shear stresses between 0 ~ 35 Pa (Sehyun Shin et al., 2004).

Osmolality gradient ektacytometry (Osmoscan) is not available on this instrument.

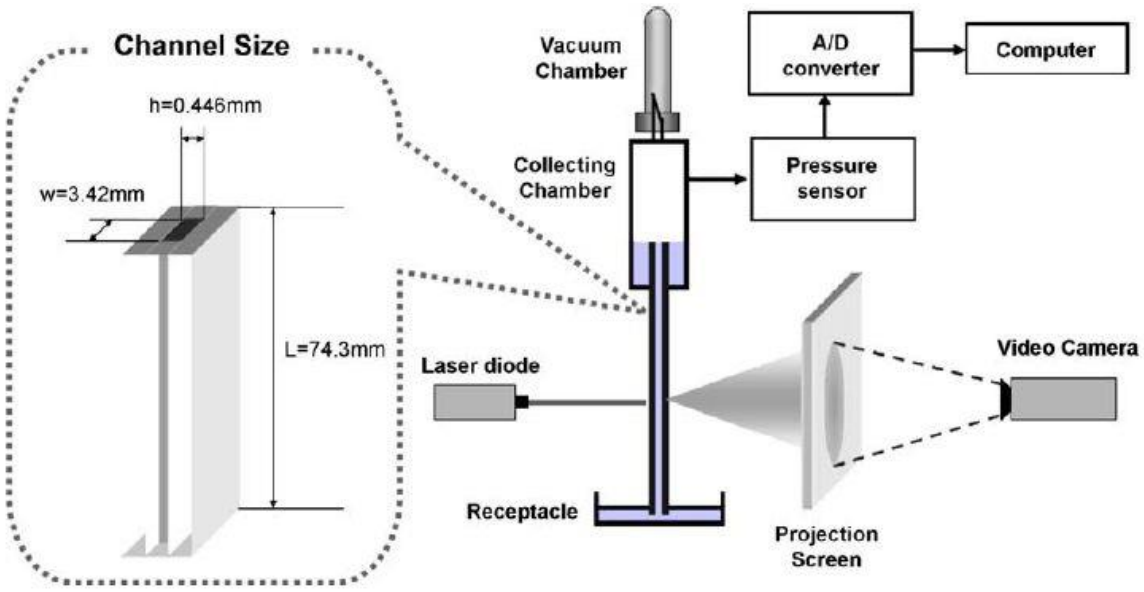

Figure 21: Schematic diagram of the RheoScan-D slit-flow ektacytometer (Shin et al., 2005a)

2.2.4 Rheodyn SSD

(Myrenne GmbH, Roetgen, Germany)

The Rheodyn SSD, is based on a shearing mechanism comprised of a couple of transparent circular plates with a gap of 0.5 mm between them. The bottom plate is stationary and the top plate rotates in eight predetermined speeds yielding shear stresses in the range of 0.3 to 60 Pa upon the RBCs suspended in Dextran solution with 24 cP viscosity. A laser beam traversing the sample in a direction perpendicular to the plates creates a diffraction pattern projected on a photodiode array. An elongation index is calculated from the light intensities recorded by the four photodiodes (Ruef et al., 1995). Osmolality gradient ektacytometry (Osmoscan) is not available on this instrument.

2.3 Conclusions

This chapter presents the state of the art in RBC deformability measurement techniques both for single cell deformability measurement and for cell population deformability measurement. Although single cell deformability measurement techniques give important details of cell structure and deformability, they are rarely suitable for clinical implementation due to their time consuming procedure.

Ektacytometry is the most suitable technique for the measurement of RBC population deformability. It uses whole blood, it is automated and it takes just several minutes to provide information on the average deformability of RBC population. Two main modes of Ektacytometers exist: Shear Scan and Osmotic scan. As explained in section 1.5, only the Osmotic Scan Ektacytometer gives proper diagnostic information for a number of hemolytic anemias. As the review of Osmotic scan Ektacytometers shows that there are only two such instruments: The Technicon whose production was halted about twenty years ago and the recent Lorca MaxSis. Both use a Couette cylinders shearing geometry. A flow channel Ektacytometer is commercially available, but it is only capable of Shear scan ektacytometry. An Osmotic Scan Flow Channel Ektacytometer, developed and presented in this thesis, has not been described or developed previously.

3 Comparison between Pressure and Shear driven flows for Osmolality Gradient Ektacytometry

3.1 Introduction

Different shearing geometries used in Ektacytometry were described in section 2.2. In these geometries RBC's are exposed to flows of different character resulting in different velocity and shear stress profiles. In this chapter the implications of these differences for Osmolality Gradient Ektacytometry are examined.

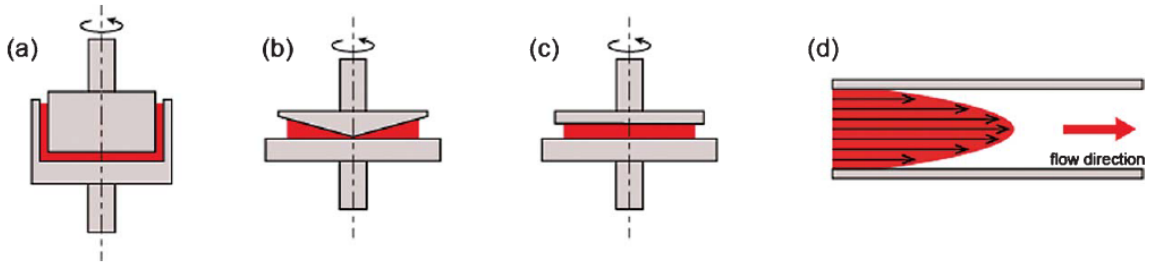

Figure 22: Various shearing geometries used to measure red blood cell deformability: (a) concentric cylinders, (b) cone and plate, (c) parallel disks, and (d) Poiseuille slit flow. From (J. Kim et al., 2015)

3.2 Theoretical background

RBC deformability is the main reason for the highly non-Newtonian behavior of blood. In Ektacytometry the interactions of cells with each other, which are present in the vascular circulation, are eliminated by creating a highly diluted suspension of blood cells in a Newtonian fluid. Obtaining a Newtonian laminar flow simplifies flow conditions and allows for the measurement of the deformability of RBC population as a function of the flow induced shear stress. Effective viscosity of highly diluted suspension of spheres (volume fraction ϕ <0.05) varies according to the following Einstein equation (Einstein, 1906)

Equation 1

$$\frac{\mu_s}{\mu_l} = 1 + 2.5\phi$$

Where $\frac{\mu_s}{\mu_l}$ is the relation between the viscosity of the suspension of spheres to the original liquid viscosity in which they are suspended, and ϕ is the volume fraction of the solid particles.

This equation was further extended to spheroids showing that the orientation of the spheroids has an influence on the effective viscosity of the suspension (Jeffery, 1922) (Leal and Hinch, 1971) (Hinch and Leal, 1972) (Mueller et al., 2010).

Figure 23 shows experimental and calculated viscosity of diluted RBC suspension at different concentrations (Shin et al., 2005a). We can conclude that the very low concentrations of RBC we use (hematocrit generally < 0.5%) allow us to neglect their influence on the solution viscosity.

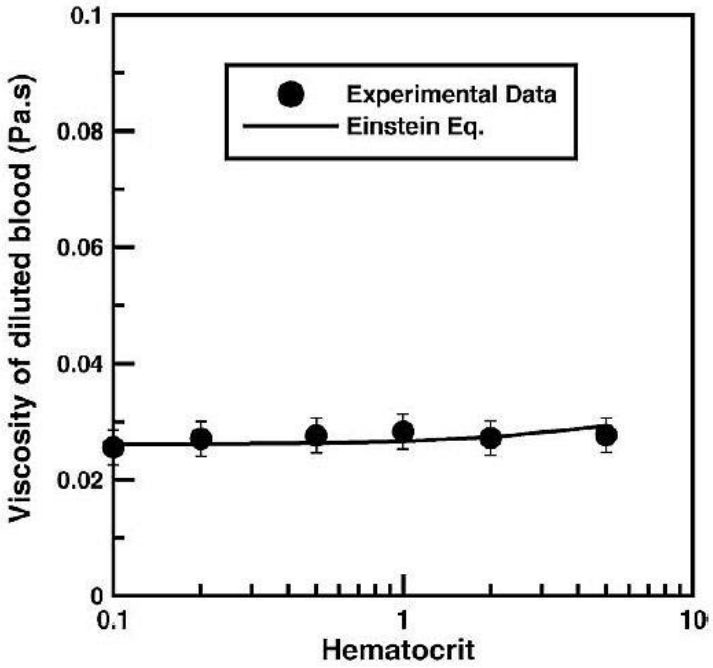

Figure 23 : Viscosity of diluted blood suspension vs. Hematocrit. From (Shin et al., 2005a)

Due to the small gap dimensions, high solution viscosity, and low velocity, in the flows used in Ektacytometry, the Reynolds numbers (ratio of inertial to viscous forces), stay far less than one (see calculated examples below). This means that shear stress is the dominant force and it allows us to neglect the inertial forces in our calculations. The Navier-Stokes equations are simplified in this case by

eliminating the terms proportional to the fluid mass, and we use the simpler Stokes equation instead. From this equation, the velocity profile is obtained by integrating it twice and applying the boundary conditions[8]. The Reynolds number (Re) is also an indication for the nature of the flow. Usually, in normal laboratory conditions, the transition from laminar to turbulent flow occurs at a Reynolds number of the order of 2000 (based on the mean velocity and the diameter) for flow in a circular pipe (Howard A. Stone, 2007) .

The equation for Reynolds Number (Re) characterizing a flow in a channel with height H much smaller than its width W is:

Equation 2
$$\mathrm{Re} = \frac{\rho \cdot U \cdot H}{\mu}$$

Where ρ,μ and U are the fluid density, viscosity and flow velocity respectively.

For instance Re for a flow rate of 1ml/min of a PVP solution (Polyvinylpyrrolidone), with a density close to that of water 10^3 kg/m^3 (Bolten and Türk, 2011) and viscosity of $\mu = 2 \cdot 10^{-2}$ Pa·sec, through a channel of H=100μm, W=5mm.

We can calculate the average flow velocity as the volumetric flow rate Q divided by the channel section area A

$U_{avg} = Q/A$ = 3.33 μm/sec

However, the distribution of flow velocity across the channel is parabolic (Equation 13), with a maximum velocity at the center. So the maximal (worst case) Reynolds number should be calculated in the lamina at the center of the channel. The maximum velocity is 1.5 times the average velocity (Equation 16). The height H that we take into account for the flow conditions around a RBC is the average

[8] Detailed calculations for the Stokes equation for the three geometries presented below can be found in (George Hirasaki, 2005) and (James O. Wilkes, 2015)

undeformed cell diameter which is 8μm (Yaginuma et al., 2013) (Sometimes the particle radius is used instead (Purcell, 1976)).

Which gives:

$\mathrm{Re} = 10^3\,(\mathrm{kg/m^3})$ x 1.5 x $3.33\cdot10^{-6}$ (m/sec) x $8\cdot10^{-6}$ (m) / $2\cdot10^{-2}$ Pa·sec = 0.00002

And for Couette cylinders (Figure 26) with R_1 = 25.35 mm, a gap of ΔR = 0.5 mm and rotation velocity of N=150 RPM, we get for the maximum velocity:

$U_{\max} = 2\pi R_2 N/60$ = 0.4 m/sec

$\mathrm{Re} = 10^3\,(\mathrm{kg/m^3})$ x 0.4 (m/sec) x $8\cdot10^{-6}$ (m) / $2\cdot10^{-2}$ Pa·sec = 0.16

We see that in both geometries (coquette cylinders and a flow channel), Re is well below 1, and hence neglecting the inertial forces is justified.

In a Newtonian fluid the shear stress τ is proportional to the gradient of velocity (shear rate). For example in an incompressible and isotropic Newtonian fluid, the viscous stress is related to the shear rate by

Equation 3
$$\tau = \mu \frac{\partial u}{\partial y} = \mu \dot{\gamma}$$

Where μ is the dynamic viscosity, u is the velocity and $\dot{\gamma}$ is the shear rate.

In Osmolality Gradient Ektacytometry, shear stress is kept constant while deformability is measured as a function of osmolality. Therefore, it is of prime importance to understand and compare the character and magnitude of shear stress in the various shearing geometries used in Ektacytometry. Since Couette cylinders and planar rotating disks produce similar shear driven flows (when measured for high radii), our main comparison will be between these two flows versus the pressure driven flow produced in a channel.

In order to find the shear stress equations for the different geometries we take the velocity profile obtained by developing the Stokes equation. We may then find the shear rate by differentiation. Finally we obtain the shear stress by multiplying the shear rate by the dynamic viscosity.

We consider in our experiments a fully developed flow where flow is in a steady state. The importance of this notion can be observed in Figure 24 and Figure 25. A fully developed flow is dependent both on the time after which pressure stabilizes and the length at which entrance effects diminish.

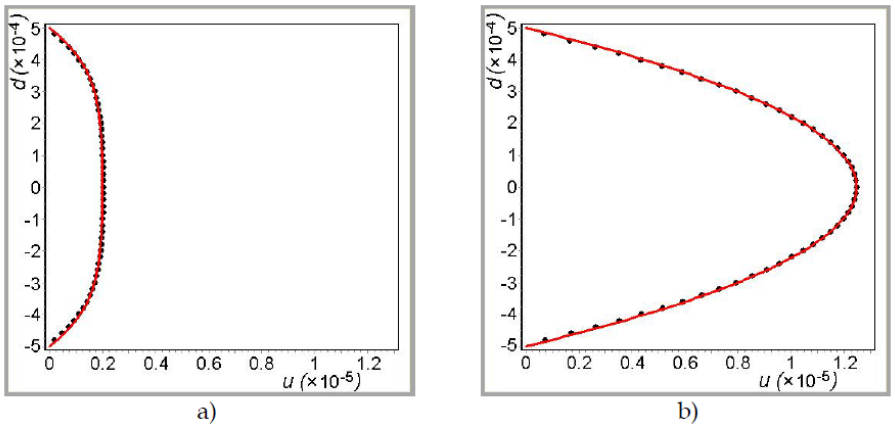

Figure 24: Velocity profiles for Poiseuille flow: a) $t = 0.02\ s$, b) $t = 0.6\ s$. From (Schulz, 2011)

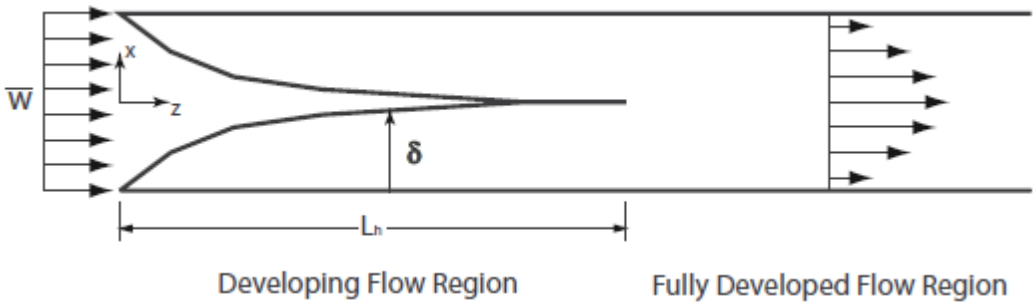

Figure 25: Entrance effect in a flow channel.

From (Muzychka and Yovanovich, 2009)

3.3 Cylindrical Couette flow

Cylindrical couette flow is a flow between two coaxial cylinders, created by their relative rotation (Figure 26). The difference of rotation speed between the cylinders

creates a velocity gradient across the gap and consequently a shear stress on cells suspended in the medium. This is the most widely used shearing geometry in Ektacytometry.

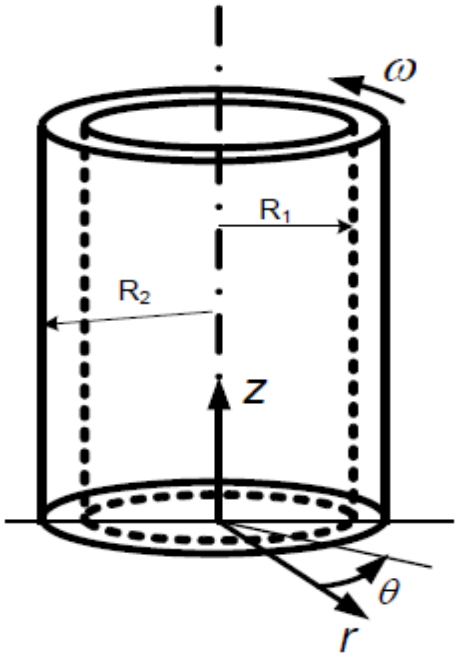

Figure 26: Couette cylinders

Assuming a unidirectional, laminar, fully developed flow, with no slip at the walls, we look for the expression of velocity distribution across the gap between the cylinders. With the internal cylinder at rest and the external cylinder rotating at an angular velocity ω, using cylindrical coordinates, we get the following expression for the tangential velocity at radius r (Chassaing, 2005):

Equation 4

$$U_\theta(r) = \frac{\omega_2 R_2^2}{R_2^2 - R_1^2} \cdot r - \frac{\omega_2 R_1^2 R_2^2}{R_2^2 - R_1^2} \cdot \frac{1}{r}$$

And the shear is obtained by differentiation of Equation 4 with respect to *r*.

Equation 5

$$\dot{\gamma} = \frac{dU_\theta(r)}{dr} = \frac{\omega_2 R_2^2}{R_2^2 - R_1^2} + \frac{\omega_2 R_1^2 R_2^2}{R_2^2 - R_1^2} \cdot \frac{1}{r^2} = \frac{\omega_2 R_2^2}{(R_2 - R_1)(R_2 + R_1)} + \frac{\omega_2 R_1^2 R_2^2}{(R_2 - R_1)(R_2 + R_1)} \cdot \frac{1}{r^2}$$

We substitute $R_2 - R_1$ by ΔR.

Assuming very large values for R_1, R_2 and a very small ΔR , we can replace $R_2 + R_1$ by $2R$. Since $R_1 \le r \le R_2$ we can approximate r by the constant R. Thus approximating the equation of shear (Equation 5) gives Equation 6 which is the same as for plane Couette flow.

We obtain flow conditions similar to that of two parallel plates with one wall stationary and the other moving at a constant velocity (plane Couette flow),

with constant shear rate across the gap for a given rotational speed.

Hence, for a Newtonian fluid, shear rate ($\dot{\gamma}$) and shear stress (τ) are constant across the gap between the cylinders.

Equation 6 $$\dot{\gamma} \approx \frac{\omega R}{\Delta R}$$

And the shear stress:

Equation 7 $$\tau \approx \mu \frac{\omega R}{\Delta R}$$

This means that the RBCs are subjected to equal shear stress, no matter what their position is across the gap ΔR.

In order to verify how close the approximation in Equation 6 is in the case of dimensions used in ektacytometry, we can calculate the non-approximated shear at the walls of the internal and external cylinders of the Technicon Ektacytometer, using Equation 5 and see how close the results are to the approximate value.

For R_1 = 25.35 mm and ΔR = 0.5 mm and rotation velocity of N=150 RPM, we get

$\dot{\gamma}_{R_1} = 820.03$ sec^{-1} and $\dot{\gamma}_{R_2} = 804.32$ sec^{-1}, compared to the approximate value of $\dot{\gamma} = 804.0$ sec^{-1}.

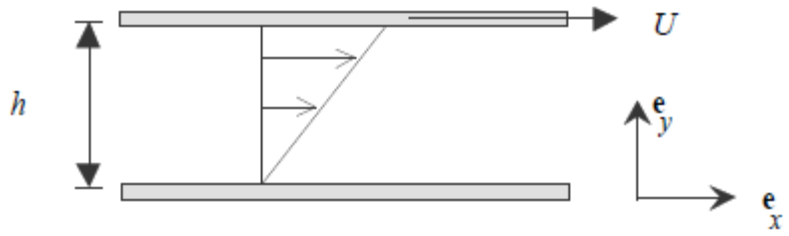

Figure 27: Plane Couette flow: velocity profile of fluid between two parallel plates with one plate moving at constant velocity. From ("ANCEY, Christophe - Notes de cours. Mécanique des Fluides")

We can now calculate the shear stress used in the Technicon Ektacytometer in the OsmoScan mode. In this mode the rotational speed is constant at 150 RPM and the viscosity of the solution is 0.02 Pa·s .

R_1= 25.35 mm

ΔR = 0.5 mm

μ = 0.02 Pa·s

N = 150 RPM

R = (25.35 + 25.85)/2 = 25.6 mm

Using Equation 7 we get:

$$\tau = 0.02 \times \frac{2 \times \pi \times 150 \times 25.6}{60 \times 0.5} = 16.08 \text{ Pa}$$

3.4 Plane rotational Couette flow

Plane rotational Couette flow is a flow between two parallel plates, created by their relative rotation as illustrated in Figure 28. The difference in rotational speed between the plates creates a velocity gradient across the gap and consequently a shear stress on cells suspended in the medium. Unlike Couette cylindrical flow, where velocity is identical at every point on the rotating cylinder surface, velocity of a point on the rotating plate is a function of the radius r. This means that the velocity of a particle in the liquid between the plates is a function not only of its distance from the rotating plate but also of its distance from the axis of rotation. Thus shear stress in direction θ is a function of velocity gradients in both r and z directions. Since measurements are taken at a radius much bigger than the gap dimensions ($r>>z$), the velocity gradient in the z direction ($\partial U/\partial z$) is dominant and the contribution to shear of the velocity gradient in r direction ($\partial U/\partial r$) is negligible (see Figure 28). The centrifugal and gravity induced flows can be neglected for small Reynolds numbers. Hence we assume a laminar unidirectional flow.

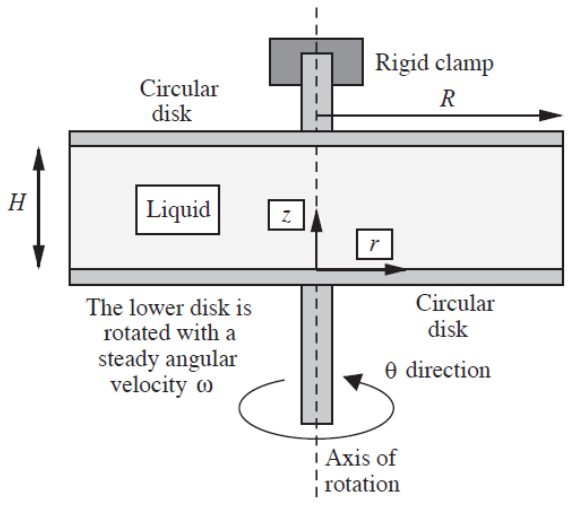

Figure 28: Cross section of parallel disk rheometer. From (James O. Wilkes, 2015)

We may calculate the velocity profile by integrating the Stokes equation twice subject to the following boundary conditions:

$U_\theta(r,0) = 2\pi rN$ at z=0

$U_\theta(r,z) = 0$ at z=H

Where N is the number of revolutions per second. Hence,

Equation 8 $$U_\theta(r,z) = -\frac{2\pi rNz}{H}$$

Since the diameter of the laser beam used in Ektacytometry is less than 1mm, we can assume that when directed in parallel to the plates axis at large values of *r*, the velocity in the *r* axis contained in the beam perimeter, is constant. In this case we replace the variable r by the constant R and we obtain a linear velocity profile.

Equation 9 $$U_\theta(z) = -\frac{2\pi RNz}{H}$$

Thus differentiating in order to obtain shear, gives constant shear and constant shear stress across the gap, as in the case of the Couette cylinders (Equation 6 and Equation 7 respectively)

Equation 10 $$\dot{\gamma}(z) = \frac{dU(z)}{dz} = -\frac{2\pi RN}{H}$$

Equation 11 $$\tau = -\frac{2\pi RN\mu}{H}$$

The minus sign comes from the fact that velocity is decreasing with increasing z value due to the rotation of the plate closer to the origin of axis.

In the case of a cone and plate geometry *H* can be expressed as a linear function of the radius r. In this case *r* and *H* are eliminated from Equation 8 and the velocity becomes linearly dependent only on *z*. Thus differentiation with respect to *z* gives a constant shear rate and shear stress throughout the sample (Equation 10, Equation 11).

3.5 Plane-Poiseuille flow

Forced flow through a rectangular channel is called Hele-Shaw flow. When the flow depends only on one variable it is called plane-Poiseuille flow. In the flow channels which we use, the width is much larger than the height (*W>>H*) and measurements are taken far from the walls, in the center of the channel. Hence, we get flow conditions that approximate a plane-Poiseuille flow.

When a fluid enters a narrow channel from a wider tube the flow profile is not immediately parabolic. The length in which entrance effects are dominant in a flow channel for low Reynolds numbers can be approximated by 0.6 times the hydraulic diameter (Shah and London, 1978) . In a rectangular channel the hydraulic diameter is conventionally defined by

Equation 12
$$D_H = \frac{2WH}{W+H}$$

For a channel 5mm wide and 200μm high we get turbulent conditions due to entrance effects for a length of 0.23mm. And for a channel of 5mm wide and 100μm high the entrance effects are for a length of 0.12mm. Thus our measurements should take place in a distance greater than these values in order to have a fully developed laminar flow.

For the sake of simplicity, we assume a unidirectional flow. However, particles in a suspension exposed to Poiseuille flow are subjected to shear induced migration from high to low shear rate regions. In a channel or tube this means that particles assume an angular trajectory away from the vessel walls, towards the center (Karnis et al., 1966). The degree of alignment of RBC with the flow direction increases with increasing flow rate (and hence shear rate) (H.L. Goldsmith, 1971). Several experiments and simulations were done in order to evaluate the scale of this migration of particles. One of these gives the scale length in which particles migrate to the center as H^3/a^2 where H is the channel height and *a* is the particle diameter

(Nott and Brady, 1994). For a RBC of 8 μm diameter in a channel of 200 μm height, this gives a length of 125 mm, while for a channel of 100μm height it is only 15.6mm. Our Channels are 50mm long hence we conclude that in the case of 200μm high channel the position of measurements along the channel is not critical as long as it's over 0.23mm from the entrance. However in the case of 100μm high channel, our measurements should take place in a distance as close as possible to the channel entrance, so the RBC distribution is nearly not altered yet, but not too close (over 0.12mm) in order to avoid entrance effects.

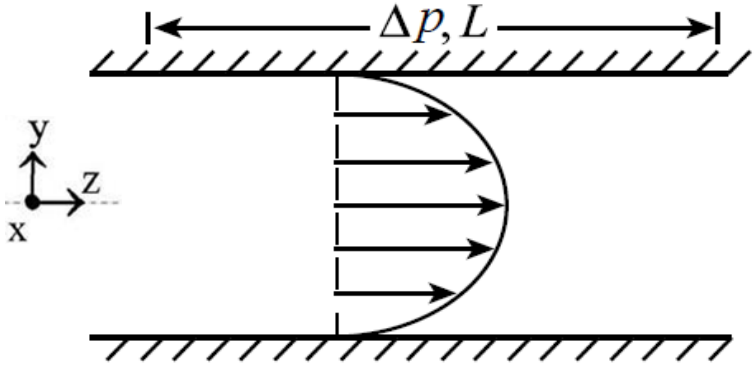

Figure 29: Pressure driven flow: velocity profile of fluid through a channel.

We assume a Newtonian incompressible fluid where the viscosity μ is constant.

For a pressure drop *Δp* that acts over a channel of length *L* we obtain a parabolic velocity profile. We assume a fully developed steady flow where the pressure drop over the channel length is constant and equal to Δp/L. Assuming *H/W*=0 (W goes to infinity) and boundary conditions of no slip at the walls (U=0), we get the following parabolic velocity profile by integrating the Stokes equation twice. We thus obtain the classical solution for plane Poiseuille flow, namely

Equation 13

$$U_z(y) = U_0\left[1-\left(\frac{2y}{H}\right)^2\right]$$

Where U_0 is the maximum velocity, at the mid-plane:

Equation 14 $$U_0 = \frac{H^2 \Delta P}{8 \mu L}$$

Integrating over the cross-sectional area A yields the volumetric flow rate Q

Equation 15 $$Q = \iint_A U_Z \cdot dA = \frac{WH^3 \Delta P}{12 \mu L}$$

The average velocity, defined as Q/WH, is

Equation 16 $$U_{avg} = \frac{2}{3} U_0 = \frac{H^2 \Delta P}{12 \mu L}$$

The shear rate profile is

Equation 17 $$\dot{\gamma}(y) = \frac{dU}{dy} = \frac{8 U_0 y}{H^2} = \frac{\Delta P}{\mu L} y$$

and the average shear rate is

Equation 18 $$\dot{\gamma}_{avg} = \frac{1}{2} \dot{\gamma}_w = \frac{3Q}{WH^2} = \frac{H \Delta P}{4 \mu L}$$

The shear stress profile is

Equation 19 $$\tau(y) = \mu \dot{\gamma}(y) = \frac{\Delta P}{L} y$$

We obtain a linear shear stress, with zero shear stress at the center of the channel and maximum shear stress at the walls (Figure 30).

The shear stress at the wall is:

Equation 20 $$\tau_W = \mu \dot{\gamma}_W = \mu \frac{6Q}{WH^2}$$

Substituting Q from Equation 15 gives

Equation 21 $$\tau_W = \mu \dot{\gamma}_W = \frac{H \Delta P}{2L}$$

The average shear stress is

Equation 22

$$\tau_{avg} = \mu\dot{\gamma}_{avg} = \frac{1}{2}\tau_W = \mu\frac{3Q}{WH^2} = \frac{H\Delta P}{4L}$$

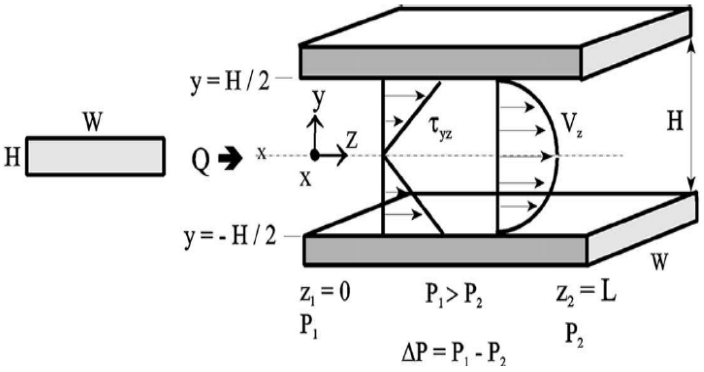

Figure 30: Velocity parabolic profile and shear stress linear profile in Plane-Poiseuille flow. From (Chung, 2000)

Since shear stress is a viscous force it seems strange to perceive, at first glance, that we succeeded in producing flow conditions where shear stress is independent of fluid viscosity (right side of Equation 19, Equation 21 and Equation 22). However, since shear stress is proportional not only to viscosity but to shear rate as well, increasing the viscosity of the solution while maintaining constant pressure across the channel, results in a decrease of flow rate and thus decrease of shear rate, by the same proportion and hence keeping shear stress constant (the solution is Newtonian, so its viscosity is constant with respect to variation of shear. The increase of viscosity is due either to replacement of the solution or to temperature variation).

In practice, a reduction in viscosity results in a reduction of pressure across the channel. This reduction is measured by the pressure sensor and our pressure regulation system increases the pumping (flow rate) by the same rate in order to maintain constant pressure. This results in a constant shear stress.

In real life, rectangular channels always have an aspect ratio *H/W* greater than zero. In our case we use channels with *W*=5 mm and H=0.2 mm or H=0.1 mm. We can check the precision of the approximated formulas we used, in both cases.

We examine the validity of the approximation assuming an aspect ratio *H/W*=0, used in Equation 15 to Equation 22. The solution to the Stokes equation should be modified to take into account the rectangular cross channel section with H/W aspect ratios we actually use (Figure 31). There is an exact solution to the Stokes equation (Cornish, 1928) and a correction factor was calculated for f^* and tabulated (Son, 2007):

Equation 23

$$\dot{\gamma}_w = \frac{6Q}{WH^2}\left(1+\frac{H}{W}\right)f^*\left(\frac{H}{W}\right)$$

For our channels aspect ratios *H/W* of 0.02 and 0.04, we choose from the table (Son, 2007) the closest value for $f^*(0.05)=0.9365$, which is slightly worse than our worst case (0.04). It gives a correction factor of $\left(1+\frac{H}{W}\right)f^*\left(\frac{H}{W}\right)=0.974$ to our equations.

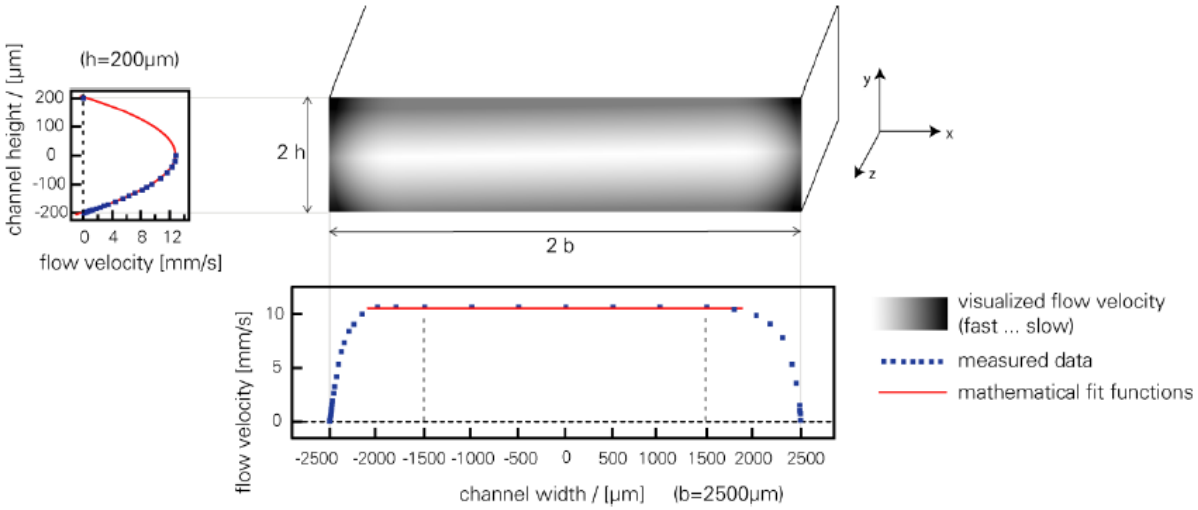

Figure 31: An illustration of the H/W ratio influence on the velocity profile, in a rectangular channel, showing a flow profile inside a channel of H= 2h=0.4mm, W= 2b = 5 mm. Measurements should be done in a width distance from the walls, comparable to at least four times the channel height. From (*Shear Stress and Shear Rates for ibidi µ - Slides - Based on Numerical Calculations*, Ibidi Application Note 11)

Finally, we can use Equation 22 to evaluate the flow rates required in order to produce, in the microchannels, an average shear stress equal to 16 Pascal, used in

the OsmoScan mode of the Technicon Ektacytometer. We calculate the pressure needed to produce such flow rates with solutions viscosity of 0.02 Pa·s.

For a channel of 50mm x 5mm x 0.2mm we get:

Q= 54 µl/sec = 3.24 ml/min

ΔP = 160.8 mbar = 2.33 psi = 16.08 kPa

For a channel of 50mm x 5mm x 0.1mm we get:

Q = 13.4 µl/sec = 0.8 ml/min

ΔP = 321.6 mbar = 4.66 psi = 32.16 kPa

Using calculated manufacturer's data (*Shear Stress and Shear Rates for ibidi µ - Slides - Based on Numerical Calculations*; Ibidi Application note 11) we get very close values to the ones we calculated: Q = 3.13ml/min compared to 3.24 in the first case and 0.794ml/min compared to 0.8 in the second. The differences are due to the manufacturer's correction for non-zero H/W aspect ratio. As expected the difference increases from 0.006 to 0.11 with an increasing H/W ratio from 0.02 to 0.04.

3.6 Conclusions

Table 2 shows a summary of compared features of the two main flows used in Osmotic Scan Ektacytometry while table 2 gives a comparison of formulas developed above. The fact that the deformability of RBCs in a flow channel is not affected by small variations in solution viscosity presents an important advantage over Couette cylinders and rotating plates. In Couette cylinders and rotating plates, variation in solution viscosity is an important source of error. This variation is not due to variation of shear (a Newtonian solution) but rather to temperature variation and also to the fact that the characteristics of PVP solutes vary not only between suppliers, but also between batches from the same supplier. For instance, Sigma-Aldrich, the producer of PVP (average mol wt 360), widely used in Ektacytometry, gives in the product specification sheet a K value range of 80 to 100 (K value is an

empirical parameter closely related to intrinsic viscosity). In order to keep experimental conditions constant, users of Ektacytometers are constrained to buy ready-made solutions with guaranteed viscosity. Therefore results with a flow channel are expected not only to reduce cost but also to have better precision and better reproducibility.

Since all RBCs are exposed to the same shear stress in Couette cylinders, their diffraction patterns can be correlated to their arithmetic mean deformability. In a flow channel RBCs are exposed to a linear distribution of shear stress varying from maximum at the wall to zero in the center. Therefore the diffraction pattern is correlated to the average shear stress which is half of the wall shear stress (τ_W /2). While some studies suggest that the diffraction pattern, in Couette cylinders, could give information regarding the distribution of deformability of a population of RBC (Dobbe et al., 2002) (Streekstra et al., 2010), this would be more difficult to achieve in a flow channel due to the non-constant shear stress field.

Table 2: Comparison of features of Cylindrical Couette flow and Plane-Poiseuille flow

Cylindrical Couette flow	Plane-Poiseuille flow
Constant wall velocity	Constant pressure
Shear driven flow	Pressure driven flow
Linear velocity profile	Parabolic velocity profile
Velocity, flow rate and shear rate independent of viscosity	Velocity, flow rate and shear rate dependent on viscosity
Homogenous shear stress	Linear shear stress distribution
Shear stress proportional to viscosity	Shear stress independent of viscosity

Table 3: Comparison of formulas for Cylindrical Couette flow *vs.* Plane-Poiseuille flow

	Cylindrical Couette flow	Plane-Poiseuille flow
Velocity profile	$U(r) \approx \frac{r - R_1}{\Delta R} \omega R_2$	$U_z(y) = \frac{H^2 \Delta P}{8 \mu L}\left[1 - \left(\frac{2y}{H}\right)^2\right]$
Average velocity	$U_{avg} = \frac{\omega R_2}{2}$	$U_{avg} = \frac{H^2 \Delta P}{12 \mu L}$
Maximum velocity	$U_{\max} = \omega R_2$	$U_{\max} = \frac{H^2 \Delta P}{8 \mu L}$
Shear rate profile	$\dot{\gamma} \approx \frac{\omega R_2}{\Delta R}$	$\dot{\gamma}(y) = \frac{\Delta P}{\mu L} y$
Shear stress profile	$\tau \approx \mu \frac{\omega R_2}{\Delta R}$	$\tau(y) = \frac{\Delta P}{L} y$
Shear stress at the walls	$\tau \approx \mu \frac{\omega R_2}{\Delta R}$	$\tau_W = \frac{H \Delta P}{2L}$
Average shear stress	$\tau \approx \mu \frac{\omega R_2}{\Delta R}$	$\tau_{avg} = \frac{H \Delta P}{4L}$

4 COMPARISON BETWEEN A CAMERA AND A FOUR QUADRANT DETECTOR, IN THE MEASUREMENT OF RED BLOOD CELL DEFORMABILITY AS A FUNCTION OF OSMOLALITY

4.1 Introduction

In this study we compared two measurement and calculation methods of average RBC deformability, both derived from the laser diffraction pattern. One method used a four quadrant silicon photodiode; the other used a CCD camera. Two distinct methods are used for the calculation of deformability from measured data.

4.2 Theoretical background

Above a certain shear stress level, the flow of RBCs mixed in a highly diluted viscous solution is laminar and they are oriented in a plane perpendicular to the shear gradient (Bayer et al., 1994). Their morphology changes with increasing shear from biconcave to tri-axial ellipsoid. Consequently, the diffraction pattern, created by the laser beam traversing the RBCs changes from a circle to an ellipse with the same

eccentricity, but its major axis is oriented perpendicularly to the direction of flow (Zahalak and Sutera, 1981) (T. Fischer and H. Schmid-Schönbein, 1977). This 90° rotation of the diffraction pattern is due to the inverse correlation of size between the diffracted image and the exposed cells. The minor axis of the image corresponds to the major axis of the exposed cells and the major axis of the image corresponds to the minor axis of the exposed cells.

In ektacytometry, two main modes are used to characterize RBC deformability: In the first the cells are mixed with a high viscosity solution of normal physiological osmolality (for human plasma 290 mOsm/Kg) then increasing shear stress is applied to the mixture. The diffraction pattern therefore shows deformability as a function of shear stress at physiologic tonicity. In the second mode the shear stress is kept constant, but RBCs are mixed in a medium where osmolality is increased gradually. The diffraction pattern then shows deformability as a function of osmolality. This mode is called "osmotic gradient ektacytometry" or "Osmoscan", and provides information on membrane stiffness, intracellular viscosity and surface-area-to-volume ratio (Clark et al., 1983). Both approaches have been used with different instrumentation and analysis methods of the diffraction pattern (Mohandas et al., 1980) (Shin et al., 2007) (Hardeman et al., 1994), and published reports have compared methods of the deformability measurements under changing shear stress (Shin et al., 2007) (Hardeman et al., 1994) (Oguz K Baskurt, 2009) (Wang et al., 1999). Both image analysis of the diffraction pattern and simple intensity measurement at discrete spots in the diffraction pattern have been used. Comparison of these different methods of analysis of the diffraction pattern, between different instrumentation, while changing osmolality is more complex as several factors affect the final result. Both the rate of osmolality change and the presence of hemolyzed cells in the population, as well as different shape changes as the result of water uptake or release may affect the diffraction pattern. In order to address this, and allow direct comparison of the two ways to measure the diffraction pattern, we designed a measuring device and method to measure the same cells simultaneously by the two methods. The approach uses the same laser source, same

optics, same viscometer, same osmolality measurement sensor, same hydraulic system and gradient maker and the same solutions to measure the same cells at the same time. This eliminates virtually all potential errors that could result from differences between two similar but yet different samples measured on two different instruments.

4.3 Experimental apparatus and methods

Several studies use a camera and image analysis in ektacytometry (Bayer et al., 1994) (Shin et al., 2005b) and there exist two such commercial apparatus: Lorca (Hardeman et al., 1994) and RheoScan-D300 (Shin et al., 2007). Our design employs a custom apparatus we built, based on a Technicon ektacytometer (Mp, 1983). Originally, RBC deformability was measured by projecting the diffracted laser beam on a mask with four equidistant holes behind which a four quadrant silicon detector was placed (Groner et al., 1980). In order to compare image analysis with the deformation computed using the simpler four quadrant detector, we designed a setup that permitted simultaneous measurement of the same sample by the two methods consisting of a beam splitter (Thorlabs) placed in the path of the post-diffraction laser beam splitting the diffraction image into two identical intensity beams, 90° apart. The design used the optical bench and the transparent Couette viscometer of an ektacytometer with a 632.8 nm helium-neon laser source of 1 mW (Lasos, Germany). An ARM microcontroller board (Embedded Artists LPC2148) provided the interface to measure osmolality and temperature and to control the speed of the viscometer and the plumbing needed to create the osmotic gradient. A mixture of whole blood was introduced into the viscometer at a hematocrit of approximately 0.08% in phosphate buffered (pH 7.35) Polyvinylpyrrolidone (PVP, Sigma, St Louis) at 0.2 poise viscosity. The tonicity of the mixture was varied between 50 and 600 mOsmol/kg with NaCl gradient, and cells were exposed to a constant shear stress of 159.3 dyn/cm^2.

One image of the diffraction pattern was projected by the beam splitter on a mask with four holes, behind which was situated the four-quadrant detector. The other diffraction pattern was projected on a translucent screen, and behind it was placed a CCD camera. Data from both measurements were recorded by a computer equipped with an interface that allowed image analysis as well as signal detection of the quadrant detector.

The elongation index (EI), a measure of RBC mean deformability, was calculated from the signals of the four quadrant photodiodes measuring the projected diffraction pattern (Figure 32), using Equation 24 where A and B are the signals on the long and short axis of the ellipsoid respectively. The use of two signals on each axis (A1, A2 and B1, B2) provides an average and compensates for slight difference in centering the beam on the mask.

Equation 24

$$EI = \frac{(A_1 + A_2) - (B_1 + B_2)}{A_1 + A_2 + B_1 + B_2}$$

In the case of the camera, we used an image analysis algorithm (modified PINK library functions (Couprie et al., 2011)) to determine the elongation index by fitting the image, using iso-intensity curves, to an ellipsoid and determining the length of the short and long axis and EI= (L-S)/(L+S) as indicated in Figure 32

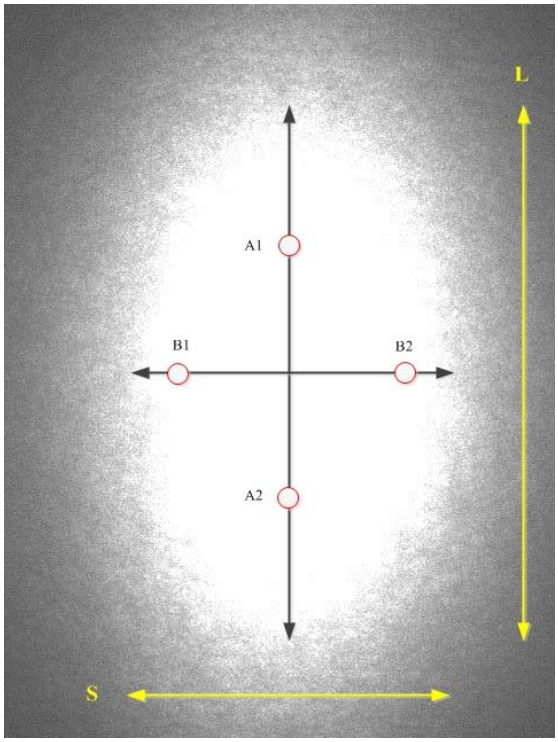

Figure 32: Screen shot of the diffraction image, indicating the position of the holes in the mask for signal detection by the quadrant detector (A1, A2, B1, B2) and the long (L) and short (S) axis of which the length is determined by the iso-intensity curves of the image analysis algorithm.

Both calculations of EI were performed simultaneously by a custom computer program as indicated in Figure 34, and plotted as EI versus osmolality.

Figure 33: Modified Technicon Ektacytometer with a beam splitter and a camera

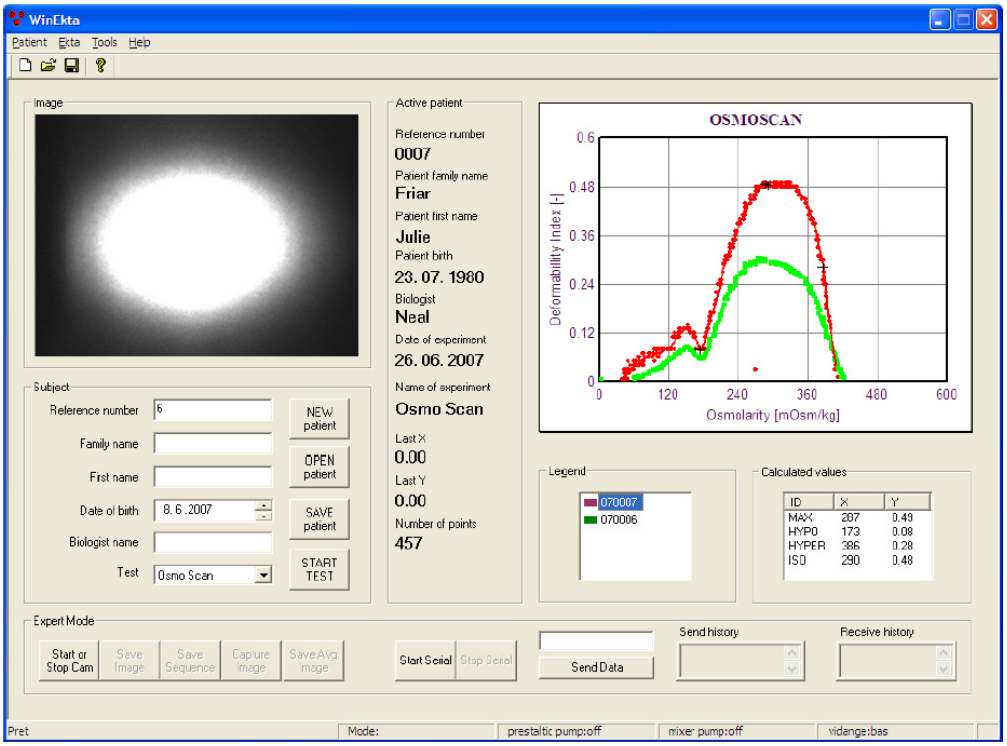

Figure 34: Screen shot of the custom application comparing two different ways to measure EI from the diffraction pattern as described in Figure 32(from (Swiač, 2007))

The EI determined by the image processing (bottom curve) could be directly compared to the one determined by the quadrant detector (top curve).

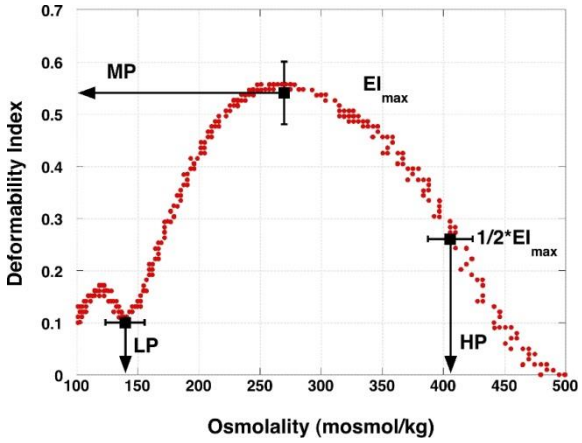

Figure 35: A typical osmotic deformability curve indicating the points used for comparison of the different measurement; the minimum at low osmolality (LP), the maximum deformability (MP), and the hypertonic osmolality (HP) at which EI= ½ EI_{max}. The use of these parameters simplifies data presentation and interpretation.

In order to facilitate the comparison of the results by these two methods, three indicator points are calculated and marked by the program on each curve, as shown in Figure 35: Hypotonic point (LP), Maximum (MP) where elongation reaches its maximum (EImax), and Hypertonic point (HP). As indicated by the average and standard deviations, LP, MP and HP vary between different individuals.

4.4 Results and discussion

Comparison of the two curves clearly showed that they closely track each other in shape (Figure 36). While the absolute value of the deformability index is different at isotonicity, the osmolality of the minimum (LP), the osmolality of the maximum (MP), and the decrease at higher osmolality are very similar using either method. The difference in amplitude can be explained by the fact that the diffraction pattern is not linear and light intensity ratio between the vertical and horizontal holes is higher than the diffracted ellipse's major to minor axes length ratio. Importantly, regardless of the method used, we find a minimum around 150 mOsmol, which has been shown to correlate with the osmolality at which approximately 50% of the RBC

have hemolyzed (Clark et al., 1983), a maximum deformability around 290 mOsmol, and a sharp drop in deformation when the cell loses water under hyper osmolalities. Different samples from control individuals show slightly different results in LP, MP. IP and HP based on the individual characteristics of the donors. These shifts are very similar with either detection method. Similarly it can be expected that differences between control and patient samples show the same trends using either of the two methods. A direct comparison of patient samples on the same machine was not performed, but a study on a family with hereditary Elliptocytosis using either the camera based LORRCA MaxSis (Mechatronics, Hoorn) or the Quadrant diode based ektacytometer showed similar results (Franck et al., 2011). Together these results indicate that either detection method identifies properly the change of RBC deformability over a large range of osmolalities and that neither method can be identified as being preferential to the other based on the final result.

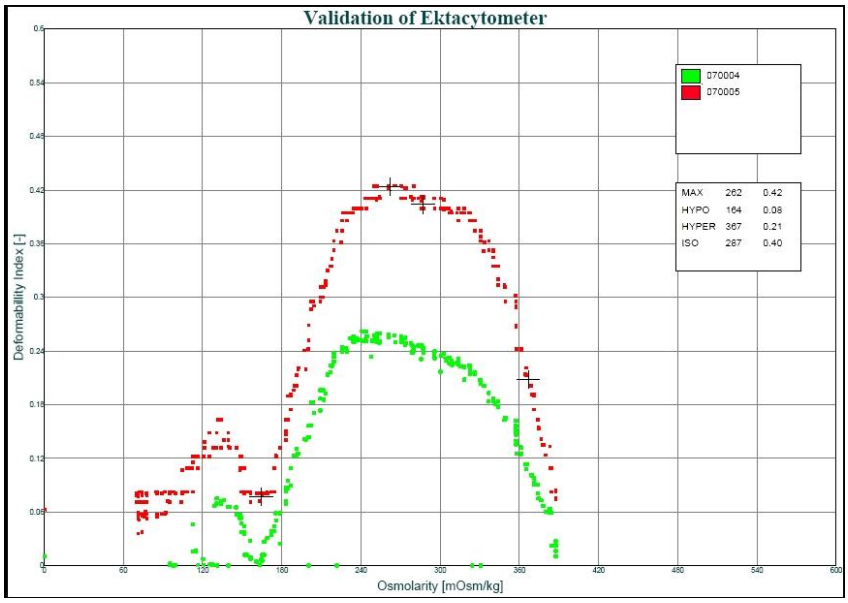

Figure 36: Experimental curve. The top curve was obtained by the four quadrant detector and the bottom one by the camera. The Y axis plots the elongation index against osmolality on the X axis. The dispersion of points at low osmolality is due to a low concentration of RBCs at the beginning of the experiment.

4.5 Conclusions

Osmotic gradient ektacytometry is a very complex but valuable tool for the diagnosis of several (hereditary) RBC disorders. Our experiments lead us to conclude that either image analysis or the use of a quadrant detector result in clinically usable interpretation of RBC deformability.

Regardless of the analysis used, proper care of solution viscosity, temperature, pH, osmolality, and oxygenation is essential. However starting with the same samples our results show that the use of a very simple detection of intensity at discrete points of the diffraction pattern renders similar results as compared to a more complex and sophisticated analysis of the image.

We cannot exclude the possibility that changes in shape to the diffraction pattern under different conditions will add more information. However, in most cases in which laser diffraction is used to routinely measure RBC deformability, either for the diagnosis of hereditary Spherocytosis or Elliptocytosis, or to monitor changes in deformability as the result of treatment, a simple measurement of four points seems fully adequate. The added complexity of image collection in real time, comparison of thousands of images, use of image analysis algorithms, adds complexity and significant cost. The addition of variables such as the choice of various possible regions of the image for interpretation, gain, aperture size, exposure time, saturation, blooming effect and sensor sensitivity degradation seem unwarranted for routine measurements. The four quadrant detector is limited by the necessity for calibration and centering, but the simplicity, constant conditions of use and simple signal processing provide the design of a simple and highly cost effective instrument for routine measurement of RBC deformability. Additional studies are required to compare repeatability for both methods, and to demonstrate that the two curves overlap for a variety of pathologies.

5 MODELLING AND MATHEMATICAL ANALYSIS

5.1 Modeling using Matlab/ Simulink

Our aim is to measure deformability as a function of osmolality, with constant shear stress. For this purpose we maintain a constant flow rate in the flow cell, and mix blood with a solution of gradually increasing osmolality.

All solutions have the same viscosity and temperature. Our hydraulic system consists of a solution preparation unit (stir tank), the sample mixing stage and the flow cell (Figure 37) .

Let's examine first the system behavior, ignoring for the moment the flow control mechanism.

In order to get a flow with increasing solution osmolality we use a stir tank filled initially to a volume V_0 with low osmolality of C_0.

A solution of constant high osmolality C_h flows into the stir tank at a flow rate f_1, increasing gradually the osmolality of the tank solution (permanently stirred).

Simultaneously, the solution flows out of the stir tank at a flow rate f_2. Since the outflow rate is higher than the inflow rate ($f_2 > f_1$), the stir tank will empty gradually.

The constant high osmolality inflow will be mixed into a decreasing volume and will increase the outflow Osmolality.

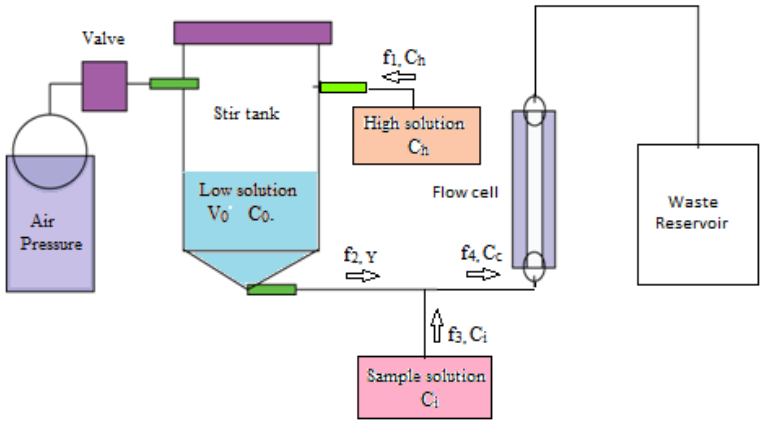

Figure 37: Schematic diagram of the FloDif hydraulic system. f_1, f_2, f_3 and f_4 denote flow rates. C_0, C_h, C_i, C_c and y denote osmolality. V denotes volume

The solution flowing out of the stir tank is mixed with the blood sample diluted in an Isotonic Osmolality C_i flowing at a rate of f_3.

Finally we obtain the blood mixed in a solution of C_c osmolality flowing into the flow cell at a rate $f_4 = f_2 + f_3$.

Let V be the volume of solution in the stir tank.

Let y be the osmolality of the solution in the stir tank.

Let f_1, f_2, f_3 *and* f_4 be flow rates as shown in Figure 37.

All the above values are always positive.

Since our aim is to (nearly) empty the solution in the stir tank at the end of the experiment the outflow is always higher than the inflow $\boldsymbol{f_2 > f_1}$.

The mass conservation equation in the stir tank may be written as

Equation 25

$$\frac{d}{dt}V = f_1 - f_2$$

In a similar manner the solution osmolality equation is

Equation 26

$$\frac{d}{dt}(yV) = c_h f_1 - y f_2$$

Developing the left hand side gives

$$y\frac{d}{dt}V + V\frac{d}{dt}y = c_h f_1 - y f_2$$

Substituting for $\frac{d}{dt}V$ from Equation 25 gives

$$y(f_1 - f_2) + V\frac{d}{dt}y = c_h f_1 - y f_2$$

Or

$$V\frac{d}{dt}y = c_h f_1 - y f_2 - y(f_1 - f_2) = c_h f_1 - y f_1$$

$$V\frac{d}{dt}y = (c_h - y) f_1$$

Finally

Equation 27

$$\frac{d}{dt}y = \frac{(c_h - y) f_1}{V}$$

Equation 25 and Equation 27 describe the behavior of the stir tank.

Compute now the flow rate f_4 through the flow cell.

Equation 28

$$f_4 = f_2 + f_3$$

And the osmolality C_c in the flow cell

Equation 29

$$C_c = \frac{y f_2 + C_i f_3}{f_2 + f_3}$$

A Matlab Simulink model lets us calculate the necessary flow rates in order to achieve a regular osmolality scan over time without running out of solution in the stir tank. The model is shown in Figure 38.

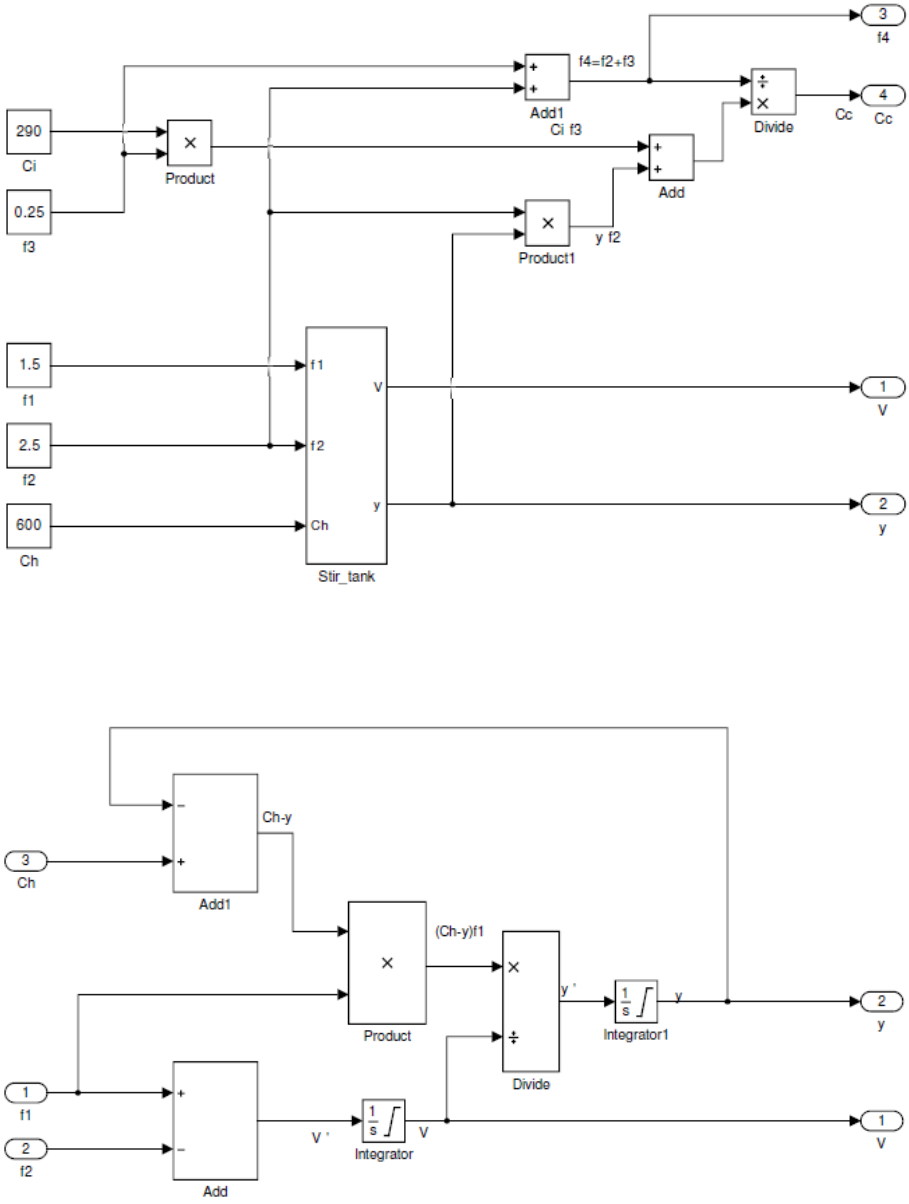

Figure 38: Hydraulic system Matlab Simulink model at the top, with Stir Tank subsystem at the bottom

Figure 39 gives curves for y obtained with different flow rates f_1 and f_2. Notice that for some values of f_1 and f_2 , the osmolality y increases in a linear manner.

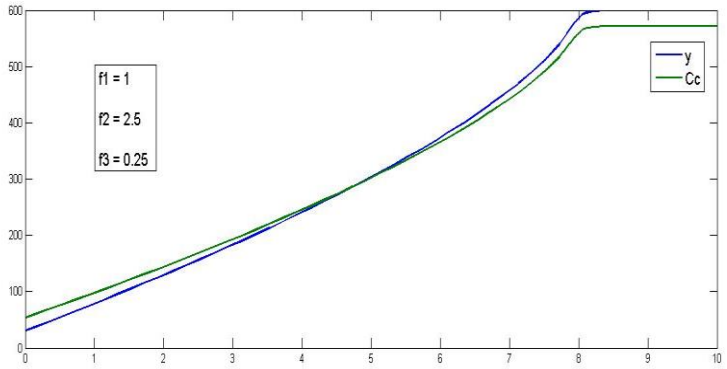

A

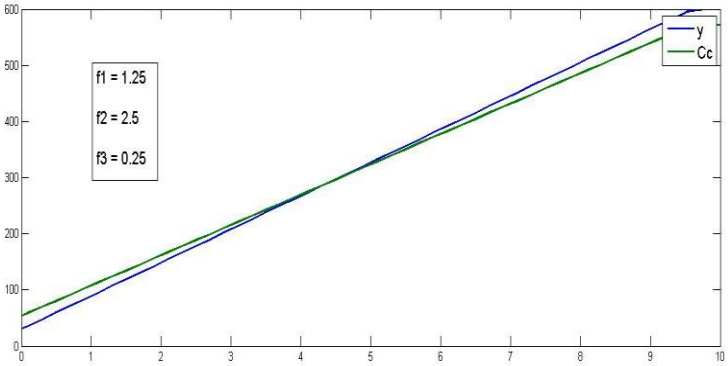

B

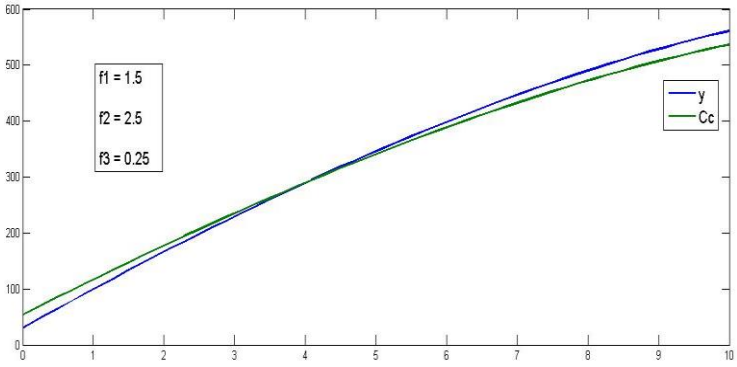

C

Figure 39: Curves of Osmolality (mOsm/kg) vs time (minutes), obtained with Matlab Simulink for several flow rates. Y (in blue) is the osmolality in the stir tank and Cc (in green) is the osmolality in the flow cell. Initial conditions are: C_h= 600mOsm/kg; C_0=30mOsm/kg; V_0=12ml

In order to get a better understanding for the influence of the f_1 and f_2 parameters on the osmolality curve, we developed Equation 27 further, so we can find the solution to the differential equation and see how it depends on the various parameters.

Assuming that the flow rates are constant throughout the experiment, we get

Equation 30 $$V = V_0 + (f_1 - f_2)t$$

Substituting V in Equation 27 gives

Equation 31 $$\frac{d}{dt}y = \frac{(c_h - y)f_1}{V_0 + (f_1 - f_2)t}$$

This equation is of the form of a first order linear ordinary differential equation.

We now find the general solution of this equation with the help of Mathematica.

We get:

Equation32

$$Y(t) = (f_1\,t - f_2 t + V_0)^{-\frac{f1}{f1-f2}}\,(C_h(f_1\,t - f_2 t + V_0)^{\frac{f1}{f1-f2}}) - (C_h - C_0)\;V_0^{\frac{f1}{f1-f2}})$$

Simplifying gives

Equation 33 $$Y(t) = C_h - (C_h - C_0)\left(\frac{V_0}{V_0 + f_1 t - f_2 t}\right)^{\frac{f_1}{f_1 - f_2}}$$

Putting the time dependent component in the denominator gives

Equation 34

$$Y(t) = C_h - (C_h - C_0)\left(\frac{V_0 + f_1 t - f_2 t}{V_0}\right)^{\frac{f_1}{f_2 - f_1}}$$

From Equation 34 we see that the exponent $\boldsymbol{f_1/(f_2 - f_1)}$ determines if the solution is linear or not.

If the exponent equals 1 ($\boldsymbol{f_2 = 2f_1}$) than we get a linear progress of the osmolality y (Figure 39B).

If the exponent is greater than 1 ($\boldsymbol{f_2 > 2f_1}$) then the curve is concave (Figure 39A).

If the exponent is lower than one ($\boldsymbol{f_1 < f_2 < 2f_1}$) then the curve is convex (Figure 39C).

Simplifying further Equation 34 for the linear case we obtain

Equation 35

$$f_2 = 2f_1 \Rightarrow Y(t) = (C_h - C_0)\left(\frac{f_1}{V_0}\right)t + C_0$$

We could actually get the results in Equation 35, in a simpler manner from Equation 31 without finding the general solution to the differential equation:

In order for *Y(t)* to be linear $\frac{d}{dt}y$ should be constant. We call this constant k and we get from Equation 31

Equation 36

$$k = \frac{(C_h - y)f_1}{V_0 + (f_1 - f_2)t}$$

And since Y(t) is linear

Equation 37 $$y = kt + C_0$$

Substituting *y* in Equation 36 gives

Equation 38 $$k = \frac{(C_h - kt - C_0) f_1}{V_0 + (f_1 - f_2)t}$$

Isolating *k* gives

Equation 39 $$k = \frac{(C_h - C_0) f_1}{V_0 + (2 f_1 - f_2)t}$$

We see from Equation 39 that in order for *k* to be constant, the same condition for linearity that we found before $2 f_1 = f_2$ must be respected, and thus we get the same result as in Equation 35.

Equation 40 $$Y(t) = (C_h - C_0)(\frac{f_1}{V_0})t + C_0$$

5.2 Practical considerations

In our design we have several imposed restrictions and guidelines for choosing the right parameters.

The range of osmolality gradient is determined by biomedical needs and is in the range of 60 to 500 mOsm/kg.

For efficiency reasons the time of scan should be as short as possible but not too short. The blood cells should be exposed long enough to a given osmolality to complete either swelling or shrinking as water crosses the membrane. This time is

determined by the flow rate (f_4) and by the volume of the tubing between the sample mixing stage (junction joining the solution f_2 and the sample f_3) and the flow cell. The flow rate through the slide (f_4) is determined by the required sheer stress, which in turn will be affected by the internal size of the flow cell, and the solution viscosity. Hence for a given viscosity and flow cell, the flow rate f_4 can be calculated to achieve a shear stress to properly deform the blood cell.

Calculations for this flow rate are found in the example below as well as in chapter 6.

f_3 is calculated in relation to f_4 in order to give the desired value of hematocrit (red cell volume relative to total volume). The desired hematocrit in the flow cell is determined by flow cell geometry and the laser intensity (see chapter 6). The hematocrit in the flow cell is a fraction of 1% and since we want to achieve a homogenous solution in the flow cell, we want f_3 to be important enough in relation to f_4. Hence whole blood (hematocrit of approximately 40%) is premixed 1 to 40 with an isotonic solution.

The initial volume of solution in the stir tank is chosen in a way that the tank is nearly empty at the end of the test, so no solution is wasted.

f_2 is determined from f_3 and f_4 by Equation 28.

Finally f1, is chosen to be half of f2 in order to give a linear progress of osmolality. Since the actual osmolality is measured by a conductivity sensor, a nonlinear increase in osmolality is not contributing to measurement errors. A close to linear rise in osmolality is preferred in order to get a roughly equal resolution of measurement points on the deformability vs osmolality curve (since acquisition rate is constant). Furthermore, it makes it easier to predict the quantities of solutions necessary for the experiment, in order to avoid running out of solution, or waste leftovers.

5.2.1 Example

Initial conditions are: C_h = 600 mOsm/kg, C_0 = 30 mOsm/kg,

Final osmolality 500 mOsmol/kg

Solution of viscosity: μ = 0.02 Pa·s

Runtime 6 minutes

Slide dimensions: L=50mm; W= 5mm; h=0.2mm

Wall shear stress for this slide: $\tau_w = 512.9\mu f_4$ (per slide manufacturer)

Shear stress required: $\tau_{avg} = 0.5\tau_w = 16$ Pa

Osmolality equilibration tubing: 1.6 mm ID

Osmolality equilibration time 20 s

5.2.2 Calculation

$$f_4 = \frac{2\tau_{avg}}{512.9\mu} = 3.10 \text{ ml/min}$$

$$f_3 = 0.1 f_4 = 0.31 \text{ ml/min}$$

$$f_2 = f_4 - f_3 = 2.80 \text{ ml/min}$$

$$f_1 = 0.5 f_2 = 1.40 \text{ ml/min}$$

Tube length for osmotic equilibration: $L_{tube} = 3.1 \cdot 20 / 60\pi \cdot 0.08^2 = 51.4$ cm

$$V_0 = \frac{(600-30)\cdot 1.4 \cdot 6}{(500-30)} = 10.19ml$$

So final conditions:

V_0 = 11 ml, C_h = 600 mOsm/kg, C_0 = 30 mOsm/kg, L_{tube}= 52 cm.

f_1= 1.4 ml/min

f_2= 2.8 ml/min

f_3= 0.3 ml/min

Further numerical examples, can be found in the experimental section in chapter 6 .

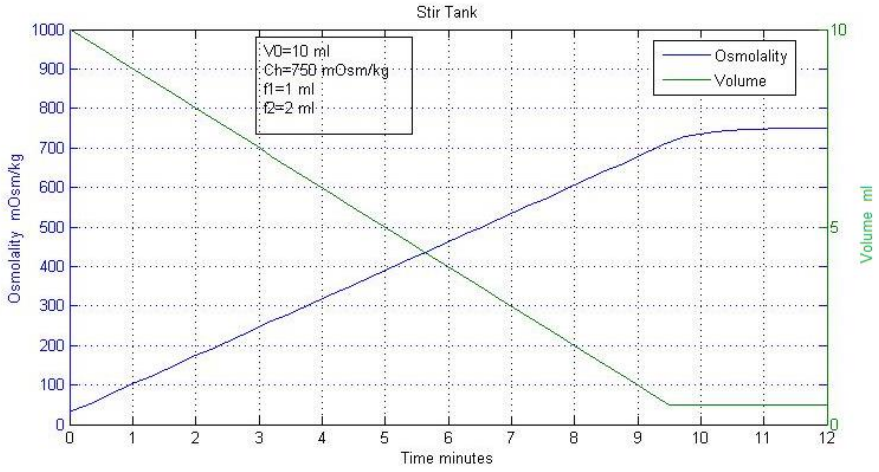

Figure 40: Simulation example of the evolution of Volume (green curve right axis) and Osmolality (blue left axis) in the steer tank for V_0=10 ml, C_h=750 mOsm/kg, f_1=1 ml, f_2=2 ml Calculations are stopped at volume 0.5ml.

5.3 Conclusions

In osmotic scan ektacytometry, deformability of RBC is measured as a function of varying osmolality. We presented in this chapter an osmolality gradient generator based on a stir tank. Finding necessary flow rate values experimentally, in order to get a, close to linear, osmolality increasing solution is very time consuming. Moreover, each time flow rates change, new experiments should be conducted in order to establish the right new values. We found by both modelling (using Matlab/Simulink) and mathematical tools (using Mathematica), that the right relations between flow rates in order to produce a linear osmolality evolving solution is $2f_1 = f_2$. We demonstrated our findings with a numerical example. Moreover we show how to calculate, from the flow rate, the tube length necessary for RBC osmotic equilibration.

6 DESIGN AND PROOF OF PRINCIPLE

6.1 Introduction

The difference between shear stress distribution in RBC population flowing under shear and pressure driven flows was explained in chapter 3. My aim in this chapter is to produce an experimental proof of concept in order to validate the possible clinical use of a pressure driven microfluidic osmolality gradient Ekyacytometer. To this end a microfluidic Ektacytometr prototype was designed and built, and experimental results are compared with these obtained on a blood sample of the same volunteer, by the Technicon (shear driven) Ektacytometer.

This section presents the different stages of design of the microfluidic osmolality gradient Ektacytometer (FloDif) and some initial experimental results providing evidence for a proof of principle.

6.1.1 Process and venue used for testing

To establish the proof of principle of the theoretical framework presented in the previous chapters, I partnered with the Red Blood Cell laboratory at Children's Hospital Oakland Research Institute (CHORI), Oakland, California.

The CHORI laboratory was useful for the following reasons:

1. Availability of blood was restricted at my institute, but widely available at CHORI, where IRB approval for our studies was gained for our protocol.

2. The Red Cell Lab at CHORI is well respected, and the credibility of data collected there was expected to stand scientific scrutiny (http://www.rbclab.com/).

3. Dr Frans Kuypers, The director of the lab, is an expert in the measurement of RBC deformability. His previous collaborations with INSERM allowed me to be able to set up this collaboration, and provided me with access to the laboratory in Oakland to test both hardware and software components that were built in Paris.

4. Dr Kuypers has been involved in the maintenance and repair of virtually all of the original 10 Couette viscometers that were built as engineering prototypes by Technicon, based on the original design of Besis and Mohandas in the 1980's (Bessis et al., 1980; Bessis and Mohandas, 1975)

5. His lab is one of the few labs in the world that is able to provide the measurement of RBC deformability as a clinical service.

(http://www.rbclab.com/Pages/200/240/240.5/240%205.html)

During this study, the functionality of the individual parts was tested in Oakland and then optimized based on data acquired there. In subsequent phases these individual parts were combined in several designs to validate a complete instrument.

The basic components and final design are described in the following sections:

- Section 6.2.3 : Flow cell chip choice. A description of several chips available and the final choice based on size considerations and test results.
- Section 6.3.2.1: Media. This was chosen based on proper environment for the red cell suspension, optimal viscosity, pH and osmolality, including the design of a conductivity assessment to continuously measure osmolality to which the cells are exposed in the flow cell.

- Section 6.2.4 : RBC concentrations. The optimized concentration of the RBC suspension that provides proper diffraction of the laser and flow in the flow cell. Access to hematology instrumentation aided this optimization.
- Section 6.2.4 : Laser and detector, including optimization of optical pathway (orientation, distance of components)

Based on the optimized components and conditions, the individual parts were combined in several designs. Two distinct systems were successfully used: One employing an ARM microcontroller (LPC2148) communicating with a PC through a serial port, and another using National Instruments acquisition system (USB6009) communicating with the host PC through a USB port. Software was designed to collect relevant data from the different elements. Coding was done in embedded C, C++/CLI Visual Studio as well as LabView. These two systems were chosen to allow future inclusion in a commercial version of the final design. The software design includes sections for the alignment of the optics, measurement of the diffraction pattern, calibration of the conductometer, and measurement of the pressure gradient in the flow path.

In section 6.2.1 and 6.2.2 two designs are described:

The first is a complete instrument with software-driven automated plumbing to show that a small bench instrument could be built for automated measurement of small amounts of collected blood. While the basic automation was successful, the final measurement of the deformability curves was hampered by the noise in the data as the result of the pumps available for testing. No budget was available to provide optimized pump replacements, but this phase set the stage for a proposed design to create a small footprint automated FloDiF for clinical lab.

The second design shown (6.2.2) is a simplified version of the first. It does not include complete automation, but still allowed measurement of samples and comparison with the Technicon ektacytometer on the same samples of blood.

The experimental results (section 6.3.4) conducted on the second design, show that the basic principles as described in the previous chapters can be applied to a

practical set up that allows commercialization of a small, efficient and cost effective instrument for measuring the deformability of RBC in small blood samples. This potential instrument can be built on well accepted principles and components to gain regulatory approval. This is important as the final design provides opportunities for this novel instrument to be used in both a research and clinical lab setting.

6.2 Hydraulic system

The hydraulic system consists of the following units: the flow cell where measurements take place, the gradient generator where osmolality-increasing solution is prepared, the equilibration unit where RBC cells are mixed with the solution and allowed to equilibrate their internal osmotic pressure, and the flow generation units (air pressure unit and syringe pumps) (see Figure 44).

6.2.1 Initial design

Initially, the design contained quite a complex hydraulic system. This system was simplified at a later stage by discarding syringe pump B and valve B (as seen in Figure 42), which also improved pressure stability in the flow cell. Picture of the initial system hydraulic system is shown in Figure 41 and a schematic description of the initial experimental setup with its five states of operation are shown in Figure 42.

Flow direction is indicated by red arrows and valve open position is in green while close position is in red. Table 4 shows the settings of valves and pump direction (push or pull) as they are applied in states 1 to 5.

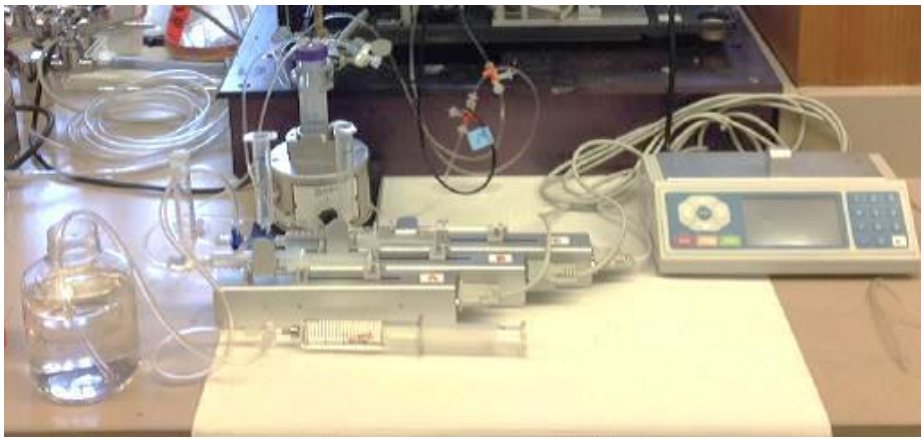

Figure 41: Picture of initial hydraulic system experimental setup.

The following schematics show the five states of operation of one experiment. By changing the valve settings, the syringe flow rate and flow direction, the process avoids opening any containers or plumbing, thus preventing pressure leaks. By replacing the manual valves with three way solenoid valves the system can be automated.

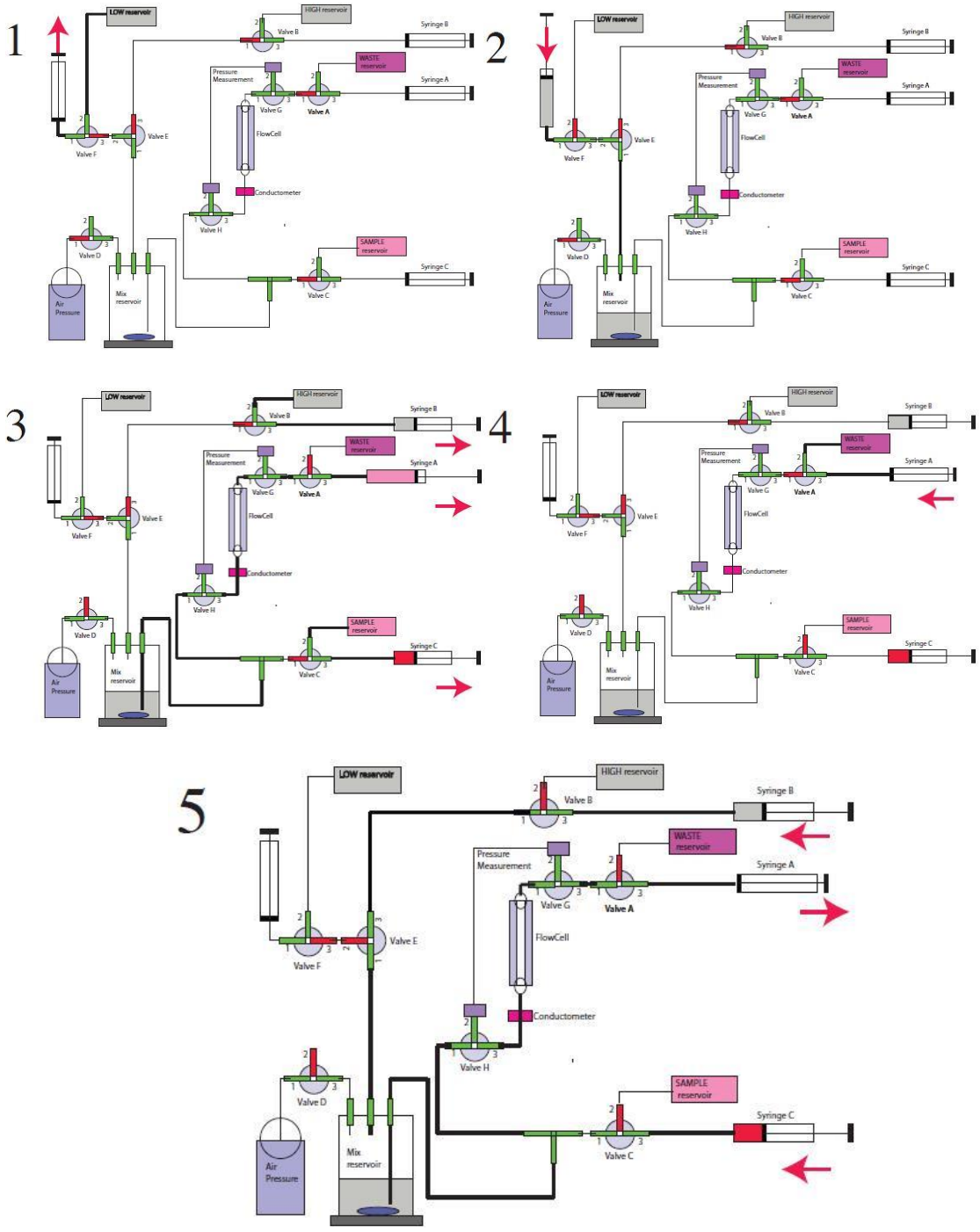

Figure 42: Five states of operation for one experiment:

<u>Step 1</u>- Fill the LOW syringe with hypotonic solution. <u>Step 2</u>- Put LOW (hypotonic) solution in the mix reservoir. Air pressure is off. <u>Step 3</u>- Fill syringe B with HIGH (hypertonic) solution, syringe C with blood sample diluted in ISO(isotonic) solution and start air pressure in order to fill the Flow Cell with LOW (hypotonic) solution. <u>Step 4</u> - empty syringe A to waste. <u>Step 5</u> - the actual blood test run. A gradually increasing osmolality solution is pushed by air pressure from the Mix reservoir to the flow cell. On its way, it is mixed with the diluted blood sample.

Table 4: The table indicates the settings as depicted in steps 1-5

VALVES: O= Open (green), X=Closed (red); PUMP: 1: push, 2: pull

step	VALVES																						PUMP SYRINGES			
	A			B			C			D			E			F			G			H			A	B	C	LOW
	1	2	3	1	2	3	1	2	3	1	2	3	1	2	3	1	2	3	1	2	3	1	2	3				
1	X	O	O	X	O	O	X	O	O	X	O	O	O	O	X	O	O	X	O	O	O	O	O	O				2
2	X	O	O	X	O	O	X	O	O	X	O	O	O	O	X	O	X	O	O	O	O	O	O	O				1
3	O	X	O	X	O	O	X	O	O	O	X	O	O	O	X	O	O	X	O	O	O	O	O	O	2	2	2	
4	X	O	O	X	O	O	X	O	O	O	X	O	O	O	X	O	O	X	O	O	O	O	O	O	1			
5	O	X	O	O	X	O	O	X	O	O	X	O	O	X	O	O	O	X	O	O	O	O	O	O	2	1	1	

6.2.2 Hydraulic system Second design

Experimenting with the initial design showed a problem with pressure stability in the flow cell. The problem arose from the fact of having two pressure sources in the flow line. One pressure source was the air pressure created in the mixing reservoir and the other was syringe A aspirating the solution (Figure 43). Having pressure and suction at the same time created pressure oscillations because of small difference in magnitude of flow created by each source. The syringe pump stepper motor added noise, with the stepper frequency, to the measured pressure. Eliminating syringe pump A solved the problem. The second design diagram and picture are shown in Figure 43 and Figure 44.

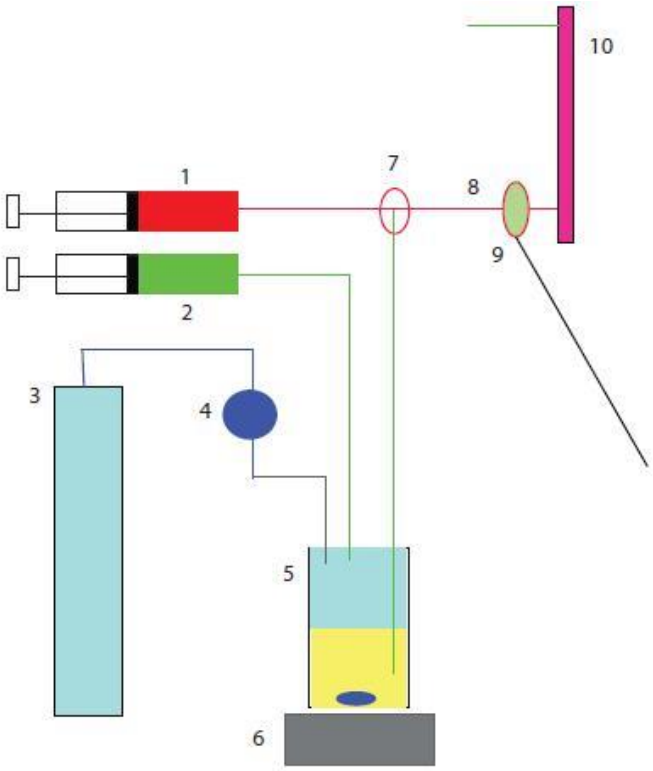

Figure 43: Second design improved hydraulic system
1: Syringe with sample blood in isotonic solution
2: PVP hypertonic solution
3: Air pump or compressed air tank
4: Pressure regulator
5: Airtight Vessel
6: Magnetic stir
7: T connection
8: Tubing of set length to equilibrate cells to osmolality
9: Conductivity and temperature sensors
10: Flow cell

Description of the hydraulic system as shown in Figure 43:

1: Syringe with blood diluted in isotonic PVP solution 290 mOsmol/kg. Rate of flow set by dual channel syringe pump rate and syringe diameter

2: PVP high osmolality solution. Rate of flow set by dual channel syringe pump rate and syringe diameter

3: Air pump or compressed air tank.

4: Pressure regulator: ControlAir Inc. Type 700

The gas pressure in 5 is tightly maintained by setting the pressure regulator 4 properly.

5: Airtight vessel.

6: Syringe 2 drops high osmolality solution to the low osmolality solution that is present in 5 and mixed with magnetic stir. The gas pressure in 5 pushes the fluid towards 7. Using syringe 2 makes sure that dropping of hypertonic solution will happen at the same rate independent of pressure in 5.

7: T where RBC from syringe 1 meet (case A: Osmoscan), or do not meet (case B: Shear scan) fluid from 5.

A: Osmotic deformability measurement: Ratio of flow from 1 and 5 determines hematocrit in the flow cell. Total flow rate (1+5) determines shear. This total flow, mainly determined by 5 (as that is the main contributor) with 1 as addition should be set constant. Also flow rate 1 << 5, to generate proper osmolality gradient.

B: No flow from 5 allows different rates from 1 for the measurement of deformability at different shear with set osmolality or fragility measurement.

8: The length of this tube together with flowrate determines the time that the RBC has to equilibrate (take up, or lose water).

9: Conductivity measurement. There is a small offset between measurement here and actual osmolality at measuring point. However this can be calibrated for a given flowrate. Importantly by filling 1,2 with known osmolalities we can calculate the change of osmolalities in time given a set low start volume.

10: Flow cell

Figure 44: Hydraulic system of the second design

6.2.3 Flow cell choice

Several microfluidic channel (slides) producers were considered:

- Ibidi Am Klopferspitz 19 D-82152 Martinsried (Munchen) Germany
- Microfluidic ChipShop GmbH Stockholmer Str. 20 D - 07747 Jena Germany

These two producers produce off the shelf, inexpensive, transparent polymer channels in a microscope slide size. Luer connector interface facilitates manipulation. While Microfluidic ChipShop have only one depth channel (150µm), Ibidi have a choice of four different channel depths (100µm, 200µm, 400µm and 800µm) and four other sizes if a line of « sticky slides » is used (150µm, 250µm, 450µm, 850µm). Since I was not sure about the optimal channel dimensions, I decided to use Ibidi slides. Another advantage of Ibidi slides is that their W/H channel dimensions ratio is double that of Microfluidic ChipShop channel (W=5mm compared to 2.5mm). This feature gives a shear field closer to unidirectional (this issue is discussed in section 3.5).

Ibidi give constants for their slides that allow calculations of wall shear stress (τ_w) with respect to flow rates (*Shear Stress and Shear Rates for ibidi µ - Slides - Based on Numerical Calculations*, Ibidi application note 11). Since we want to achieve an

average shear stress equal to that used in the Technicon Ektacytometer in osmoscan mode, we use these constants (k) in Equation 41 in order to calculate the flow rates (Q), necessary in our experiments. The constants are given (with no units specified) so they yield flow rates in ml/min. In order to stay in international units we use k'=60· k which is the value given by the manufacturer multiplied by 60.

Equation 41

$$Q = \frac{\tau_w}{k'\mu} = \frac{2\tau_{avg}}{k'\mu}$$

The units used for Equation 42 are as follows:

Q - Flow rate (cm^3/s)

$\tau_w = 2\tau_{avg}$ - wall shear stress (Pa) (identical to $kg/m{\cdot}s^2$)

μ - Viscosity (Pa· s)

k' - Slide constant ($1/cm^3$)

The average shear stress we want to achieve is τ_{avg}= 16 Pa (τ_w=32 Pa) (see calculation at the end of section 3.3). We calculate flow rates for each Ibidi channel (0.2mm, 0.15mm and 0.1mm) and for two viscosity (μ) values 0.02 Pa·s and 0.03 Pa·s. Once we get the flow rates, we can calculate the pressures necessary in order to achieve these flow rates using Equation 42 (L=50 mm, W= 5mm). So for each channel height, we get the flow rates and the pressures using two different solution viscosities.

Equation 42

$$\Delta P = \frac{12\mu LQ}{WH^3}$$

The units used for Equation 42 are as follows:

ΔP – Pressure (Pascal)

μ - Viscosity (Pa· s)

Q - Flow rate (m^3/s)

L,W,H - slide dimensions (m)

We also calculate the length of a tube of 1.6 mm ID, necessary in order to equilibrate the cells for osmolality variations (between the T and the channel. See Figure 43). We use 20 seconds as a reference time for osmotic cellular equilibration (which is the same as the Technicon Ektacytometer). The necessary tube length is calculated from the flow rates column.

We can calculate the fluidic resistance of the channel, and assuming adapters and tubing leading to the channel have much lower fluidic resistance, we can use this value to convert measured pressure to flow rate. Fluidic resistance is calculated in the last column. Note that the 0.15 mm slides are actually 0.1 mm sticky µ-Slide I Luer, intended to be fixed on a standard microscope slide. The additional height comes from the thickness of the sticky film.

Table 5: Calculated flow rates, pressures and tube lengths for three different height Ibidi slides (L=50mm, W= 5mm). See more details above.

µSlide	Viscosity	Flow Rate	Flow Rate	Pressure	Tube length	Slide constant k'
mm	Pa·s	cm^3/s	ml/min	Kpa	cm	$1/cm^3$
0.2	0.02	0.0520	3.120	15.60	51.717	30774.00
0.2	0.03	0.0347	2.080	15.60	34.478	30774.00
0.15	0.02	0.0294	1.766	20.93	29.278	54360.00
0.15	0.03	0.0196	1.177	20.93	19.519	54360.00
0.1	0.02	0.0132	0.790	31.60	13.096	121530.00
0.1	0.03	0.0088	0.527	31.60	8.731	121530.00

6.2.3.1 Selecting the optimal slide dimensions for this work.

The selection of the slide determines the range of shear stress that can be applied. In our case, since we wish to compare our results to those obtained by the Technicon Ektacytometer in osmoscan mode, we use the same magnitude of shear stress which is 16 pascal (as calculated at the end of section 3.3). From Table 5 we see that for a 0.1mm height channel the flow rate is a quarter of the flow rate in a 0.2 mm channel. The lower flow rate presents an advantage of using smaller quantities of blood and solutions. However, the lower channel height (of 0.1mm) has more important dimensional variations, compromising reproducibility.

According to the manufacturer, ibidi Luer slides are made of a polyethylene-derivative with linear expansion coefficient of 7x10-5 cm/cm·°C (method: ASTM D696). This makes a negligible expansion of height of 0.007 µm/°C, for the 0.1 mm channel and of 0.014 µm/°C for the 0.2mm channel. Variation of height within one batch for µslide I 0.1mm is +/-13% and µslide I 0.2mm is +/-5%.

Table 6 shows dimensions of three different flow cells from the same batch as provided by the producer. In order to minimize errors due to variations in channel height it is necessary to measure flow rate each time the flow cell is replaced. This way it's possible to compensate variations in channel height by variation in pressure in order to keep shear stress constant (see Equation 22 section 3.5). Another option would be to pre-select channels within a certain height tolerance. In conclusion, 0.1 mm height channel is preferable for our application.

Table 6: Channel height measurements, within same batch, for Ibidi µ-Slide I (provided by Ibidi)

	µ-Slide I Luer (standard bottom)					µ-Slide I Luer sticky (assembled by hand)			
Target height	100µm	200µm	400µm	600µm		100µm	200µm	400µm	600µm
Measured height in µm	87.7	196.8	399.2	602.8		152.4	268.3	461.25	656.98
	87.6	192.8	402.1	600.4		146.6	269.7	464.00	653.13
	87.3	195.4	399.8	605.0		150.8	269.7	466.80	653.53

6.2.4 Optical system

The optical system consists of the HeNe 632.6 nm laser source, the adjusting mirrors, the microchannel diffraction unit and the photodetector measurement unit

(Figure 45 to Figure 47). In order to eliminate possible sources of errors due to stability and collimation of the laser beam, we chose to use a Helium-Neon laser source for our prototype. Once a proof of principle is established, a small footprint laser diode can replace the HeNe tube. The vertical position of the flow cell is advantageous for a quick air bubble evacuation. The filter covering the photo-detector is a 10 nm narrow filter which eliminates ambient light influence on measurements.

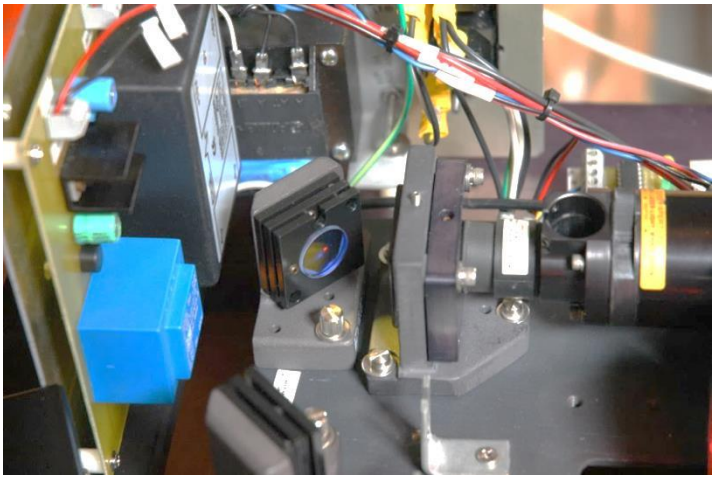

Figure 45: Laser tube with optical system. The laser light path can be adjusted with two mirrors (vertical/horizontal) adjusted by set screws.

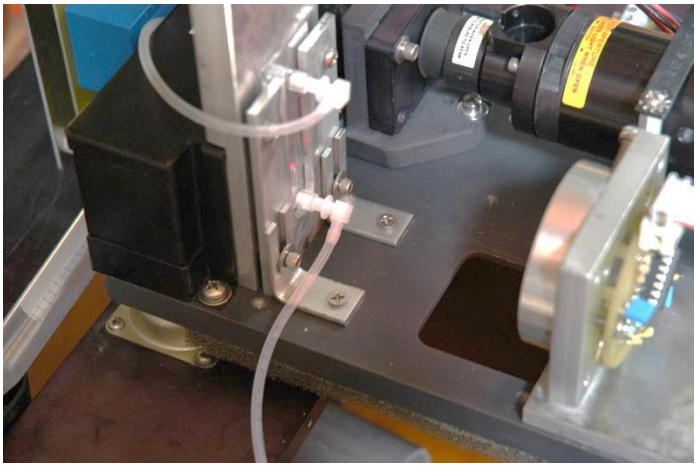

Figure 46: Flow cell with bottom feed line and top waste line. Flow cells can be easily switched out by loosening screws of the cell holder and sliding in or out.

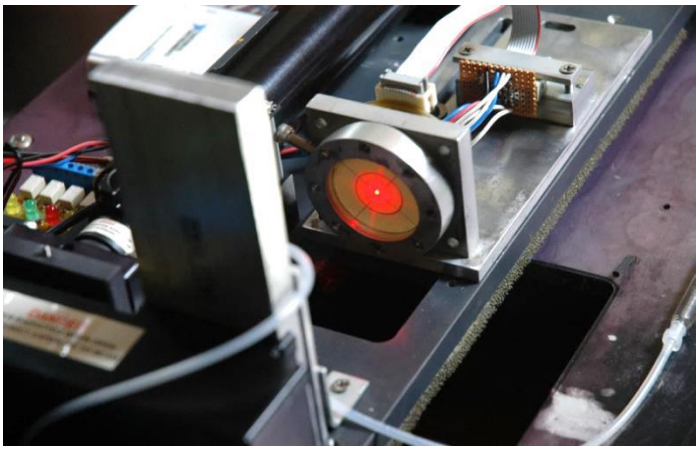

Figure 47: Four quadrant detector on sliding base. The detector front is covered with a filter.

6.2.5 Hardware composition

6.2.5.1 Analog to digital (A/D) conversion unit

We use analog sensors for measurement of conductivity and light intensity. The signals generated are conditioned and amplified in order to generate voltages in levels required by the A/D converters inputs. A/D converters are used in order to allow the use of the measured analog data by the computer. Two distinct A/D systems were used. One employing an ARM (LPC2148) microcontroller equipped with a 10 bit resolution A/D converter sending conductivity, pressure and four photodiode readings to the host PC through a serial port (Figure 52), The second A/D system using National Instruments acquisition system with a 12 bit resolution A/D converter (USB6009) sending the same measurements from the sensors to the host PC through a USB port (Figure 48). These two systems were used alternatively according to the software option chosen: Labview or the custom software application. Further information can be found in section 6.2.6 describing software.

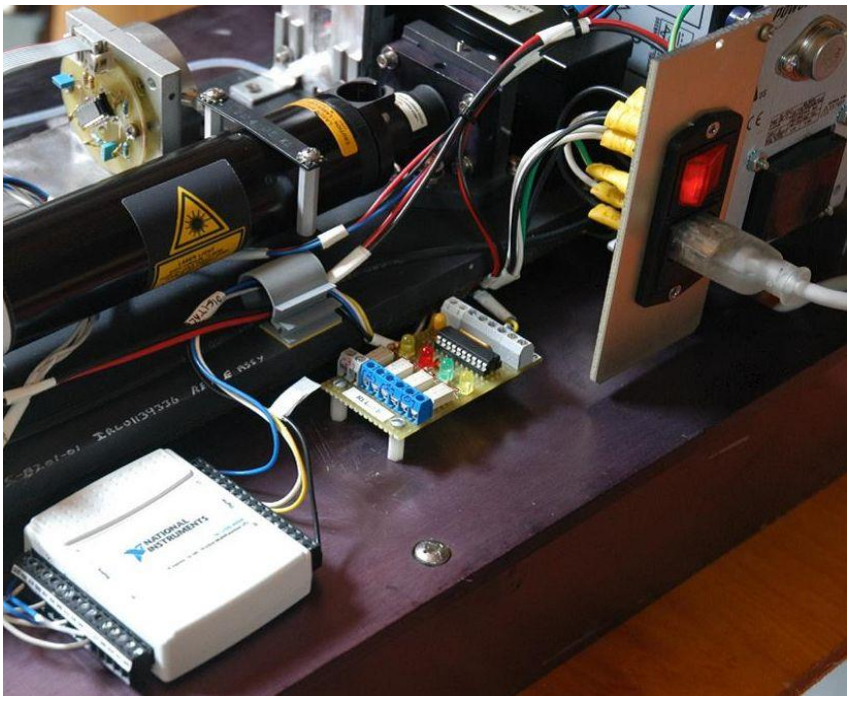

Figure 48: Analog to digital conversion unit (NI USB6009) with relay card for solenoid valve automation.

6.2.5.2 Conductivity measurement

Osmolality measurement is necessary in order to produce osmotic scan curves, where RBC deformability is depicted with respect to osmolality. The usual way to measure osmolality is either by a freezing point depression or a vapour pressure depression osmometer. These techniques are expensive and difficult to implement in a small footprint instrument. We use, instead, conductivity measurement as an indicator for the osmolality of our solutions. The ability of a solution to conduct electricity depends on its ionic character and the solute concentration. Our solution's osmolality is dominated by variation in Sodium chloride (NaCl) concentration. All other components in the solutions have constant concentrations throughout the measurement (see section 6.3.2.1). A calibration procedure records conductivity with respect to calibrated solutions in seven different osmolalities (see 6.3.3 Osmolality calibration). A second order polynomial approximation gives the approximation parameters for calculation of osmolalities between the values of calibrated points (Figure 58). In the first stage a conductivity cell using two electrode platinum wires, and a 10kΩ NTC temperature sensor, were placed in a

measurement unit connected in the flow line very close to the channel (Figure 49 right). This was later replaced by two platinum wires introduced into the channel serving as the electrodes of the conductivity measurement cell. In order to avoid electrolysis, the circuit injects into the measured solution, a low level alternating voltage of 1.5 KHz. The voltage drop between the electrodes depends on the solution conductivity. This signal is fed to a log amplifier, then rectified and followed by an integrator. The last stage of the circuit compensates the measured values for temperature variations with the help of a signal obtained by a negative temperature coefficient sensor (NTC) introduced in the flow channel. The conductivity board and sensors are shown in Figure 49. Table 7 shows the relation between conductivity and output voltage for the conductivity board. A variable resistance (potentiometer) was connected instead of the conductivity cell and a precision voltmeter was connected at the output. The potentiometer was adjusted to give several output levels. The resistance was measured for each given voltage. All measurements were conducted in a controlled room temperature of 25°C.

Table 7: Conductivity board Voltage measurement for several conductivity values

Resistance (Ω)	Conductivity ($m\Omega^{-1}$)	Voltage (volts)
20000	0.050	0.120
10000	0.100	0.150
5870	0.170	0.300
3471	0.288	0.600
2274	0.440	1.000
800	1.250	2.997
456	2.193	5.000
256	3.906	7.990
186	5.376	10.000

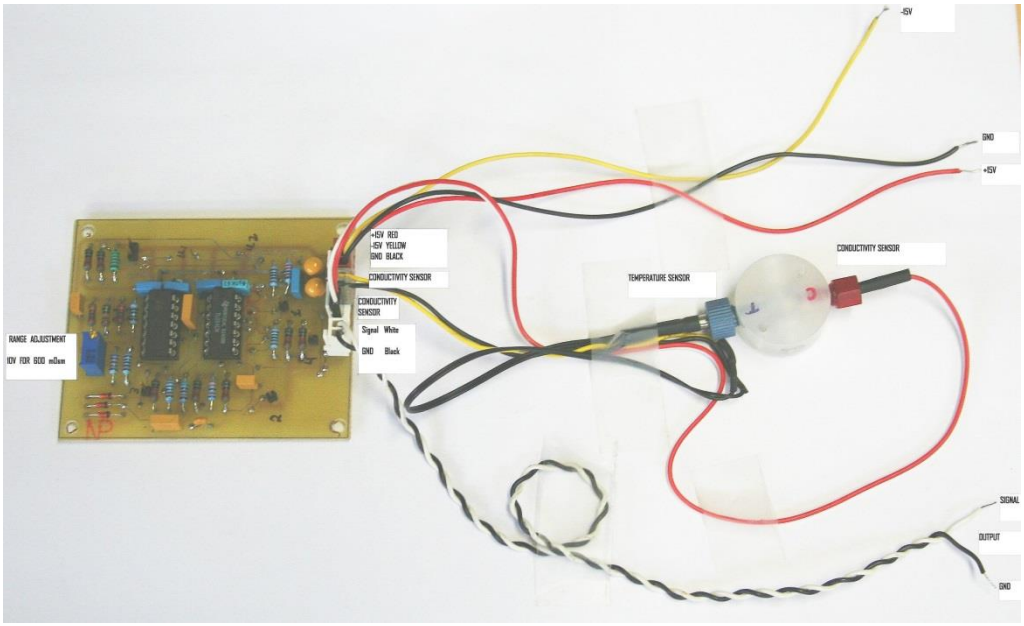

Figure 49: Conductivity measurement card with conductivity and temperature measurement unit. The conductivity measurement unit was integrated into the flow cell at a later stage.

6.2.5.3 Optodetector unit

The Optodetector unit (Figure 50) has a four quadrant detector measuring light intensities in four separate zones (Figure 51 left). The detector is placed behind a mask with four holes allowing measurement of light intensity at four points equidistant from the center of the laser beam (Figure 51 right). A narrow band pass filter protects the sensor readings from errors corresponding to ambient light. Transimpedance amplifiers convert the low currents generated by the photodiodes into voltage levels between 0 and 10V.

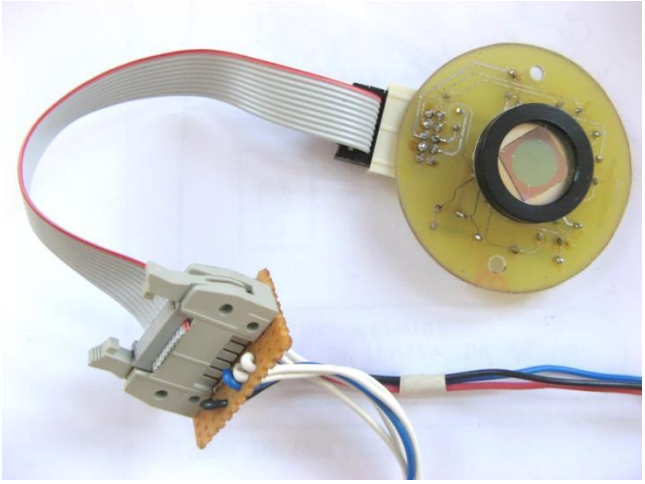

Figure 50: Four quadrant detector circuit

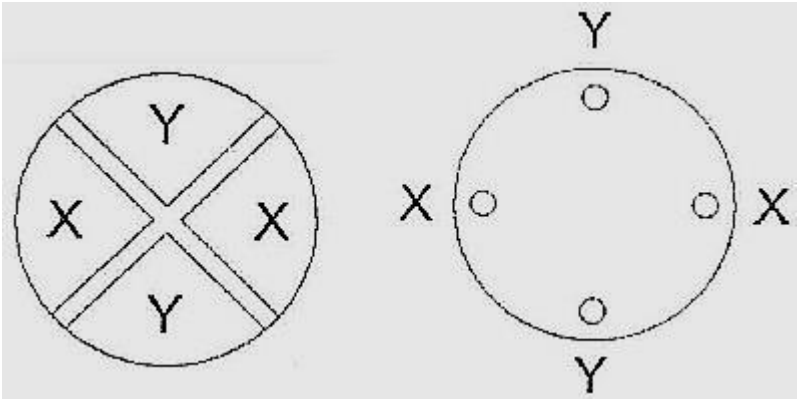

Figure 51: Orientation of the four quadrant detector (left) and its mask (right)

6.2.5.4 Microcontroleur board

An ARM LPC2148 microcontroller produced by NXP is used for the control, measurements and communication with a host PC. This microcontroller has 14 inputs of 10 bit A/D converter as well as one 10bit D/A output for eventual pressure control. The inputs are used to measure conductivity, pressures and four levels of voltages coming from the four quadrant detector unit, and two voltages from pressure sensors. It has both a serial port and a USB port to allow communication with the host PC.

Embedded artists quickstart prototype board was chosen for development since it has a large breadboard area allowing the placement of the conductivity board as well as analog inputs interface circuit (placed below the conductivity board). See Figure 52.

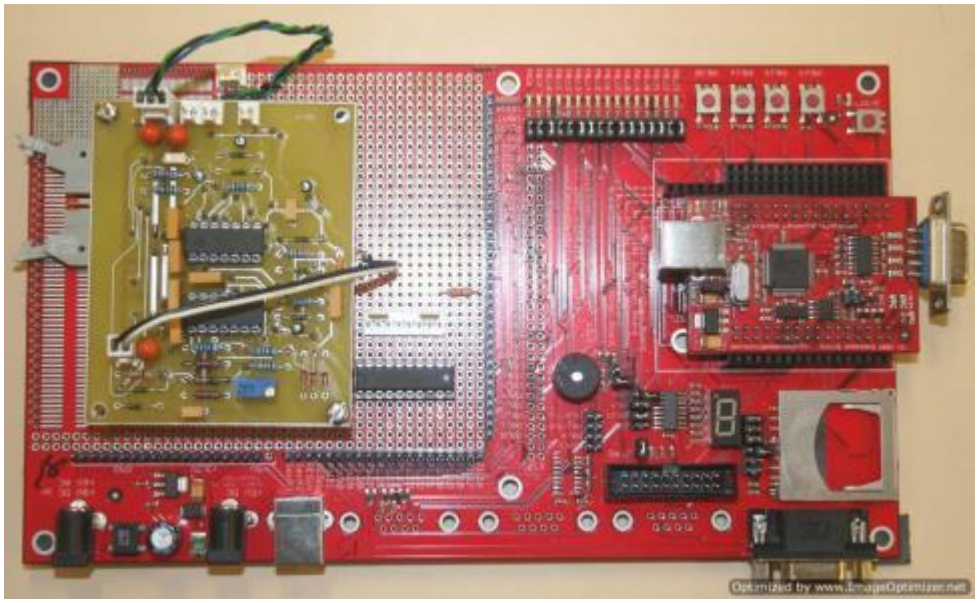

Figure 52: ARM LPC2148 microcontroller board (right), conductivity measurement board (left) and quadrature photodetector analog interface (on breadboard)

6.2.5.5 Power supply unit

The power supply is composed of three units. The switching power supply of 12V is designed to provide power to the valves and pressure pump. An analog +/-15V symmetric low noise power supply provides power to the opto-detector unit (5mA), the conductivity measurement board (19mA) and the pressure sensors (13mA). A 5V power supply provides power to the Microcontroller board and the Relay board. The power supplies are seen in Figure 53 and Figure 54. The HeNe laser tube and the syringe pumps are powered by their own dedicated power supplies.

Figure 53: Analog power supply unit with 5V and +/-15v, powering the four quadrant detector unit, the conductivity measurement circuit and the pressure sensor card.

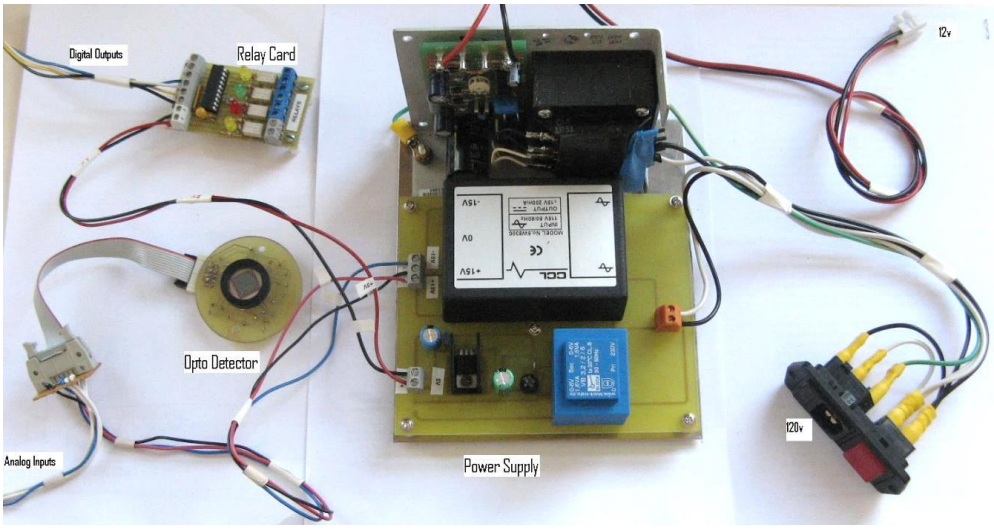

Figure 54: Analog and switching power supplies, photodetector card and relay card

6.2.5.1 Pressure measurement card

The pressure sensors were introduced in order to allow close monitoring of pressure during experiments, and eventually a feedback controlled pressure pump system.

Two pressure sensors are used. One for the source pressure measurement and one for the pressure drop on the microchannel. Since the pressure on the channel determines the shear stress on the flow cell, I chose a higher precision Honeywell sensor (HSCDRRT005PG2A5) with a totale error inferior to +/- 0.25% of full span. The source pressure is measured by a cheaper Motorola sensor (MPXV5050DP) with a totale error inferior to +/- 2.5% of full span.

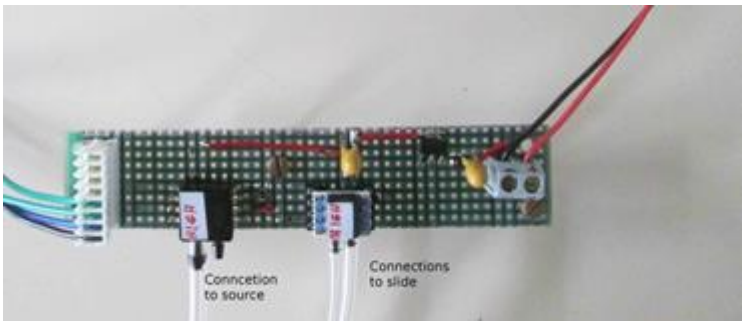

Figure 55: Pressure Sensors Card

Calculations of pressures from measured voltages are done as follows:
- for the Freescale sensor V_{i0} the measured voltage is

$V_{i0} = V_s \cdot (P \cdot 0.018 + 0.04)$

Where V_s=5V. P is in kPascal.

So $P = ((V_{i0}/5) - 0.04)/0.018$ (in kPascal)

- for the Honeywell sensor Vi1 the measured voltage is

$V_{i1} = P \cdot (0.8Vs)/Pmax + 0.1Vs$

Where Vs= 5v and Pmax = 5 PSI

So $P = (Vi1/5\text{-}0.1) \cdot 5/0.8$ (in PSI)

In order to validate the pressure measurement chain I connected a needle gauge pressure meter and the two pressure sensors to the same pressure source. The pressure source was a Xavitech V200 Pump. Table 8 shows the pressure measured by the three options for different values set by the pump. The needle gauge scale was in Cm/Hg while the sensors output was in Volts. Freescale specifies the formula to convert Volts to pressure in kPascal while Honeywell's conversion formula gives pressure in PSI. Columns 3, 6 and 9 show calculated values, all in kPascal for the sake of comparison. Since the data sheets for the sensors give detailed information about precision and temperature drift of the sensors, we didn't need to go through repetitive set of measurements and statistical calculations.

Table 8: Comparison of pressure measurements between a needle gauge and two pressure sensors used in our experiments. All three were connected to the same pressure source controlled by an adjustable pressure regulator. See calculation formulae above.

Pressure (needle gauge)			Freescale Vi0	Freescale P		Freescale P	Honeywell Vi1	Honeywell P	Honeywell P
Cm/Hg	psi	kPa	Volts	psi		kPa	Volts	psi	kPa
5	0.967	6.666	0.8	0.967		6.667	1.275	0.969	6.679
10	1.934	13.332	1.403	1.939		13.367	2.055	1.944	13.402
15	2.901	19.998	1.99	2.885		19.889	2.804	2.880	19.857
20	3.867	26.664	2.61	3.884		26.778	3.605	3.881	26.760
25	4.834	33.331	3.258	4.928		33.978	4.42	4.900	33.784
27	5.221	35.997	3.47	5.270		36.333	4.71	5.263	36.284
* Pressure source is Xavitech Pump V200									
* * Both sensors connected to same pressure with T connection									

6.2.6 Software

Two distinct options were designed. These systems were chosen to allow future inclusion in a commercial version of the final design.

One system has an integrated microcontroller communicating with a host PC with a user interface program. Crossworks for ARM microcontroller, by Rowley was used as the embedded C development environment on a PC. The Rowley CrossConnect

Jtag adapter was used to program and debug the board. The ARM program (ArmEkta) reads analog inputs from the conductivity, pressure and optodetector boards and sends them to a PC through a serial port.

Microsoft Visual Studio 2010 was used to develop the user interface program (WinEkta). This program communicates with the microcontroller board. It converts the conductivity into osmolality, and the four quadrant detector readings into deformability index. The resulting curve is presented on the computer screen as the blood test progresses, and finally stored on the hard disk. It allows comparison of curves and indicator points calculations. Figure 56 shows the software application in comparison mode displaying two curves of the same blood sample taken before and after calibration.

In the second option, reading of conductivity, pressures and optodetector measured signals is performed by NI USB6009 A/D acquisition unit communicating with Labview program on a host PC, through a USB port (Figure 48 and Figure 57).

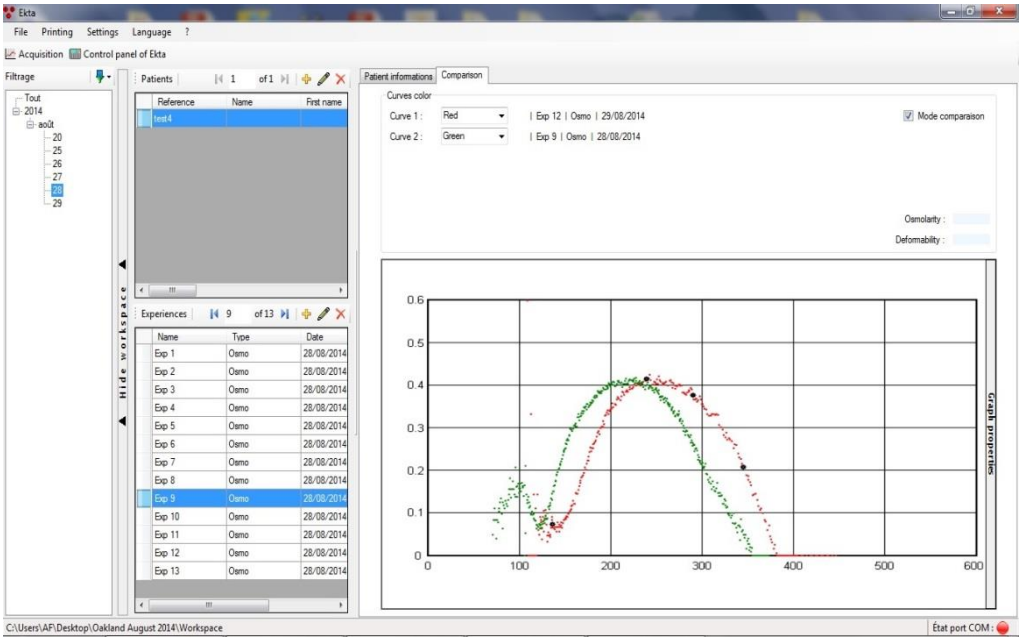

Figure 56: Screenshot of WinEkta Program

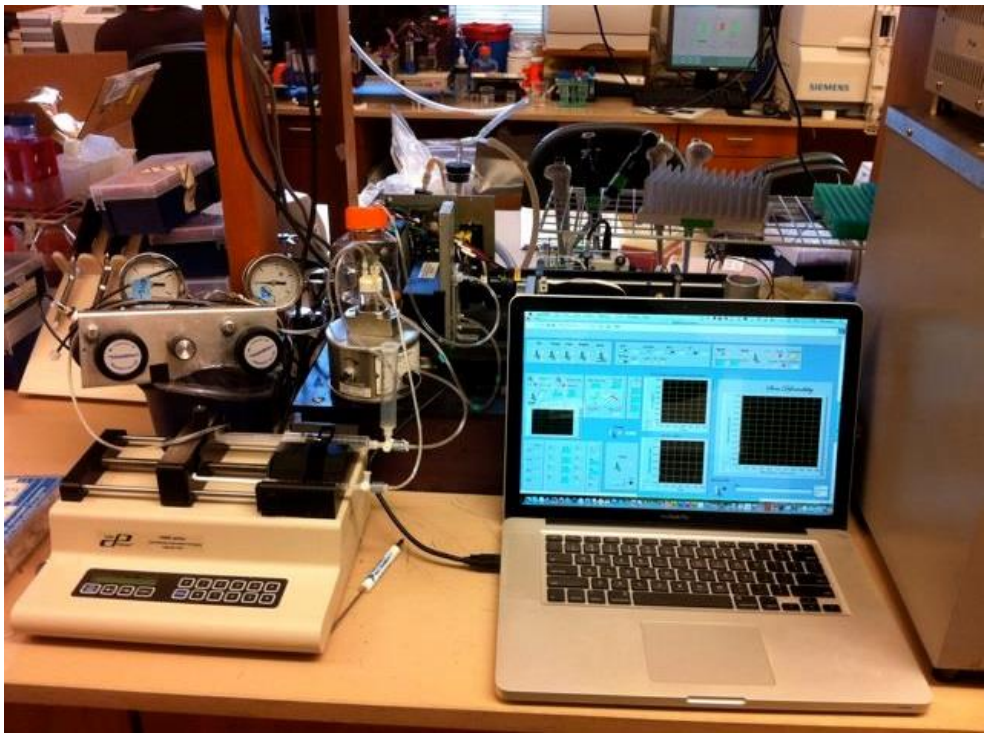

Figure 57: Computer program for user interface using Labview

6.3 Proof of principle

6.3.1 Sample preparation

Venous blood sample was obtained from a healthy volunteer. Two 6 ml tubes with ACD-B solution where used and kept refrigerated for the three days of experiments

6.3.1.1 Estimation of dilution rate of blood

Experiments performed on a Couette cylinder Ektacytometer equipped with a four quadrant detector, show negligible errors due to variations in cell concentration and in mean cell hemoglobin content (MCHC) (Groner et al., 1980; Mohandas et al., 1980). However, in order to be able to validly compare results between the microfluidic device and the Technicon Ektacytometer, we aimed to have, using both devices, approximately the same number of cells in the volume of solution exposed to the laser beam. Since we used laser beams of roughly the same diameter and intensity, we could increase the hematocrit by the ratio of the gap size between the

Technicon cylinders divided by the microchannel height. So for a 0.1 mm height microchannel, compared to a 0.5mm gap between the cylinders, we need 5 times higher hematocrit. The solution containing whole blood, introduced into the Technicon viscometer is at a hematocrit of approximately 0.08%, thus we need to use in the microchannel blood at hematocrit of around 0.4%. That makes a dilution of whole blood at a rate of around 1 to 100 compared to 1 to 500 dilution in the Technicon Ektacytometer. We can estimate the number of cells diffracted by the laser beam. The number of RBC in normal blood is around 5 million per µl. Since we dilute blood by 100, while using the microchannel, we have 50 thousand cells per µl. The volume exposed by a 1mm diameter laser beam in a channel of 0.1 mm height is: $0.1 \cdot \pi \cdot 0.5^2$ mm^3 = 0.0785 µl. So the number of cells exposed to the laser beam is $5 \cdot 10^4 \cdot 0.0785 \sim 3926$. The actual amount of blood used and required in the experiments described in section 6.3.4, is 70 µl. This can be further reduced by increasing the laser intensity.

6.3.2 Solution preparation[9]

Three kinds of aqueous solutions are used in osmotic gradient ektacytometry: hypotonic, isotonic and hypertonic. Isotonic solution is used as the sample diluent in Shear Scan mode and as pre-diluent in Osmoscan mode. The hypotonic and hypertonic solutions are used in order to create osmolality gradient for Osmoscan mode.
Polyvinyl Pyrollidone (PVP) is a polymer used to achieve the necessary viscosity.
Sodium chloride (NaCl) is used to achieve the right tonicity.
Dibasic and monobasic anhydrous sodium phosphates (Na2HPO4, NaH2PO4) are used to achieve the right pH ("Technicon Ektacytometer User's manual,").

[9] In many publications Dextran is used as an alternative thickening polymer instead of PVP (Groner et al., 1980; Kuypers et al., 1990)

6.3.2.1 Reagents[10]

1. Low (hypotonic) solution

   31.0g - PVP K90 (MW360.00)

   0.90g - Na2HPO4

   0.24g - NaH_2PO_4

   Add distilled water to a final volume of one liter.

   Specifications:

Osmolality	40 ± 5 mOsm/kg
Viscosity	20 ± 1 centipoise @ 22 °C
pH	7.35 ± 0.05

2. Sample (isotonic) solution

   31.0g - PVP K90 (MW360.00)

   0.90g - Na_2HPO_4

   0.24g - NaH_2PO_4

   7.938g - NaCl

   Add distilled water to a final volume of one liter.

   Specifications:

Osmolality	290 ± 5 mOsm/kg
Viscosity	20 ± 1 centipoise @ 22 °C
pH	7.35 ± 0.05

3. High (hypertonic) solution

   31.0g - PVP K90 (MW360.00)

   0.90g - Na_2HPO_4

   0.24g - NaH_2PO_4

[10] Based on ("Technicon Ektacytometer User's manual," n.d.).

22.428 g - NaCl

Add distilled water to a final volume of one liter.

Specifications:

Osmolality	750 ± 10 mOsm/kg
Viscosity	20 ± 1 centipoise @ 22 °C
pH	7.35 ± 0.05

6.3.3 Osmolality calibration

Osmolality calibration is achieved by measuring conductivity for several calibration solutions of known osmolality. Curve fitting is performed by using the measured calibration points. The coefficients obtained are stored and used to determine osmolality from measured conductivity during experiments.

Calibration solutions are obtained by mixing high and low solutions in ratios specified in Table 9.

Table 9: Composition of calibration solutions

Final Osmolality	%LOW (40 mOsm/kg)	%HIGH (750 mOsm/kg)
40	100	0
100	91.6	8.4
150	84.5	15.5
200	77.5	22.5
300	63.4	36.6
400	49.3	50.7
750	0	100

Using the calibration solutions and distilled water, I measure conductivity at 8 points. Measurement values are shown in Table 10. Measured conductivity values are the output of a 10 bit analog to digital converter.

Table 10: Measured values for osmolality calibration

Osmolality	Conductivity
750	1023
400	758
300	654
200	502
150	400
40	80
0	24

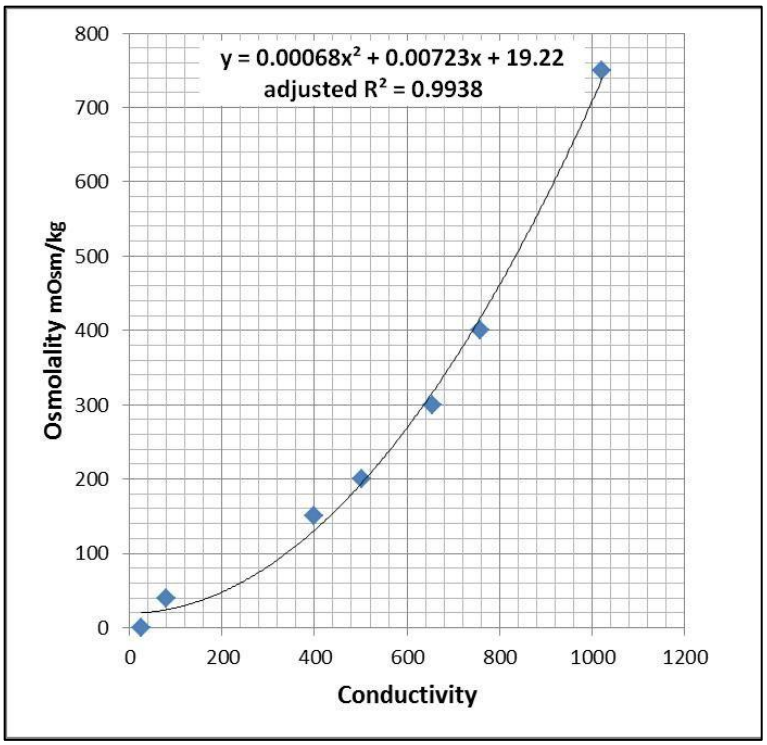

Figure 58: Osmolality calibration curve obtained from Table 10

6.3.4 Osmoscan curves

Figure 59 shows curves of three experiments (green purple and blue). We can see that the curves nearly overlap.

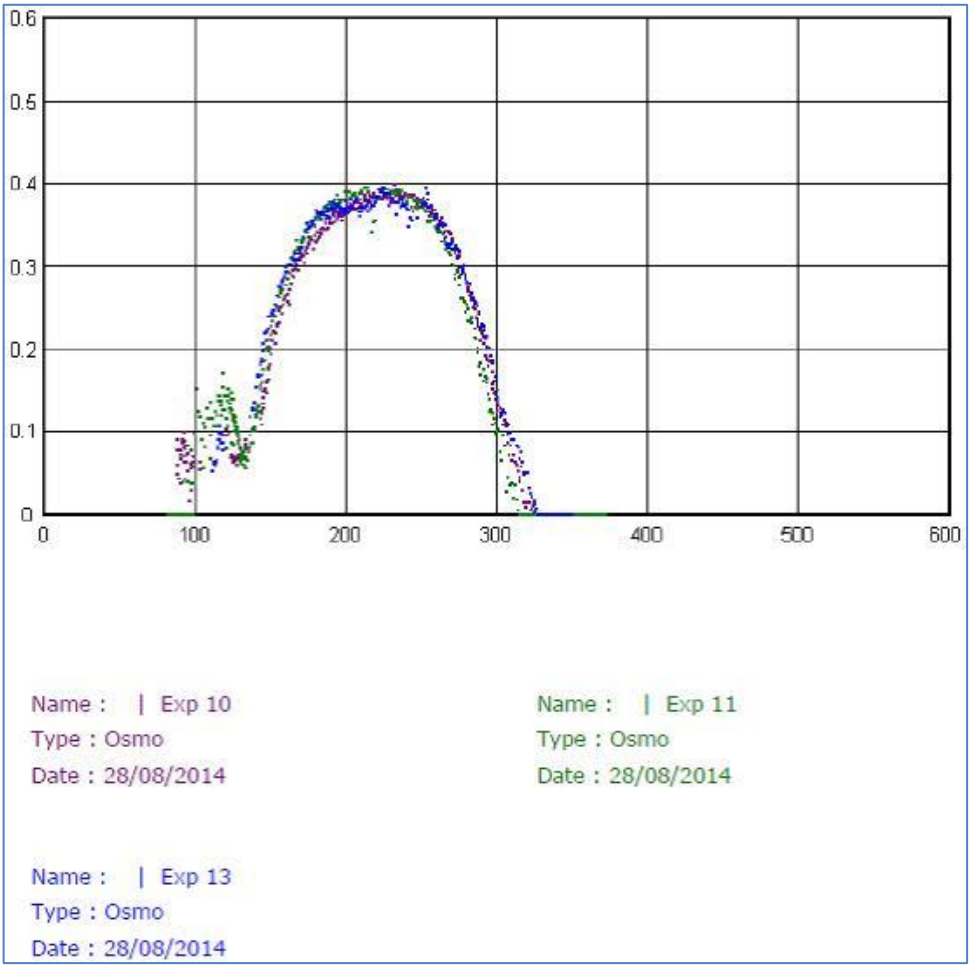

Figure 59: Curves obtained on the 0.1mm flow cell before osmolality calibration. We can observe a good repeatability between the blue, green and purple curves. Pressure on channel is 2.5 psi.

Figure 60 shows an experiment with 0.1 mm flow cell, after osmolality calibration. The duration of the experiment was 7 minutes. Pressure on the channel was 2.84 psi Solutions consumption was: Sample 1 ml (composed of 300µl of blood per 10ml of isotonic solution), High 1.5 ml, and Stir Tank 3 ml. The recommended 2:1 flow

relations of stir tank outflow to high solution inflow, was respected. Consumption of blood in this experiment was 30 µl.

Figure 61 shows results obtained by the Technicon Ektacytometer on the same blood sample used in Figure 60. In order to facilitate the comparison of the results obtained by these two methods, three indicator points are calculated and marked on each curve, as shown in section 4.3 Figure 35: Hypotonic point where deformability is minimal in the hypotonic osmolality region, Maximum point where deformability reaches its maximum and Hypertonic point where deformability has a value of half of maximum point. The designers of these methods chose different denominations for these same points. These points are marked Hypo, Max and Hyper in Figure 60 and Omin, DImax and Ohyp in Figure 61.

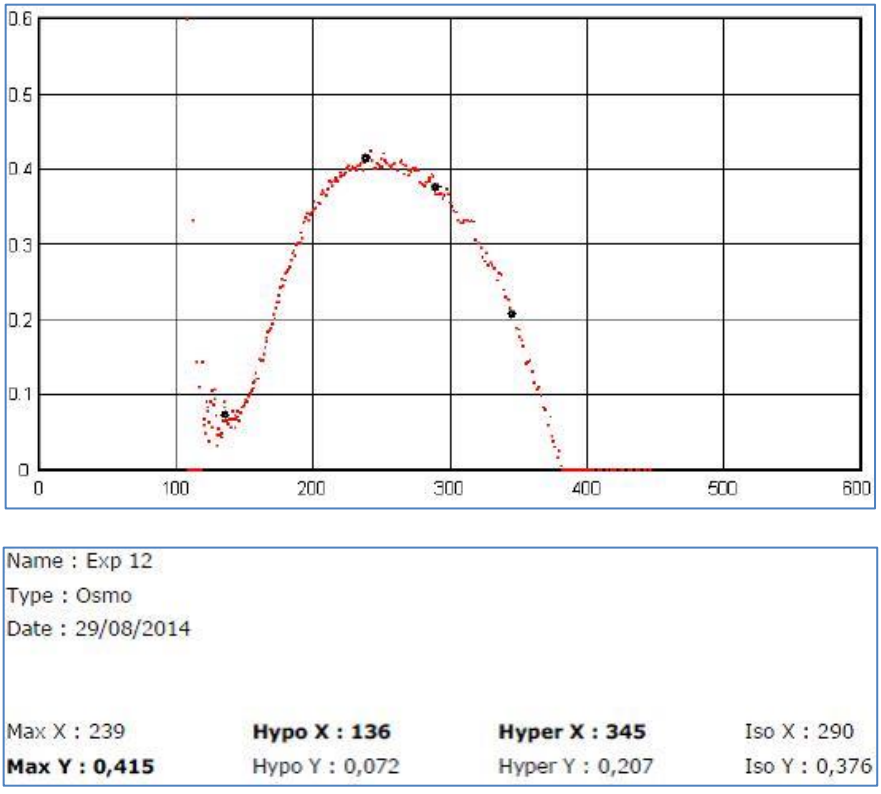

Figure 60: Curve obtained on the flow cell of H=0.1mm after osmolality calibration. Pressure on channel is 2.84 psi.

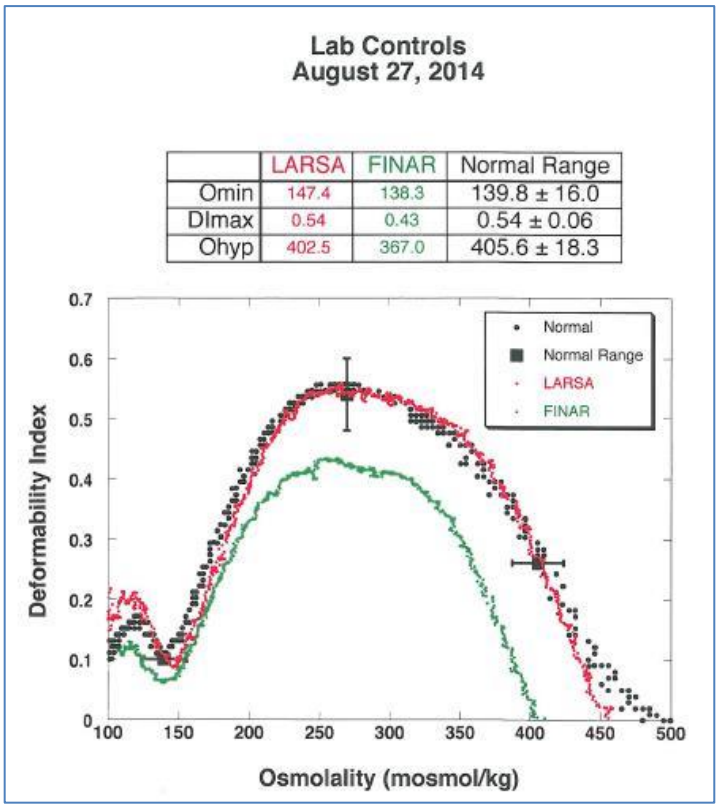

Figure 61: Curve obtained on the Technicon Ektacytometer. Green curve shows the test curve while the red curve is a normal control curve.

The dispersion of points on the left of the curves in Figure 59 and Figure 60 results from the fact that flow of sample was started too late. A low concentration of cells at the beginning gives this dispersion.

Table 11: Comparing the indicator points on curves in Figure 60 and Figure 61 for the same blood sample obtained by the Microchannel device and the Technicon ektacytometer

Point on Curve	Microchannel	Technicon Ektacytometer
Omin = Hypo	136	138.3
DImax = Max	0.415	0.43
Ohyp = Hyper	345	367

6.4 Conclusions

A microfluidic Osmotic Scan Ektacytometer was designed and built as a prototype. Unlike in a Couette cylinder Ektacytometer, where shear stress is constant across the gap between the cylinders, a cell population flowing in a microfluidic channel is subjected to a linear distribution of shear stress across the channel. For this reason, comparing results of both methods should be conducted with special care. Equation 22 in section 3.4 shows that in order to have the same average shear stress in both techniques the value of wall shear stress, in a micro-channel, should be double of that normally used in the Couette cylinders. Since the distribution of sheer stress across the channel and across the gap between the cylinders is very different, an experimental proof of principle was necessary in order to validate results obtained by a microfluidic osmotic scan Ektacytometer.

Osmoscan curves, obtained by the FloDif are comparable to these obtained by the Technicon Ektacytometer, under equal average shear, for one blood sample. Both the curve shape and magnitudes are very close (Figure 60 and Figure 61). A comparison of indicator points on both curves is shown in Table 11. The osmolality of the minimum point (LP point marked Omin or Hypo), the osmolality of the maximum (MP point marked DImax or Max), and the decrease at higher osmolality (HP point marked Ohyp or Hyper) are very similar using either method. Since this data is based on a single experiment, the significance of results is more in the closely tracking shapes rather than in the close magnitude of values. Importantly, regardless of the method used, we find a minimum around 150 mOsmol, which has been shown to correlate with the osmolality at which approximately 50% of the RBC have hemolyzed (Clark et al., 1983), a maximum deformability around 290 mOsmol, and a sharp drop in deformation when the cell loses water under hyper osmolalities. Different samples from control individuals show slightly different results in LP, MP and HP based on the individual characteristics of the donors. These shifts are very similar with either detection method. It indicates clearly that the microfluidic method identifies properly the change of RBC deformability over a large range of

osmolalities. Due to lack of resources and time, a very small number of experiments were performed. Nevertheless, this encouraging achievement can be considered as a proof of principle. It has still to be validated in a series of experiments on both normal and pathological blood samples, and a range for normal indicator points values should be established. Moreover, the repeatability and reproducibility of results should be further experimentally verified.

7 CONCLUSIONS

In this thesis I describe, for the first time, the design and construction of a prototype of a diagnostic instrument for several hereditary RBC disorders based on Osmotic scan ektacytometry in a micro-channel. I provide experimental results that can serve as a proof of principle for a further development. That was my main goal in this thesis, and that was accomplished.

This new technique presents several advantages over the currently used rotating cylinder technique :

- Lower quantities of blood sample are required - important for newborn babies and experimental mouse models used in bio clinical studies.

- Closed circuit design giving better sterile conditions and lowering sample contamination risk.

- Closed circuit allows monitoring of additional parameters like oxygenation and temperature. It also permits the instrument to be more compact in size and lighter.

- No moving parts in the flow channel (compared to the concentric rotating cylinders) leading to lower power consumption, lower production/manufacturing cost, and simplification of maintenance.

- Test conditions closer to blood vessel physiology.

- Provides better precision because shear stress does not depend on viscosity when constant pressure is maintained across the channel.

This new technique opens up the possibility of building a simple small footprint instrument that can be used with finger prick amounts of blood. Finger pricks are used for many applications (e.g. diabetes glucose monitoring) as it is much less invasive as compared to a needle in the arm. It could prove useful in many applications.

This new technique should still be validated by a series of experiments on both normal and pathological blood samples. Moreover, the claim that the flow channel presents a better measurement precision, has to be assessed in detail for each factor contributing to the potential cumulative measurement error and experimentally proven.

8 REFERENCES

Abkarian, M., Faivre, M., Viallat, A., 2007. Swinging of Red Blood Cells under Shear Flow. Phys. Rev. Lett. 98, 188302. doi:10.1103/PhysRevLett.98.188302

Allard, C., Mohandas, N., Bessis, M., 1978. Red Cell Deformability Changes in Hemolytic Anemias Estimated by Diffractometric Methods (Ektacytometry) Preliminary Results, in: Bessis, Marcel, Shohet, S.B., Mohandas, N. (Eds.), Red Cell Rheology. Springer Berlin Heidelberg, pp. 209–221.

Allison, A.C., 1964. Polymorphism and Natural Selection in Human Populations. Cold Spring Harb Symp Quant Biol 29, 137–149. doi:10.1101/SQB.1964.029.01.018

Amato, D., Booth, P.B., n.d. Hereditary ovalocytosis in Melanesians. [WWW Document]. PNG Med J VOLUME 20, NO. 1, MARCH, 1977. URL https://www.docphin.com/research/article-detail/14197732/PubMedID-269577/Hereditary-ovalocytosis-in-Melanesians (accessed 4.24.17).

ANCEY, Christophe - Notes de cours. Mécanique des Fluides.pdf ; page 141 [WWW Document], Scribd. URL https://www.scribd.com/doc/220887281/ANCEY-Christophe-Notes-de-cours-Mecanique-des-Fluides-pdf (accessed 6.23.16).

Artmann, G.M., Kelemen, C., Porst, D., Büldt, G., Chien, S., 1998. Temperature transitions of protein properties in human red blood cells. Biophys J 75, 3179–3183.

Ashkin, A., 1970. Acceleration and Trapping of Particles by Radiation Pressure. Phys. Rev. Lett. 24, 156–159. doi:10.1103/PhysRevLett.24.156

Ashkin, A., Dziedzic, J.M., 1971. Optical Levitation by Radiation Pressure. Applied Physics Letters 19, 283–285. doi:10.1063/1.1653919

Ashkin, A., Dziedzic, J.M., Bjorkholm, J.E., Chu, S., 1986. Observation of a single-beam gradient force optical trap for dielectric particles. Opt. Lett. 11, 288–290. doi:10.1364/OL.11.000288

Baskurt, O.K., Boynard, M., Cokelet, G.C., Connes, P., Cooke, B.M., Forconi, S., Liao, F., Hardeman, M.R., Jung, F., Meiselman, H.J., Nash, G., Nemeth, N., Neu, B., Sandhagen, B., Shin, S., Thurston, G., Wautier, J.L., International Expert Panel for Standardization of Hemorheological Methods, 2009. New guidelines for hemorheological laboratory techniques. Clin. Hemorheol. Microcirc. 42, 75–97. doi:10.3233/CH-2009-1202

Bayer, R., Caglayan, S., Guenther, B., 1994. Discrimination between orientation and elongation of RBC in laminar flow by means of laser diffraction, in: Bonner, R.F., Cohn, G.E., Laue, T.M., Priezzhev, A.V. (Eds.), . pp. 105–113. doi:10.1117/12.180777

Bessis, M., Delpech, G., 1981. Discovery of the red blood cell with notes on priorities and credits of discoveries, past, present and future. Blood Cells 7, 447–480.

Bessis, M., Mohandas, N., 1975. Diffractometric Method for Measurement of Cellular Deformability. Blood Cells 1, 307–313.

Bessis, M., Mohandas, N., Feo, C., 1980. Automated ektacytometry: a new method of measuring red cell deformability and red cell indices. Blood Cells 6, 315–327.

Bessis, N., Mohandas, N., 1974. Mesure continue de la déformabilité cellulaire par une méthode diffractométrique. CR Acad Sci Paris 278, 3–263.

Bhaduri, B., Pham, H., Mir, M., Popescu, G., 2012. Diffraction phase microscopy with white light. Opt. Lett., OL 37, 1094–1096. doi:10.1364/OL.37.001094

Binnig, G., Quate, C., Gerber, C., 1986. Atomic Force Microscope. Phys. Rev. Lett. 56, 930–933. doi:10.1103/PhysRevLett.56.930

Block, S.M., 1992. Making light work with optical tweezers. Nature 360, 493–495. doi:10.1038/360493a0

Bolten, D., Türk, M., 2011. Experimental Study on the Surface Tension, Density, and Viscosity of Aqueous Poly(vinylpyrrolidone) Solutions. Journal of Chemical & Engineering Data 56, 582–588. doi:10.1021/je101277c

Bransky, A., Korin, N., Nemirovski, Y., Dinnar, U., 2006. An automated cell analysis sensing system based on a microfabricated rheoscope for the study of red blood cells physiology. Biosensors and Bioelectronics 22, 165–169. doi:10.1016/j.bios.2005.12.006

Brochard, F., Lennon, J.F., 1975. Frequency spectrum of the flicker phenomenon in erythrocytes. J. Phys. France 36, 1035–1047. doi:10.1051/jphys:0197500360110103500

Brooks, D.E., Evans, E.A., 1987. Rheology of blood cells, in: Chien, S., Dormandy, J., Ernst, E., Matrai, A. (Eds.), Clinical Hemorheology, Developments in Cardiovascular Medicine. Springer Netherlands, pp. 73–96.

Canham, P.B., 1970. The minimum energy of bending as a possible explanation of the biconcave shape of the human red blood cell. Journal of Theoretical Biology 26, 61–81. doi:10.1016/S0022-5193(70)80032-7

Chassaing, P., 2005. Mécanique des fluides: PC-PSI. Bréal, Rosny-sous-Bois.

Chien, S., 1987. Red Cell Deformability and its Relevance to Blood Flow. Annual Review of Physiology 49, 177–192. doi:10.1146/annurev.ph.49.030187.001141

Chien, S., 1978. Principles and Techniques for Assessing Erythrocyte Deformability, in: Bessis, M., Shohet, S.B., Mohandas, N. (Eds.), Red Cell Rheology. Springer Berlin Heidelberg, pp. 71–99.

Chien, S., 1975. Biophysical behavior of red cells in suspensions. The red blood cell 2, 1031–1133.

Chien, S., Sung, K.L., Skalak, R., Usami, S., Tözeren, A., 1978. Theoretical and experimental studies on viscoelastic properties of erythrocyte membrane. Biophysical Journal 24, 463–487. doi:10.1016/S0006-3495(78)85395-8

Chung, C.I., 2000. Extrusion of Polymers: Theory and Practice. Hanser Publishers.

Clark, M.R., Mohandas, N., Shohet, S.B., 1983. Osmotic gradient ektacytometry: comprehensive characterization of red cell volume and surface maintenance. Blood 61, 899–910.

Cornish, R.J., 1928. Flow in a Pipe of Rectangular Cross-Section. Proceedings of the Royal Society A: Mathematical, Physical and Engineering Sciences 120, 691–700. doi:10.1098/rspa.1928.0175

Couprie, M., Marak, L., Talbot, H., others, 2011. Pink image processing library, in: Poster European Python Scientific Conference.

Dao, M., Lim, C.T., Suresh, S., 2003. Mechanics of the human red blood cell deformed by optical tweezers. Journal of the Mechanics and Physics of Solids 51, 2259–2280. doi:10.1016/j.jmps.2003.09.019

Dhermy, D., Schrével, J., Lecomte, M.-C., 2007. Spectrin-based skeleton in red blood cells and malaria. Curr. Opin. Hematol. 14, 198–202. doi:10.1097/MOH.0b013e3280d21afd

Dobbe, J.G.G., 2002. Engineering developments in hemorheology. s.n.], S.l.

Dobbe, J.G.G., Streekstra, G.J., Hardeman, M.R., Ince, C., Grimbergen, C.A., 2002. Measurement of the distribution of red blood cell deformability using an automated rheoscope. Cytometry 50, 313–325. doi:10.1002/cyto.10171

Eaton, P., West, P., 2010. Atomic Force Microscopy. Also available as: eBook.

Eber, S., Lux, S.E., 2004. Hereditary spherocytosis—defects in proteins that connect the membrane skeleton to the lipid bilayer. Seminars in Hematology 41, 118–141. doi:10.1053/j.seminhematol.2004.01.002

Einstein, A., 1906. Eine neue Bestimmung der Moleküldimensionen. Annalen der Physik 324, 289–306. doi:10.1002/andp.19063240204

Evans, E., Fung, Y.C., 1972. Improved measurements of the erythrocyte geometry. Microvasc. Res. 4, 335–347.

Evans, E.A., 1983. Bending elastic modulus of red blood cell membrane derived from buckling instability in micropipet aspiration tests. Biophys J 43, 27–30.

Evans, E.A., 1973. New Membrane Concept Applied to the Analysis of Fluid Shear- and Micropipette-Deformed Red Blood Cells. Biophys J 13, 941–954.

Evans, E.A., Waugh, R., Melnik, L., 1976. Elastic area compressibility modulus of red cell membrane. Biophys J 16, 585–595.

Fahraus, R., Lindqvist, T., 1931. The viscosity of the blood in narrow capillary tubes. American Journal of Physiology 96, 562–568.

Fedosov, D.A., Peltomäki, M., Gompper, G., 2014. Deformation and dynamics of red blood cells in flow through cylindrical microchannels. Soft Matter 10, 4258–4267. doi:10.1039/C4SM00248B

Finkelstein, A., Talbot, H., Topsu, S., Cynober, T., Garçon, L., Havkin, G., Kuypers, F., others, 2013. Comparison between a Camera and a Four Quadrant Detector, in the Measurement of Red Blood Cell Deformability as a Function of Osmolality. Journal of Medical and Bioengineering 2, 62–65.

Fischer, T., Stohr-Lissen, M., Schmid-Schonbein, H., 1978. The red cell as a fluid droplet: tank tread-like motion of the human erythrocyte membrane in shear flow. Science 202, 894–896. doi:10.1126/science.715448

Fischer, T.M., 2004. Shape Memory of Human Red Blood Cells. Biophysical Journal 86, 3304–3313. doi:10.1016/S0006-3495(04)74378-7

Fischer, T.M., Korzeniewski, R., 2013. Threshold shear stress for the transition between tumbling and tank-treading of red blood cells in shear flow: dependence on the viscosity of the suspending medium. Journal of Fluid Mechanics 736, 351–365. doi:10.1017/jfm.2013.496

Franck, P.H.F., Postma, C., Veuger, M., Wijermans, P., Kuypers, F.A., 2011. A Family with Hereditary Elliptocytosis: Variable Clinical Severity Caused by Three Mutations in the α- Spectrin Gene, in: ASH Annual Meeting Abstracts. p. 3167.

Frank, R.S., Hochmuth, R.M., 1987. An Investigation of Particle Flow Through Capillary Models With the Resistive Pulse Technique. Journal of Biomechanical Engineering 109, 103. doi:10.1115/1.3138650

Generic Optical Tweezer Diagram - Optical tweezers - Wikipedia, the free encyclopedia [WWW Document], n.d. URL https://en.wikipedia.org/wiki/Optical_tweezers#mediaviewer/File:Generic_Optical_Tweezer_Diagram.jpg (accessed 12.15.14).

George Hirasaki, 2005. Chapter 8- laminar flows with dependence on one dimension, college study notes - Transport phenomena [WWW Document]. URL http://www.docsity.com/en/chapter_8-_laminar_flows_with_dependence_on_one_dimension__college_study_notes_-_transport_phenomena_/194928/ (accessed 6.26.16).

Grier, D., 2003. A revolution in optical manipulation. Nature 424, 810–816. doi:10.1038/nature01935

Groner, W., Mohandas, N., Bessis, M., 1980. New optical technique for measuring erythrocyte deformability with the ektacytometer. Clin. Chem. 26, 1435–1442.

Haldane, J.B.S., 1949. The Rate of Mutation of Human Genes. Hereditas 35, 267–273. doi:10.1111/j.1601-5223.1949.tb03339.x

Hardeman, M.R., Goedhart, P.T., Dobbe, J.G.G., Lettinga, K.P., 1994. Laser-assisted optical rotational cell analyser (L.O.R.C.A.). I: A new instrument for measurement of various structural hemorheological parameters. Clinical hemorheology 14, 605–619.

Heinrich, V., Rawicz, W., 2005. Automated, high-resolution micropipet aspiration reveals new insight into the physical properties of fluid membranes. Langmuir 21, 1962–1971. doi:10.1021/la047801q

Hénon, S., Lenormand, G., Richert, A., Gallet, F., 1999. A new determination of the shear modulus of the human erythrocyte membrane using optical tweezers. Biophys J 76, 1145–1151.

Hereditary Stomatocytosis - Anaemias - Enerca [WWW Document], n.d. URL http://www.enerca.org/anaemias/58/hereditary-stomatocytosis (accessed 4.24.17).

Hinch, E.J., Leal, L.G., 1972. The effect of Brownian motion on the rheological properties of a suspension of non-spherical particles. Journal of Fluid Mechanics 52, 683. doi:10.1017/S002211207200271X

H.L. Goldsmith, 1971. Deformation of human red cells in tube flow. Biorheology 7, 235–242.

Hochmuth, R.M., 2000. Micropipette aspiration of living cells. Journal of Biomechanics 33, 15–22. doi:10.1016/S0021-9290(99)00175-X

Howard A. Stone, 2007. Introduction to Fluid dynamics for microfluidics flows.pdf, in: CMOS Biotechnology. Springer Science & Business Media.

Ibidi Application note 11, accessed 27.04.2017; http://ibidi.com/fileadmin/support/application_notes/AN11_Shear_stress.pdf

James O. Wilkes, 2015. Chapter 6. Solution of Viscous-Flow Problems - Fluid Mechanics for Chemical Engineers with Microfluidics and CFD, Second

Edition [Book], in: Fluid Mechanics for Chemical Engineers with Microfluidics and CFD. Prentice Hall.

Jeffery, G.B., 1922. The Motion of Ellipsoidal Particles Immersed in a Viscous Fluid. Proceedings of the Royal Society A: Mathematical, Physical and Engineering Sciences 102, 161–179. doi:10.1098/rspa.1922.0078

Johnson, R.M., Ravindranath, Y., 1996. Osmotic scan ektacytometry in clinical diagnosis. J. Pediatr. Hematol. Oncol. 18, 122–129.

Karnis, A., Goldsmith, H.L., Mason, S.G., 1966. The kinetics of flowing dispersions. Journal of Colloid and Interface Science 22, 531–553. doi:10.1016/0021-9797(66)90048-8

Keller, S.R., Skalak, R., 1982. Motion of a tank-treading ellipsoidal particle in a shear flow. Journal of Fluid Mechanics 120, 27–47. doi:10.1017/S0022112082002651

Kim, J., Lee, H., Shin, S., 2015. Advances in the measurement of red blood cell deformability: A brief review. Journal of Cellular Biotechnology 1, 63–79. doi:10.3233/JCB-15007

Kim, Y., Kim, K., Park, Y., 2012. Measurement Techniques for Red Blood Cell Deformability: Recent Advances, in: Moschandreou, T. (Ed.), Blood Cell - An Overview of Studies in Hematology. InTech.

Kim, Y., Shim, H., Kim, K., Park, H., Jang, S., Park, Y., 2014. Profiling individual human red blood cells using common-path diffraction optical tomography. Sci. Rep. 4. doi:10.1038/srep06659

King, M.-J., Garçon, L., Hoyer, J.D., Iolascon, A., Picard, V., Stewart, G., Bianchi, P., Lee, S.-H., Zanella, A., the International Council for Standardization in Haematology, 2015. ICSH guidelines for the laboratory diagnosis of nonimmune hereditary red cell membrane disorders. Int. Jnl. Lab. Hem. 37, 304–325. doi:10.1111/ijlh.12335

Koutsouris, D., R, G., Jc, L., Mt, G., P, B., Y, B., M, B., 1987. Determination of erythrocyte transit times through micropores. I--Basic operational principles. Biorheology 25, 763–772.

Kuypers, F.A., Scott, M.D., Schott, M.A., Lubin, B., Chiu, D.T., 1990. Use of ektacytometry to determine red cell susceptibility to oxidative stress. J. Lab. Clin. Med. 116, 535–545.

Kwiatkowski, D.P., 2005. How Malaria Has Affected the Human Genome and What Human Genetics Can Teach Us about Malaria. Am J Hum Genet 77, 171–192.

Lazarova, E.,. DIAGNOSIS OF HEREDITARY SPHEROCYTOSIS [WWW Document]. URL http://www.lesjeudisdefleurus.org/uploads/files/page/Sph%c3%a9rocytose_E_Lazarova.pdf.pdf (accessed 4.21.17).

Lazarova, E., Gulbis, B., Oirschot, B. van, van Wijk, R., 2017. Next-generation osmotic gradient ektacytometry for the diagnosis of hereditary spherocytosis: interlaboratory method validation and experience. Clin. Chem. Lab. Med. 55, 394–402. doi:10.1515/cclm-2016-0290

Leal, L.G., Hinch, E.J., 1971. The effect of weak Brownian rotations on particles in shear flow. Journal of Fluid Mechanics 46, 685. doi:10.1017/S0022112071000788

Lee, K., Kim, K., Jung, J., Heo, J., Cho, S., Lee, S., Chang, G., Jo, Y., Park, H., Park, Y., 2013. Quantitative Phase Imaging Techniques for the Study of Cell Pathophysiology: From Principles to Applications. Sensors 13, 4170–4191. doi:10.3390/s130404170

Lenard, J.G., 1974. A note on the shape of the erythrocyte. Bltn Mathcal Biology 36, 55–58. doi:10.1007/BF02461190

Linda M. Mcmanus, 2014. Pathobiology of Human Disease: A Dynamic Encyclopedia of Disease Mechanisms. Elsevier.

Linderkamp, O., Wu, P.Y.K., Meiselman, H.J., 1983. Geometry of Neonatal and Adult Red Blood Cells. Pediatr Res 17, 250–253. doi:10.1203/00006450-198304000-00003

Liu, S.C., Jarolim, P., Rubin, H.L., Palek, J., Amato, D., Hassan, K., Zaik, M., Sapak, P., 1994. The homozygous state for the band 3 protein mutation in Southeast Asian Ovalocytosis may be lethal. Blood 84, 3590–3591.

McLaren, C.E., Brittenham, G.M., Hasselblad, V., 1987. Statistical and graphical evaluation of erythrocyte volume distributions. American Journal of Physiology - Heart and Circulatory Physiology 252, H857–H866.

Mills, J.P., Qie, L., Dao, M., Lim, C.T., Suresh, S., 2004. Nonlinear elastic and viscoelastic deformation of the human red blood cell with optical tweezers. Mech Chem Biosyst 1, 169–180.

Mir, M., Bhaduri, B., Wang, R., Zhu, R., Popescu, G., 2012. Chapter 3 - Quantitative Phase Imaging, in: Wolf, E. (Ed.), Progress in Optics, Progress in Optics. Elsevier, pp. 133–217. doi:10.1016/B978-0-44-459422-8.00003-5

Mitchison, J.M., Swann, M.M., 1954. The Mechanical Properties of the Cell Surface I. The Cell Elastimeter. J Exp Biol 31, 443–460.

Mohandas, N., Clark, M.R., Jacobs, M.S., Shohet, S.B., 1980. Analysis of factors regulating erythrocyte deformability. Journal of Clinical Investigation 66, 563–573. doi:10.1172/JCI109888

Mohandas, N., Gallagher, P.G., 2008. Red cell membrane: past, present, and future. Blood 112, 3939–3948. doi:10.1182/blood-2008-07-161166

Mohandas, N., Lie-Injo, L.E., Friedman, M., Mak, J.W., 1984. Rigid membranes of Malayan ovalocytes: a likely genetic barrier against malaria. Blood 63, 1385–1392.

Mokken, F.C., Kedaria, M., Henny, C.P., Hardeman, M.R., Gelb, A.W., 1992. The clinical importance of erythrocyte deformability, a hemorrheological parameter. Ann Hematol 64, 113–122. doi:10.1007/BF01697397

Molloy, J.E., Padgett, M.J., 2002. Lights, action: Optical tweezers. Contemporary Physics 43, 241–258. doi:10.1080/00107510110116051

Mp, N., 1983. The Technicon Ektacytometer: automated exploration of erythrocyte function. Biorheology Suppl 1, 291–295.

Mueller, S., Llewellin, E.W., Mader, H.M., 2010. The rheology of suspensions of solid particles. Proceedings of the Royal Society of London A: Mathematical, Physical and Engineering Sciences 466, 1201–1228. doi:10.1098/rspa.2009.0445

Musielak, M., 2009. Red blood cell-deformability measurement: Review of techniques. Clinical Hemorheology and Microcirculation 42, 47–64. doi:10.3233/CH-2009-1187

Muzychka, Y.S., Yovanovich, M.M., 2009. Pressure Drop in Laminar Developing Flow in Noncircular Ducts: A Scaling and Modeling Approach. J. Fluids Eng 131, 111105–111105. doi:10.1115/1.4000377

Nott, P.R., Brady, J.F., 1994. Pressure-driven flow of suspensions: simulation and theory. Journal of Fluid Mechanics 275, 157. doi:10.1017/S0022112094002326

Oguz K Baskurt, M.R.H., 2009. Comparison of three commercially available ektacytometers with different shearing geometries. Biorheology 46, 251–64. doi:10.3233/BIR-2009-0536

Park, H., Lee, S., Ji, M., Kim, K., Son, Y., Jang, S., Park, Y., 2016. Measuring cell surface area and deformability of individual human red blood cells over blood storage using quantitative phase imaging. Sci Rep 6. doi:10.1038/srep34257

Park, Y., Best, C.A., Kuriabova, T., Henle, M.L., Feld, M.S., Levine, A.J., Popescu, G., 2011. Measurement of the nonlinear elasticity of red blood cell membranes. Phys Rev E Stat Nonlin Soft Matter Phys 83, 051925.

Park, Y., Diez-Silva, M., Popescu, G., Lykotrafitis, G., Choi, W., Feld, M.S., Suresh, S., 2008. Refractive index maps and membrane dynamics of human red blood cells parasitized by Plasmodium falciparum. PNAS 105, 13730–13735. doi:10.1073/pnas.0806100105

Pasvol, G., 2009. Are Children with Homozygous Sickle Cell Disease Really at a Disadvantage in the Face of Malaria? The Malaria Hypothesis Revisited. Clin Infect Dis. 49, 223–224. doi:10.1086/599835

Picard, V., Proust, A., Eveillard, M., Flatt, J.F., Couec, M.-L., Caillaux, G., Fénéant-Thibault, M., Finkelstein, A., Raphaël, M., Delaunay, J., Bruce, L.J., Pissard, S., Thomas, C., 2014. Homozygous Southeast Asian ovalocytosis is a severe

dyserythropoietic anemia associated with distal renal tubular acidosis. Blood 123, 1963–1965. doi:10.1182/blood-2014-01-548149

Platt, O.S., Brambilla, D.J., Rosse, W.F., Milner, P.F., Castro, O., Steinberg, M.H., Klug, P.P., 1994. Mortality In Sickle Cell Disease – Life Expectancy and Risk Factors for Early Death. New England Journal of Medicine 330, 1639–1644. doi:10.1056/NEJM199406093302303

Popescu, G., Badizadegan, K., Dasari, R.R., 2006a. Observation of dynamic subdomains in red blood cells. J. Biomed. Opt 11, 040503-040503-3. doi:10.1117/1.2221867

Popescu, G., Ikeda, T., Goda, K., Best-Popescu, C.A., Laposata, M., Manley, S., Dasari, R.R., Badizadegan, K., Feld, M.S., 2006b. Optical Measurement of Cell Membrane Tension. Phys. Rev. Lett. 97, 218101. doi:10.1103/PhysRevLett.97.218101

Puig-de-Morales-Marinkovic, M., Turner, K.T., Butler, J.P., Fredberg, J.J., Suresh, S., 2007. Viscoelasticity of the human red blood cell. Am. J. Physiol., Cell Physiol. 293, C597-605. doi:10.1152/ajpcell.00562.2006

Purcell, E.M., 1976. Life at low Reynolds number, in: AIP Conference Proceedings. Presented at the Physics and Our World: A Symposium in Honor of Victor F. Weisskopf, AIP Publishing, pp. 49–64. doi:10.1063/1.30370

Rand, R.P., Burton, A.C., 1964. Mechanical Properties of the Red Cell Membrane: I. Membrane Stiffness and Intracellular Pressure. Biophysical Journal 4, 115–135. doi:10.1016/S0006-3495(64)86773-4

Reid, H.L., Barnes, A.J., Lock, P.J., Dormandy, J.A., Dormandy, T.L., 1976. A simple method for measuring erythrocyte deformability. J Clin Pathol 29, 855–858.

Reinhart, W.H., Huang, C., Vayo, M., Norwich, G., Chien, S., Skalak, R., 1991. Folding of red blood cells in capillaries and narrow pores. Biorheology 28, 537–549.

Ruef, P., Pöschl, J.M.B., Linderkamp, O., 1995. The rheodyn SSD for measuring erythrocyte deformability. Biorheology 32, 357–358. doi:10.1016/0006-355X(95)92349-F

Sackmann, E., 1995. Biological Membranes Architecture and Function, in: Handbook of Biological Physics, (Ed. R.Lipowsky and E.Sackmann). Elsevier, Structure and Dynamics of Membranes (Ed: R. Lipowsky E. Sackmann).

Schmid-Schoenbein, H., Wells, R., Schildkraut, R., 1969. Microscopy and viscometry of blood flowing under uniform shear rate(rheoscopy). Journal of Applied Physiology 26, 674–678.

SCHMID-SCHöNBEIN, H., Wells, R., Goldstone, J., 1969. Influence of Deformability of Human Red Cells upon Blood Viscosity. Circulation Research 25, 131–143. doi:10.1161/01.RES.25.2.131

Schmid-Schönbein, P.D.D.H., Weiss, J., Ludwig, H., 1973. A simple method for measuring red cell deformability in models of the microcirculation. Blut 26, 369–379. doi:10.1007/BF01632746

Schulz, H.E. (Ed.), 2011. Hydrodynamics - Optimizing Methods and Tools. InTech.

Sehyun Shin, Yunhee Ku, Myung-Su Park, Jang-Soo Suh, 2004. Measurement of red cell deformability and whole blood viscosity using laser-diffraction slit rheometer. Korea-Australia Rheology Journal 85–90.

Shah, R.K., London, A.L., 1978. Laminar flow forced convection in ducts: a source book for compact heat exchanger analytical data. Academic Press.

Shin, S., Hou, J.X., Suh, J.S., Singh, M., 2007. Validation and application of a microfluidic ektacytometer (RheoScan-D) in measuring erythrocyte deformability. Clin. Hemorheol. Microcirc. 37, 319–328.

Shin, S., Ku, Y., Park, M.-S., Jang, J.-H., Suh, J.-S., 2005a. Rapid cell-deformability sensing system based on slit-flow laser diffractometry with decreasing pressure differential. Biosens Bioelectron 20, 1291–1297. doi:10.1016/j.bios.2004.04.025

Shin, S., Ku, Y., Park, M.-S., Suh, J.-S., 2005b. Slit-flow ektacytometry: Laser diffraction in a slit rheometer. Cytometry 65B, 6–13. doi:10.1002/cyto.b.20048

Shojaei-Baghini, E., Zheng, Y., Sun, Y., 2013. Automated Micropipette Aspiration of Single Cells. Ann Biomed Eng 41, 1208–1216. doi:10.1007/s10439-013-0791-9

Son, Y., 2007. Determination of shear viscosity and shear rate from pressure drop and flow rate relationship in a rectangular channel. Polymer 48, 632–637. doi:10.1016/j.polymer.2006.11.048

Stier, A., Bize, P., Schull, Q., Zoll, J., Singh, F., Geny, B., Gros, F., Royer, C., Massemin, S., Criscuolo, F., 2013. Avian erythrocytes have functional mitochondria, opening novel perspectives for birds as animal models in the study of ageing. Frontiers in Zoology 10, 33. doi:10.1186/1742-9994-10-33

Streekstra, G.J., Dobbe, J.G.G., Hoekstra, A.G., 2010. Quantification of the fraction poorly deformable red blood cells using ektacytometry. Opt Express 18, 14173–14182.

Stuart, J., 1985. Erythrocyte rheology. J Clin Pathol 38, 965–977.

Sutera, S.P., Gardner, R.A., Boylan, C.W., Carroll, G.L., Chang, K.C., Marvel, J.S., Kilo, C., Gonen, B., Williamson, J.R., 1985. Age-related changes in deformability of human erythrocytes. Blood 65, 275–282.

Swiač, I., 2007. Design of a Graphical User Interface to control a Medical Analysis System (Master Thesis). Brno University of Technology.

T. Fischer, H. Schmid-Schönbein, 1977. Tank tread motion of red cell membranes in viscometric flow: behavior of intracellular and extracellular markers. Blood Cells 351–365.

Technicon Ektacytometer User's manual, n.d.

Van Leeuwenhoek, A., 1674. Microscopical observations concerning blood, milk, bones, the brain, spittle, and cuticula. Philos Trans 121–128.

Wang, N., Butler, J.P., Ingber, D.E., 1993. Mechanotransduction across the cell surface and through the cytoskeleton. Science 260, 1124–1127.

Wang, X., Zhao, H., Zhuang, F.Y., Stoltz, J.F., 1999. Measurement of erythrocyte deformability by two laser diffraction methods, in: Clinical Hemorheology and Microcirculation. Presented at the Hemorheology and Tissue Oxygenation in Hypertension and Vascular Diseases. International Conference, IOS Press, pp. 291–295.

Weisenhorn, A.L., Khorsandi, M., Kasas, S., Gotzos, V., Butt, H.-J., 1993. Deformation and height anomaly of soft surfaces studied with an AFM. Nanotechnology 4, 106.

Yaginuma, T., Oliveira, M.S.N., Lima, R., Ishikawa, T., Yamaguchi, T., 2013. Human red blood cell behavior under homogeneous extensional flow in a hyperbolic-shaped microchannel. Biomicrofluidics 7. doi:10.1063/1.4820414

Zahalak, G.I., Sutera, S.P., 1981. Fraunhofer diffraction pattern of an oriented monodisperse system of prolate ellipsoids. Journal of Colloid and Interface Science 82, 423–429. doi:10.1016/0021-9797(81)90384-2

Zhao, R., Antaki, J.F., Naik, T., Bachman, T.N., Kameneva, M.V., Wu, Z.J., 2006. Microscopic investigation of erythrocyte deformation dynamics. Biorheology 43, 747–765.

9 APPENDIX

9.1 Scientific communications by Arie Finkelstein

A list of my scientific communications is presented below. Some of them were conducted in the framework of this thesis.

9.1.1 International journals

Arié Finkelstein, Hugues Talbot, Suat Topçu, Loïc Garçon, Gregor Havkin, Frans Kuypers Comparison between a camera and a four quadrant detector, in the measurement of Red blood cell deformability, Journal of Medical and Bioengineering (JOMB) Volume 2, No.1, March, 2013 , pp. 62-65 ISSN 2301-3796

Picard, V., Proust, A., Eveillard, M., Flatt, J.F., Couec, M.-L., Caillaux, G., Fénéant Thibault, M., Finkelstein, A., Raphaël, M., Delaunay, J., Bruce, L.J., Pissard, S., Thomas, C. Homozygous Southeast Asian ovalocytosis is a severe dyserythropoietic anemia associated with distal renal tubular acidosis. Blood 123, pages : 1963–1965. 2014. doi:10.1182/blood-2014-01-548149

9.1.2 Conferences

Arié Finkelstein, Hugues Talbot, Suat Topçu, Loïc Garçon, Frans Kuypers Validation of an Image Processing Algorithm for the Measurement of Red Blood cell Deformability, poster and short abstract, ISBI The 2013 IEEE *International Symposium on Biomedical Imaging*, San Francisco, Ca. 7-11 April 2013

Arié Finkelstein, Hugues Talbot, Suat Topçu, Loïc Garçon, Gregor Havkin, Frans Kuypers Comparison between a camera and a four quadrant detector, in the measurement of Red blood cell deformability, 2013 ICMIB 2nd International Conference on Medical Information and Bioengineering Bali Island, Indonesia, 16 - 17 March 2013

V. Picard, S. Pissard, M-L. Couec, A. Proust, R. Kokode, M. Fénéant-Thibault, A. Finkelstein, J. Delaunay, M. Raphaël, C. Thomas "Une ovalocytose mélanésienne homozygote chez un enfant présentant une hémolyse sévère et une acidose tubulaire rénale distale", *Congrès de la Société Française d'Hématologie,* SFH/GEHT. CNIT, Paris La Défense, France. du 10 au 12 Mars 2011.

9.1.3 Internal communications

Arié Finkelstein Résultats des expériences de validation de l'ektacytomètre au CHU de Bicêtre 05.06.2007

This document classified in « INTRANET de la Recherche ESIEE », was not published due to an examination of eventual patent application.

Arié Finkelstein Camera assisted measurement and control, Informatics Center of ESIEE-Paris, Research Report 2008-2009 page 34

Arié Finkelstein Mesure et contrôle assistés par une caméra, Département Systèmes Embarqués, Rapport d'activité ESIEE Engineering 2006-2007 page 75 -77

CONCEPTION ET ÉVALUATION D'UN NOUVEL OUTIL DE DIAGNOSTIC UTILISANT L'EKTACYTOMÉTRIE À GRANDIENT OSMOLAIRE

Résumé

La capacité des globules rouges à modifier leur forme en fonction de conditions externes spécifiques représente une propriété fondamentale permettant aux cellules de traverser des capillaires de diamètres plus petits que leur propre diamètre. L'ektacytométrie est une technique utilisée pour mesurer la déformabilité des globules rouges en exposant un échantillon très dilué de sang à des contraintes de cisaillement et en mesurant l'élongation resultante des globules par l'analyse de la figure de diffraction laser. Ce travail contribue à la conception et l'évaluation d'un nouveau dispositif de diagnostic basé sur la méthode microfluidique d'ektacytométrie à gradient osmolaire. Elle permet de mesurer la déformabilité d'une population de globules rouges (RBC), en fonction de l'osmolalité de milieu. Cette mesure permet un diagnostic différentiel d'un certain nombre d'anomalies du globule rouge présentant des symptômes similaires. Elle permet également de suivre les effets de certains traitements. Des aspects théoriques qui s'appuient sur les équations des écoulements et une preuve de principe sont discutés. Cette nouvelle technique ouvre la possibilité de construire un instrument simple et peu encombrant, décrit dans ce travail, ne nécessitant qu'un prélèvement de sang au bout du doigt.

DESIGN AND EVALUATION OF A NEW DIAGNOSTIC INSTRUMENT FOR OSMOTIC GRADIENT EKTACYTOMETRY

Abstract

The ability of red blood cells (RBC) to change their shape under varying conditions is a crucial property allowing these cells to go through capillaries narrower than their own diameter. Ektacytometry is a technique for measuring deformability by exposing a highly diluted blood sample to shear stress and evaluating the resulting elongation in RBC shape using a laser diffraction pattern. This work contributes to the design and evaluation of a new diagnostic technique based on osmotic scan ektacytometry, using a microfluidic method. It allows the measurement of deformability of an RBC population, as a function of varying medium osmolality. This measurement makes possible a differential diagnosis for any one of a number of RBC disorders presenting similar symptoms. It also permits the physician to follow the effects of treatments. Both theoretical aspects based on flow equations and a proof of principle are discussed. This new technique opens up the possibility of building a simple, small footprint instrument described in this work that can be used with finger prick amounts of blood.